A Torque Ripple Analysis on Reluctance Synchronous Machines

By

ALWYN NICOLAAS HANEKOM

Submitted to the Department of Electrical Engineering in Fulfilment of the Requirements for the Magister Technologiae in Electrical Engineering at the

CAPE PENINSULA UNIVERSITY OF TECHNOLOGY

SUPERVISOR: E. VOSS

SEPTEMBER 2006

Declaration

I, ALWYN NICOLAAS HANEKOM, submit this thesis as fulfilment of the requirements for the degree of Magister Technologiae (MTech) in Electrical Engineering.

I claim that his is my own original work and that it has not been submitted in this or similar form for a degree at any other tertiary institution.

.....

Alwyn N. Hanekom

Candidate

.....

Date

Acknowledgements

I wish to express my gratitude to all of the following:

- First of all, I would like to praise the Heavenly Father for his spiritual guidance during this project.

- I would like to express my deepest gratitude and appreciation to my supervisor, Mr Egon Voss, for his expert advice, encouragement and commitment during this project.

- The financial assistance of the University Research Fund (URF) of the Cape Peninsula University of Technology towards this research is acknowledged.

- I also would like to thank the staff of the Cape Peninsula University of Technology for providing a stimulating and friendly atmosphere.

- Finally, I would like to thank those closest to me. My parents, Johan and Hettie, for their support, encouragement and giving me this opportunity to further my education. I would like to thank my girlfriend, Nadia Oosthuizen, for her devotion and loving support.

Synopsis

Reluctance Synchronous Machines (RSM) have, due to their rotor geometry, an inherently high torque ripple. This torque ripple is defined as the deviation of the minimum and maximum torque from the average value. It is unwanted as it indicates uneven pull on the rotor causing deformation of it and hence different air-gaps along the rotor circumference as well as acoustic noise. In applications such as power steering, robotics and radar positioning systems where high precision movement is vital, oscillating torque will lead to the malfunction of these devices and therefore suppressed the use and development of RSMs.

Unlike the Induction machine (IM), the RSM has no copper losses in the rotor, which reduces the operating temperature significantly. With the development of electronic drives the quality of the output torque could be improved by means of accurate current- and flux space phasor control methods with much success and made the RSM a possible replacement for the IM. However, reducing torque ripple by means of purely geometrical changes is still a challenge to the machine designer.

This thesis will focus on the reduction of torque ripple while leaving the average torque relatively unchanged by changing the rotor geometry. The rotor changes will take place by means of flux barriers and cut-outs while the stator has either semi-closed slots or magnetic wedges.

In this work rotor structures with equal harmonic magnitudes but their angles 180° apart, will be combined to form one machine and identify how torque harmonics respond. The change in average torque and power factor will be evaluated with all geometrical changes made to these machines throughout this work.

Table of Content

List of Figures and Tables

Table **Title** **Page**

List of Symbols and Abbreviations

Roman Alphabet

A	cross-sectional area of circuit (m^2)
A_{avg+}	average magnetic vector potential at the enter side of a coil (Vs/m)
A_{avg-}	average magnetic vector potential at the return side of a coil (Vs/m)
A_{mi}	vector potential of element m at node i (Vs/m)
A_n	magnitude of the n^{th} harmonic
$A_{(R1,2,3)}$	average magnetic vector potential at enter side of phase R (Vs/m)
$A_{(Y1,2,3)}$	average magnetic vector potential at enter side of phase Y (Vs/m)
$A_{(B1,2,3)}$	average magnetic vector potential at enter side of phase B (Vs/m)
$A_{(r1,2,3)}$	average magnetic vector potential at return side of phase R (Vs/m)
$A_{(y1,2,3)}$	average magnetic vector potential at return side of phase Y (Vs/m)
$A_{(b1,2,3)}$	average magnetic vector potential at return side of phase B (Vs/m)
a_n	imaginary part of the n^{th} harmonic
$\bar{B}$	flux density vector (Vs/m^2)
B_r	radial component of flux density (Vs/m^2)
B_t	tangential component of flux density (Vs/m^2)
b_n	real part of the n^{th} harmonic
$\cos\varphi$	power factor
F	magnomotive force (MMF) (At)
I_{rms}	input rms supply current (A)
I_S	current space phasor ($A\angle$ deg)
$\lvert I_S \rvert$	magnitude of current space phasor (A)
i	point on node (where i = 1, 2 or 3) of element m
i_a	instantaneous current in phase a (A)
i_b	instantaneous current in phase b (A)

i_c	instantaneous current in phase c (A)
i_d	steady state d-axis stator current (A)
i_q	steady state q-axis stator current (A)
i_0	zero sequence component of the stator current (A)
$[K]$	Park's transformation matrix
k_d	distribution factor
k_p	pitching factor
k_w	winding factor
L_d	d-axis synchronous inductance (Am)
L_q	q-axis synchronous inductance (Am)
$L_d^{'}$	transient self inductance of rotor d-axis (Am)
$L_q^{'}$	transient self inductance of rotor q-axis (Am)
ℓ	effective winding length in the z direction (m)
ℓ_{mi}	effective length of winding filament at element m and node i (m)
ℓ_s	effective rotor stack length (m)
M	number of elements in meshed region of slot
$M_d^{'}$	transient mutual inductance of rotor d-axis (Am)
$M_q^{'}$	transient mutual inductance of rotor q-axis (Am)
m	corresponding element
N	number of turns per slot winding
N_{ph}	number of turns per phase
P_d	developed output power (W)
p	number of pole pairs
q	number of slots per pole phase group
$\Re$	magnetic reluctance (At/Vs)
r	radius of the air-gap (m)
r_{mi}	radius of location of node i at element m (m)
r_s	resistance of all the conductors of a phase winding (Ω)

S	area of integration (m^2)
S_m	sum of all elements
T	torque, (Nm)
T_{avg}	average torque (Nm)
T_d	torque from dynamic variables (Nm)
T_{dq}	torque from dq-variables (Nm)
T_m	torque from Maxwell's stress tensor (Nm)
$T_{\max}$	maximum instantaneous torque (Nm)
$T_{\min}$	minimum instantaneous torque (Nm)
T_{ripple}	torque ripple (%)
$\|T\|$	magnitude of instantaneous torque (Nm)
t	time (s)
v_{abc}	instantaneous values of fundamental supply phase voltages a, b and c (V)
V_d	steady state values for d- axis stator voltage component (V)
V_q	steady state values for q- axis stator voltage component (V)
V_0	zero sequence component of the stator voltage (V)
V_S	voltage space phasor (V $\angle$ deg)

Greek Alphabet

α_s	slot pitch (degrees)
Γ	contour of integration (m)
γ	torque angle (deg)
Δ_m	cross-sectional area of element m (m^2)
δ	rotor angle (deg)
δ_S	angle of stator flux linkage space phasor (deg)
θ	sum of rotational speed ωt and current space phasor angle $\hat{v}$ (deg)
$\hat{v}$	angle of current space phasor referenced to rotor d-axis (deg)
λ	flux linkage of a given coil (Vs)

λ_a	instantaneous flux linkage in phase a (Vs)
λ_b	instantaneous flux linkage in phase b (Vs)
λ_c	instantaneous flux linkage in phase c (Vs)
λ_d	d-axis fundamental stator flux linkage component (Vs)
λ_q	d-axis fundamental stator flux linkage component (Vs)
λ_0	zero sequence component of the stator flux linkage component (Vs)
λ_S	flux linkage space phasor (Vs$\angle$deg)
$\lvert\lambda_S\rvert$	space phasor magnitude of stator flux linkages (Vs)
μ_0	permeability of free space (Vs/Am)
μ_r	relative magnetic permeability of a material (Vs/Am)
σ	saliency ratio of L_d / L_q
σ_r	radial stress vector component (N/m)
σ_s	resultant stress vector component (N/m)
σ_t	tangential stress vector component (N/m)
τ_c	coil span (deg)
τ_p	pole span (deg)
υ	ratio of i_q / i_d
Φ	magnetic flux (Vs)
Φ_m	average flux of element m (Vs)
Φ_{mi}	flux of winding filament to node i at element m (Vs)
φ_n	angle of the n^{th} harmonic (deg)
ω	angular velocity (deg/s)

Abbreviations:

RSM	Reluctance Synchronous Machine
IM	Induction Machine
FA	Fourier analysis
FE	Finite element

1. Introduction

1.1 The development of RSM's

Alternating current (ac) machines have been part of our history from as early as the 19th century when Faraday produced the first ac electrical machine in 1821. At this time direct current (DC) machines found more attention due to the availability of a DC source by Volta's battery which could store energy. Even thought the invention of the induction motor was made by Nicola Tesla in 1888, this machine at the time, received little attention due to the profound research and applications DC machines was exposed to. Only later when the development of alternating systems by Tesla, which became very popular, and the introduction of power electronics research into the induction motor led to numerous contributions. (Levi 1966 & Richardson 1978)

From as early as the beginning of the 20th century, research has been conducted on the design of the reluctance rotor. Thomson (1911) proposed a salient-type rotor with a slitted field pole which reduced the armature reaction. Kostko (1923) moved away from this salient-type rotor towards a more round rotor with initial flux barriers. During the next 30 years, important publications were those of Brüderlin (1924), Trickey (1933, 1946), Taalat (1951), Lin (1951) and Douglas (1956), who all concentrated in different areas on rotor design. In this period all models were theory-based, since it was before the computer age and Finite Element (FE) software was unavailable.

Between the 1960s and 1970s the main concerns were stability problems and substantial research was concentrated on this problem. Leaders in this field were Lawrenson (1964, 1967) with his contribution to segmental-rotor reluctance motors, Kurscheidt (1961), and Brinkman (1965) for investigating flux barrier rotors with saturation bridges. Cruickskank (1971) were the first to investigate the possibilities of axially laminated rotors. The analysis of Honsinger (1971) on a two flux barrier per pole rotor created much interest and later a study on the steady-state performance was continued by Kamper (1996).

From the 1970s to the 1990s, attention was drawn to the single-salient RSM rotor. Weh (1985) again investigated an axially laminated rotor but on a special multi-phase reluctance

machine while El-Antably (1985) focussed on fibre glass between the rotor laminations. From 1990 until the present, considerable research attention has been given to both the single- and double salient reluctance machine. Vagati (1992) moved away from axially laminated rotors, due to iron loss problems, toward the punched flux barrier rotor.

Fratta (1993) mention that the most straightforward way to "compensate" for one harmonic component of the torque ripple is to divide the rotor into two sections, shifted with respect to each other by the proper angle. This, however, is not a complete harmonic compensation, owing to the rotor anisotropic behaviour. This statement was verified by Vagati (1998).

Chiricozzi (1996) focussed his attention on minimising the inductances as they affect the static torque enormously. He proposed a multi cross-sectional 2D FE analysis with a skewed rotor. This was done by means of stacking the rotor in four parts with no parallel flux barriers.

Lee (2004) approached the problem of torque ripple reduction by means of a completely new design and proposed to create asymmetry in the rotor teeth. These experiments, however, were done on a switched reluctance machine but presented the same possibilities for the RSM.

All of the above-mentioned authors based their research on different rotor geometries but concentrated mainly on inductances, magnetic fields and permeance harmonics. Very few published on torque harmonics and their relation to the rotor structure. In fact, before 1998 hardly anything was done with respect to this. Only Fratta (1993) and Malesani (1994) made a substantial contribution while most publications concentrated on obtaining high anisotropy and high torque-per-volume values.

1.2 Problem statement

The principle of using reluctance differences in the rotor to produce torque in electrical machines has been known for more than 1½ centuries. Researchers like Thompson (1911) and Kostko (1923) referred to this occurrence as 'reaction' changes in the machine which

was related to the armature reaction effect in DC machines. The term 'magnetic reluctance' defined as the resistance of a material to a magnetic field (in ampere-turns per weber) was coined in May 1888 by Oliver Heaviside and he described this phenomenon as the ratio of magnomotive force (MMF) to the magnetic flux (Heaviside 1888).

$$\Re = \frac{F}{\Phi} \tag{1.2.1}$$

The reluctance of a uniform magnetic circuit can be calculated accordingly

$$\Re = \frac{\ell}{\mu_0 \mu_r A} \tag{1.2.2}$$

where ℓ is the length of the circuit, μ_0 the permeability of free space, μ_r the relative magnetic permeability of the material and A the cross-sectional area of the circuit. Reluctance differences can be achieved by geometrical asymmetry in the rotor, known as 'cut-outs' or 'flux barriers' which consist of air openings in the rotor itself. This asymmetry causes different reluctances in the rotor, causing flux lines passing through it to experience different directional changes. Such a rotor can be defined as homogeneous (physical characteristics don't vary from point to point) and nonisotropic (properties are dependent on direction). Based on these facts the design of different rotor structures was exposed to an infinite amount of possibilities and led to important findings. From the mid 90's hardly anything was published specifically on torque ripple and the harmonic torque spectrum present and how to compensate for it. Only later researchers like Chiricozzi (1996), Conti (1996) and Vagati (1998, 2000) published their findings on this topic, but from there onwards torque ripple and torque harmonics have been neglected.

The contributions made with respect to torque ripple reduction gave clear rotor design procedures and theoretical explanations. Since the development of power electronics and machine drives, the quality of the output torque can be altered by means of accurate current and flux control methods with much success. These methods were partly responsible, for the past few years, that the focus on rotor design have been neglected. Torque ripple optimization has only lately received attention and still is not been thoroughly investigated

as to other performance characteristics like average torque, power factor, efficiency, etc. This torque ripple is defined as the deviation of the minimum and maximum torque from the average value. The cogging of instantaneous torque is unwanted since it creates uneven pull on the rotor which causes its deformation, leading to audible noise and mechanical resonance. In applications such as power steering, robotics and radar positioning systems where precision movement is vital, oscillating torque will lead to the malfunction of these devices. The different approaches to eliminate the latter led to acceptable results but the problem was not entirely solved in some cases. Some of the approaches and remedies are briefly explained:

(i) One approach to compensate for torque ripple was skewing of the rotor, which was a method adapted from induction machines. Skewing is normally done over one slot pitch but this angle, however, is decided upon empirically which will present problems if the torque harmonic content changes with each design. Another disadvantage of skewing is that the manufacturing cost of motors will increase, especially for mass production. The author wishes to introduce a new method where the rotor will be divided into two sections where each section consists of different flux barrier and cut-out geometries. The aim is to cancel a specific dominant harmonic. The combination methodology will be explained in more detail in the following chapters.

(ii) Previous research has shown that this torque ripple could be eliminated to a certain extent by short pitching (chording) the windings by typically one or two slots to reduce lower-order MMF space harmonics (Bomela 2002). Although this method has proved itself worthy no clear statement has been made how winding- and rotor design influence the torque ripple, as only brief discussion were made towards a singular rotor design. Consequently the necessity exists to identify how rotor structures with different geometrical dimensions react, with respect to parameters such as torque ripple, towards an optimized chorded winding.

(iii) On the stator side is a slotted structure which is also responsible for high torque ripple. To reduce this effect the air-gaps needs to be magnetically 'smooth' which in fact has a negative effect on the average torque. Semi-closed slots have shown positive results with respect to torque ripple reduction (Deodhar 1992).

This work will introduce the use of 'magnetic wedges', which is the total closure of the slot region towards the air-gap, to identify how the performance of such machines is altered.

The problem statement is therefore: "How can the torque ripple created by Reluctance Synchronous Machines be reduced by means of rotor geometrical alterations rather than electronic design techniques?"

1.3 Problem approach

Contributions of numerous scientists and engineers over the years have made impressive progress in the development of RSMs or any machine for that matter. They provided a good insight to the physical picture and performance properties like power density, efficiency, power factor and the overall performance of machines while the approach to eliminate torque ripple have in fact not been a topic discussed and researched for many years. This provided an opportunity to deliver commentary on new approach methods to counter torque ripple. This work will provide a clear layout with design methods and recommendations. The aim of this thesis will not be to provide an intense mathematical derivation but rather a practical method with brief mathematical explanations on the magnetic properties of RSMs. The methodology will be provided with more detail in the following chapters.

From literature research it was engineering wise always a good approach to use an existing machine and rectify geometrical ratios where the parameters would be the objection function. The approach therefore is the use of an existing single-salient vector controlled RSM. The stator structure used will consists of double layer windings chorded by 2 slots as used by Trübenbach (1993) where he did a compatibility study of the RSM and the Induction machine (IM).

The rotor structure chosen will be that of Honsinger (1971) where his focus was on the self-inductances L_d and L_q and proved with measured and calculated results that the whole machine performance could be calculated with knowledge of the machine's admittance. Kamper (1994) later contributed with his findings on cross magnetisation with

respect to L_d and L_q and said that if cross magnetization is ignored in any design optimization, the optimization itself will not be true. Further more this machine provided an acceptable torque-per-current output with a rotor geometry which presented high anisotropy but left much room for improvement. Although this machine prove to be adequate with respect to numerous performance properties it in fact does lag a specific one, namely low torque ripple, which is essential for applications where precision movement is of immense importants.

Firstly, the machine as a whole has to be analysed and 'revamped' as Vagati (1992) made it clear that the rotor can not be optimized by itself, but stator and rotor laminations have to be optimized as a whole. The structure is as follows:

(i) The Finite Element (FE) method together with an integrated source code software will be used for modulation and analysis accompanied by an optimization procedure for geometrical and performance changes. A refined mesh description along the air-gap and near flux barriers will be applied in this model to ensure high accuracy. This work will only consider the design optimization and abbreviations made for steady state operation.

(ii) The influence of the rotor flux barrier pitch will be investigated where the diagonal part of the barriers is changed with respect to each other in 2° steps leaving the horizontal part stationary.

(iii) Secondly the influence of double rotor flux barriers sets with diagonal barrier pitch changes similar to the previous and those with different geometries and positions.

(iv) The best performing machines in (ii) to (iii), with low torque ripple as main performance parameter, will be subjected to geometrical changes by means of adding of cut-outs. The pitch and horizontal height of the cut-out will vary from a minimum to a maximum position, depending on the pitch of the flux barriers, and best machines identified.

(v) The best performing machines in (ii) to (iv) will be optimized with respect to the best current space phasor angle where all parameters will be investigated.

(vi) Changes to the stator slots by means of magnetic wedges will be made for all machines from (ii) - (iv) to identify how these wedges alter the parameters, especially the torque ripple. The same procedure as in (iv) will be followed to identify the most optimum machines with respect to lowest torque ripple. For this machine the height of the magnetic wedges will be changed from 1mm to 5mm in steps of 1mm to identify the effect of the height on the performance of the machine.

(vii) The machines with semi-closed and closed slots will be subjected to a harmonic analysis to identify dominant harmonics and their angles. The aim of this is to identify how the pitch of the flux barriers or the changes to the cut-out geometry influence the harmonic content in the torque.

(viii) The torque data for all the modelled machines will be accumulated and introduced to an algorithm topology where different rotor groupings will be tested. The combination topology model will divide the rotor into sections and combine rotor structures with different geometries but not shifted with respect to each other. The justified aim of this is to achieve harmonic cancellation.

A detailed investigation and explanation of the above mentioned statements will be given in the following chapters.

1.4 Outline of thesis

The layout of the remaining part of the thesis is done accordingly:

Chapter 2: This section explain the method on how parameters are calculated for RSMs. The use of an existing machine will be subject to dimensional analysis and brief statements made towards possible design improvements. The occurrence of torque ripple will be discussed and possible methods to eliminate the latter investigated.

Chapter 3: This chapter investigate rotor geometrical changes to an existing RSM where dimensional changes such as flux barrier pitch, number of flux barriers present, cut-out pitch and cut-out height are investigated. The influence on

performance parameters such as average torque, torque ripple, power factor and saliency will be discussed consequently.

Chapter 4: In this section the best performing machines from Chapter 3 would be subject to an analysis of optimum current angles per given parameter. The introduction of magnetic wedges to the stator slots will be simulated with all machines from the previous chapter and conclusions drawn on how they affect the performance of RSMs.

Chapter 5: The machines modelled in Chapter 3 with semi-closed slots and magnetic wedges will be subjected to a Fourier analysis (FA), to identify how the changing geometry of the rotor affects the dominant torque harmonics in RSMs. The torque data of all these machines will be used in an algorithm and all possible rotor combinations be tested. This will identify the best combinations of two machines which show maximum torque harmonic cancellation.

Chapter 6: This chapter will conclude on how the geometry of the rotor with minor changes to the stator alters the torque ripple in RSMs. Conclusions and recommendations will be made to the design engineer. Areas not covered by this work will be highlighted and future research will be indicated.

2. Overview of an RSM

This section describes the physical geometry and nature of an unskewed RSM consisting of a rotor structure similar to that of the originally proposed model of Honsinger (1971). The rotor has air openings in it defined as flux barriers and cut-outs. With the presents of these barriers and cut-outs the opportunity presents itself to address certain geometrical dimensions and accordingly facilitate the opportunity of possible dimensional ratios. These ratios will be discussed in the following chapters as part of machine optimization with respect to certain parameters. In order to draw these comparisons the parameters such as torque, power factor and power must be calculated first. They will be derived from fundamental variables like the current, flux linkage, voltage, inductance, etc accordingly.

2.1 Mathematical model of the machine

This thesis will only deal with the analysis of steady-state machine operation and therefore the calculations will be based on the latter. The fundamental variables will be transformed from a stationary time dependent system (stator) to a rotating but time independent system (rotor) by means of the *dq*-transformation method.

2.1.1 Calculation of basic quantities

In order to calculate parameters like torque, power and power factor fundamental variables like currents, flux linkages, voltages and inductances must be established first. For the vector controlled RSM the input currents will be sinusoidal and defined as

$$\begin{bmatrix} i_a \\ i_b \\ i_c \end{bmatrix} = \sqrt{2} \cdot I_{rms} \begin{bmatrix} \cos(\omega t) \\ \cos(\omega t - 120^\circ) \\ \cos(\omega t + 120^\circ) \end{bmatrix} \tag{2.1.1}$$

with I_{rms} being the rms current and ωt being the rotational speed. These stator quantities i_a, i_b, i_c can be transformed by means of a Park transformation matrix K (Appendix A.1) in to three individual rotor quantities i_d, i_q, i_0 accordingly

$$i_d = \frac{2}{3}\left(i_a \cos(\omega t) + i_b \cos(\omega t - 120°) + i_c \cos(\omega t + 120°)\right) \tag{2.1.2}$$

$$i_q = -\frac{2}{3}\left(i_a \sin(\omega t) + i_b \sin(\omega t - 120°) + i_c \sin(\omega t + 120°)\right) \tag{2.1.3}$$

$$i_0 = \frac{1}{3}\left(i_a + i_b + i_c\right) \tag{2.1.4}$$

For sinusoidal systems the zero sequence component i_0 becomes zero and can be neglected. From eq (2.1.2) & (2.1.3) the magnitude of the stator current space phasor I_S and the current angle ϑ can be calculated accordingly

$$|I_S| = \sqrt{i_d^{\,2} + i_q^{\,2}} \tag{2.1.5}$$

$$\vartheta = \angle I_S = \tan^{-1}\left(\frac{i_q}{i_d}\right) \tag{2.1.6}$$

The stator flux linkages $\lambda_a, \lambda_b, \lambda_c$ for this unskewed machine, excluding end-winding linkages, are calculated from the weighted average vector potentials by means of the finite element (FE) method (Appendix A.2) and given by

$$\lambda = N\ell\left(A_{avg+} - A_{avg-}\right) \tag{2.1.7}$$

where ℓ is the effective winding length in the z direction, N the number of turns in the winding, A_{avg+} and A_{avg-} being the average vector potential of the "enter" and "return" side respectively. From experience it can be said that the calculation of the flux linkages is done more accurately using average vector potentials than from a magnetic field surface integral. Another advantage of this method is that the effect of cross magnetization and saturation are taken into account as this is fundamental for accurate calculation of flux linkages (Kamper 1996). Since the method of flux linkage calculation being established for two slots, let us consider the model used for analysis in this thesis as seen in Fig 2.1.1.

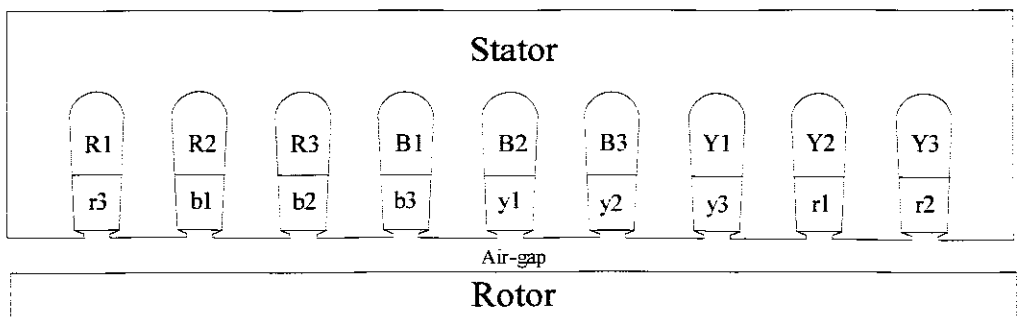

Fig 2.1.1 Cross-sectional view of 1-pole pitch for a 36-slot double layer machine which is short pitched by 2 slots

The calculation of winding to winding flux linkages can be expressed in numerous ways all depending on the definition of the input currents. Due to rotor symmetry the total flux linkage per pole phase group can be calculated accordingly

$$\lambda_a = N_{ph}\ell\left[\left(A_{(R1)} - A_{(r1)}\right) + \left(A_{(R2)} - A_{(r2)}\right) + \left(A_{(R3)} + A_{(r3)}\right)\right] \tag{2.1.8}$$

$$\lambda_b = N_{ph}\ell\left[\left(A_{(Y1)} + A_{(y1)}\right) + \left(A_{(Y2)} + A_{(y2)}\right) + \left(A_{(Y3)} + A_{(y3)}\right)\right] \tag{2.1.9}$$

$$\lambda_c = -N_{ph}\ell\left[\left(A_{(B1)} + A_{(b1)}\right) + \left(A_{(B2)} + A_{(b2)}\right) + \left(A_{(B3)} + A_{(b3)}\right)\right] \tag{2.1.10}$$

where N_{ph} is the number of turns per phase, $A_{(R1,2,3)}, A_{(Y1,2,3)}$ and $A_{(B1,2,3)}$ are the weighted average vector potentials on the "enter" side of the red-, yellow- and blue phase winding and $A_{(r1,2,3)}, A_{(y1,2,3)}$ and $A_{(b1,2,3)}$ are weighted average vector potentials on the "return" side of the red-, yellow- and blue phase winding. These stator quantities can be transformed into the rotor quantities $\lambda_d, \lambda_q, \lambda_0$ which results in the following equations

$$\lambda_d = \frac{2}{3}\left(\lambda_a \cos(\theta) + \lambda_b \cos(\theta - 120°) + \lambda_c \cos(\theta + 120°)\right) \tag{2.1.11}$$

$$\lambda_q = -\frac{2}{3}\left(\lambda_a \sin(\theta) + \lambda_b \sin(\theta - 120°) + \lambda_c \sin(\theta + 120°)\right) \tag{2.1.12}$$

$$\lambda_0 = \frac{1}{3}\left(\lambda_a + \lambda_b + \lambda_c\right) \tag{2.1.13}$$

where the angle θ being the sum of the current space phasor angle ϑ and the rotational speed ωt. The stator flux linkage space phasor magnitude λ_S and its angle δ_S can be calculated from the individual *dq*-components, from eq (2.1.11) & (2.1.12) as follows

$$|\lambda_S| = \sqrt{\lambda_d{}^2 + \lambda_q{}^2} \tag{2.1.14}$$

$$\delta = \angle\lambda_S = \tan^{-1}\left(\frac{\lambda_q}{\lambda_d}\right) \tag{2.1.15}$$

Even though the stator flux linkages have a harmonic content, it is of such a nature that the zero sequence linkage component λ_0, with a dominant 3rd harmonic, can be neglected as the sum of the linkages $\lambda_a, \lambda_b, \lambda_c$ is approximately zero. With this said the current- and flux linkage space phasors can be represented on the following space phasor diagram where the angle γ between the current space phasor I_S and the flux linkage space phasor λ_S is defined as the torque angle.

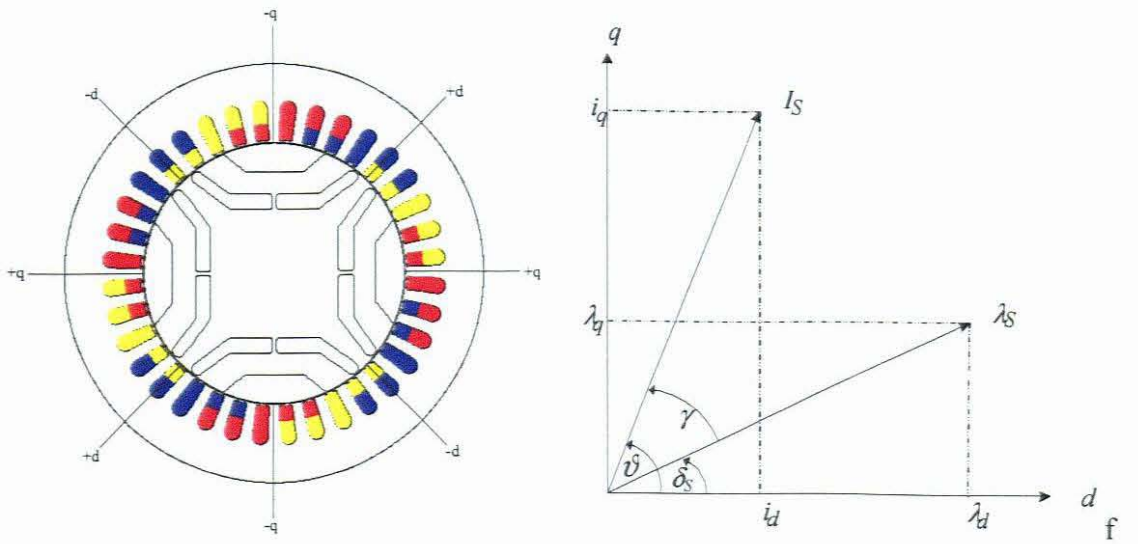

a) Cross section of RSM b) Space phasor diagram

Fig 2.1.2 Cross sectional view of RSM with space phasor representation of the currents and flux linkages in rotating frame.

The stator voltage equation of all rotating field machines from classic machine theory can be expressed as

$$v_{abc} = r_s i_{abc} + \frac{d}{dt}\lambda_{abc} \tag{2.1.16}$$

where r_s is the winding resistance and $(d/dt)\lambda_{abc}$ the emf created in each phase. The voltages can be transformed from stationary- to the rotating frame by applying the Park transformation matrix K and can be expressed as

$$V_{dq0} = r_s i_{dq0} + A\omega\lambda_{dq0} + \frac{d}{dt}\lambda_{dq0} \tag{2.1.17}$$

where

$$A = K\left[(d/d\theta)K^{-1}\right] \tag{2.1.18}$$

and ω is the reference frame angular velocity. Eq (2.1.17) can be rewritten in three individual voltage equations namely

$$V_q = r_s i_q + \omega\lambda_d + \frac{d}{dt}\lambda_q \tag{2.1.19}$$

$$V_d = r_s i_d - \omega\lambda_q + \frac{d}{dt}\lambda_d \tag{2.1.20}$$

$$V_0 = r_s i_0 + \frac{d}{dt}\lambda_0 \tag{2.1.21}$$

For a wye- (with neutral point not grounded) or delta connected machine the zero sequence voltage V_0 would be zero. The above equations indicate that the flux linkages are dependent on certain fundamental variables and must therefore be expressed as a function of the following.

$$\lambda_q = \lambda_q(i_q, i_d, \theta) \tag{2.1.22}$$

$$\lambda_d = \lambda_d(i_d, i_q, \theta) \tag{2.1.23}$$

This indicates that the flux linkage is a function of the *dq*-currents and the angle θ, thus the term $(d/dt)\lambda_{dq}$ in eq (2.1.19) & (2.1.20) has to be broken down into it's individual components namely

$$V_q = r_s i_q + \omega\lambda_d + \frac{\partial\lambda_q}{\partial i_q}\frac{di_q}{dt} + \frac{\partial\lambda_q}{\partial i_d}\frac{di_d}{dt} + \frac{\partial\lambda_q}{\partial\theta}\frac{d\theta}{dt} \tag{2.1.24}$$

$$V_d = r_s i_d - \omega\lambda_q + \frac{\partial\lambda_d}{\partial i_d}\frac{di_d}{dt} + \frac{\partial\lambda_d}{\partial i_q}\frac{di_q}{dt} + \frac{\partial\lambda_d}{\partial\theta}\frac{d\theta}{dt} \tag{2.1.25}$$

where $d\theta/dt$ is the angular velocity. From these individual fundamental quantities, function values such as the torque, power and power factor can be calculated.

2.1.2 Torque from basic quantities

The torque created is axially along the rotor surface and is perpendicular to the *dq*-reference frame. The simplest and most established method for torque calculation is done by using the cross-product between the stator flux linkage space phasor λ_S and current space phasor I_S and written as

$$T = \frac{3}{2}(\lambda_S \times I_S) \tag{2.1.26}$$

The magnitude can be calculated by the following equation:

$$|T| = \frac{3}{2}|\lambda_S||I_S|\sin(\gamma) \tag{2.1.27}$$

where λ_S and I_S being the magnitudes of the given space phasors and γ the torque angle. To present this torque in terms of its individual *dq*-components the voltage equations have

to be refurbished according to the nature of the RSM model. The *dq*-voltage equation of the RSM (ignoring iron losses) derived from eq (2.1.24) & (2.1.25) are given by

$$V_q = r_s i_q + L_q' \frac{di_q}{dt} + M_q' \frac{di_d}{dt} + \frac{\partial \lambda_q}{\partial \theta}\omega + \lambda_d \omega \tag{2.1.28}$$

$$V_d = r_s i_d + L_d' \frac{di_d}{dt} + M_d' \frac{di_q}{dt} + \frac{\partial \lambda_d}{\partial \theta}\omega - \lambda_q \omega \tag{2.1.29}$$

These voltages consist of three individual parts being the heat loss $r_s i_{dq}$, the energy stored in the magnetic field $L_{dq}'(di_{dq}/dt) + M_{dq}'(di_{qd}/dt)$ and the mechanical output which is $(\partial \lambda_{dq}/\partial \theta)\omega + \lambda_{dq}\omega$. The transient- self and mutual inductances as a function of the individual *dq*-currents are given by Fick (2004) as

$$L_q' = \left.\frac{\partial \lambda_q}{\partial i_q}\right|_{id=constant} \quad \& \quad L_d' = \left.\frac{\partial \lambda_d}{\partial i_d}\right|_{iq=constant} \tag{2.1.30}$$

and

$$M_q' = \left.\frac{\partial \lambda_q}{\partial i_d}\right|_{iq=constant} \quad \& \quad M_d' = \left.\frac{\partial \lambda_d}{\partial i_q}\right|_{id=constant} \tag{2.1.31}$$

The voltages from eq (2.1.28) & (2.1.29) can be physically represented in terms of an equivalent circuit which is shown below.

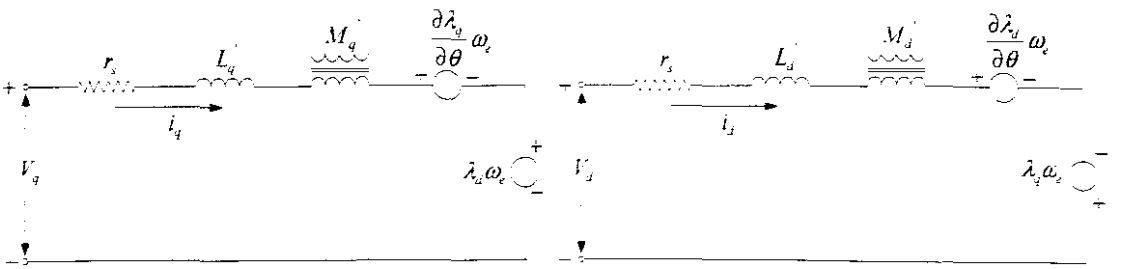

Fig 2.1.3 The *dq*-equivalent circuits of a RSM with respect to the voltages

For further evaluation it must be made clear if the machine consist of a smooth- or slotted air-gap. For a smooth air-gap, meaning that the circumference of the stator (closed slots for

example magnetic wedges) and the rotor (non-salient for example no cut-outs) is round, it is known that such a machine with no flux barriers in the rotor present will produce no torque. Thus assuming no variation in the d- and q-axis flux linkages with each rotor position, the terms $(\partial\lambda_q/\partial\theta)\omega$ and $(\partial\lambda_d/\partial\theta)\omega$ from eq (2.1.28) & (2.1.29) will become zero. The new reduced equivalent circuit becomes

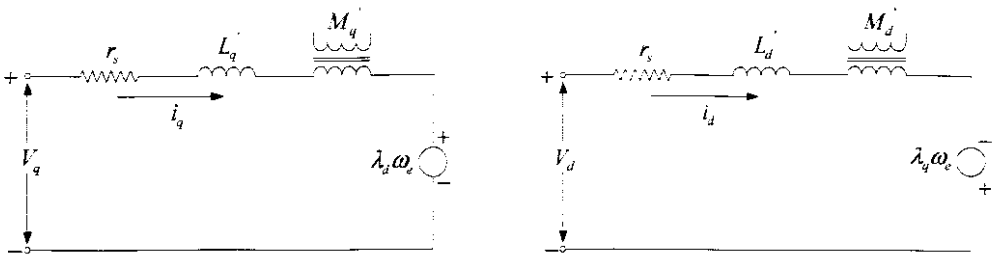

Fig 2.1.4 The dq-equivalent circuits of a RSM with smooth air gap

Note that L_d', L_q', M_d' and M_q' in this case are not a function of the rotor position θ for a machine with a smooth air-gap. The developed power of the smooth air-gap RSM is

$$P_d = \frac{3}{2}\left(\lambda_d i_q \omega - \lambda_q i_d \omega\right) = \frac{3}{2}\omega\left(\lambda_d i_q - \lambda_q i_d\right) \tag{2.1.32}$$

It must be remembered that this definition is excluding the losses (specifically the heat losses) in the stator. Thus the developed torque of the smooth air-gap machine is given by

$$T_{dq} = \frac{2P_d}{p\omega_n} = \frac{3}{4}p\left(\lambda_d i_q - \lambda_q i_d\right) \tag{2.1.33}$$

From this scalar presented equation it can be seen that the smooth air-gap RSM produce hardly any torque ripple since the terms $i_d(\partial\lambda_d/\partial\theta)$ and $i_q(\partial\lambda_q/\partial\theta)$ is responsible for the latter. Even though with all the assumptions made, this equation in fact give a good indication of the average torque created. However, this thesis will concentrate more on torque ripple than on average torque which justifies a further investigation for a more suitable method for torque calculation. Fratta (1993) and Chiricozzi (1996) indicted that to

accurately establish torque quality from dynamic variables the following method should be used

$$T_d = \frac{3}{4} p \left(i_q \lambda_d - i_d \lambda_q + \frac{1}{2} \left(i_q \frac{\partial \lambda_q}{\partial \theta} \omega_e + i_d \frac{\partial \lambda_d}{\partial \theta} \right) \right) \tag{2.1.34}$$

This is an approximate equation for the torque of the RSM and the second part of the equation is based on a linear magnetic circuit and thus no cross coupling is assumed. It's been made clear by Conti (1996) that eq (2.1.34) permits the best theoretical torque ripple analysis if *dq*-fluxes versus operating currents and rotor positions are known. Although many assumptions were made and fundamental occurrences neglected the equation does show that to have smooth torque the linkages λ_d and λ_q must be smooth (meaning their rate of change equal to zero) with rotor position or movement. In order to evaluate the precision of this method a comparison has to be made with respect to the well established method given by Maxwell which is presented next.

2.1.3 Torque from Maxwell's stress tensor

Maxwell developed a set of equations which explained the magnetic field phenomena with respect to a longitudinal tension and a transverse pressure, both equal in magnitude (Howe 1935). He suggested that the stress on a segment of the path due to the flux density field can be broken down into two individual components namely the radial and tangential component which is calculated accordingly:

$$\sigma_r = \frac{B_r^{\,2} - B_t^{\,2}}{2\mu_0} \tag{2.1.35}$$

$$\sigma_t = \frac{B_r B_t}{\mu_0} \tag{2.1.36}$$

where μ_0 is the permeability of free space, σ_r and σ_t are the radial and tangential stress components with B_r and B_t the flux density vectors components all along the defined

path. From these individual stresses the total force distribution can be calculated from the surface integral

$$F = \oint_S \sigma_s \cdot dS \tag{2.1.37}$$

where σ_s is the resultant stress tensor on the contour S. The radial and tangential force components can be obtained from the product between the individual stress vectors and the path length. The use of the Maxwell stress tensor method is probably the simplest method from a computational point of view since it requires only the local flux density distribution along a specific contour around the air-gap of the machine. However, studies have indicated that its accuracy can be markedly dependent on the model discretization and on the selection of the integration contour (Chang 1989). In this thesis the machine analysis is done with respect to a two-dimensional model as seen below in Fig 2.1.5

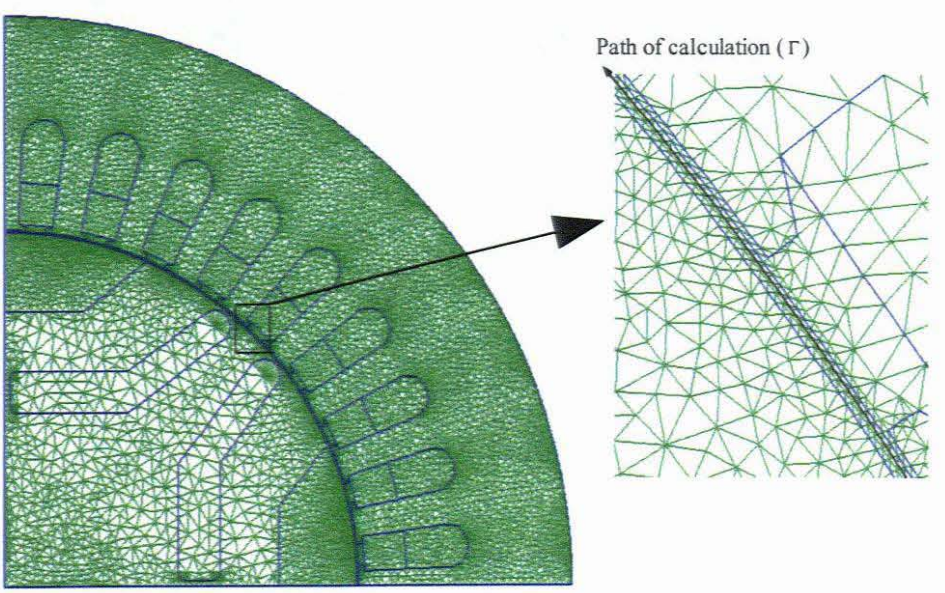

Fig 2.1.5 Contour Γ where torque will be calculated

Calculation of force or any other parameter for that matter is done more accurate in FE analysis when the defined path or contour goes through the middle of the elements and not through the nodes. In this analysis the middle of the air-gap has been chosen as path of calculation. With a two-dimensional model, eq (2.1.37) can be reduced to a line integral along a closed contour Γ in the air-gap and can be represented by

$$T_m = \frac{1}{\mu_0} \oint_{\Gamma} r B_t B_r d\Gamma \times \ell_s \tag{2.1.38}$$

where ℓ_s is the effective stack length of the rotor and r the radius between the centre of the shaft and contour Γ. From eq (2.3.38) it can be seen that only the components of the flux density on the contour of integration are invoked which make the computation less complex and rather quick (Chang 1989). This equation also indicates that rotational motion in a machine is created purely from the tangential component of the force and not from the radial one. With the different methods of torque calculation it now needs to be established how they compare to each other for the given RSM model as seen in Fig 2.1.6.

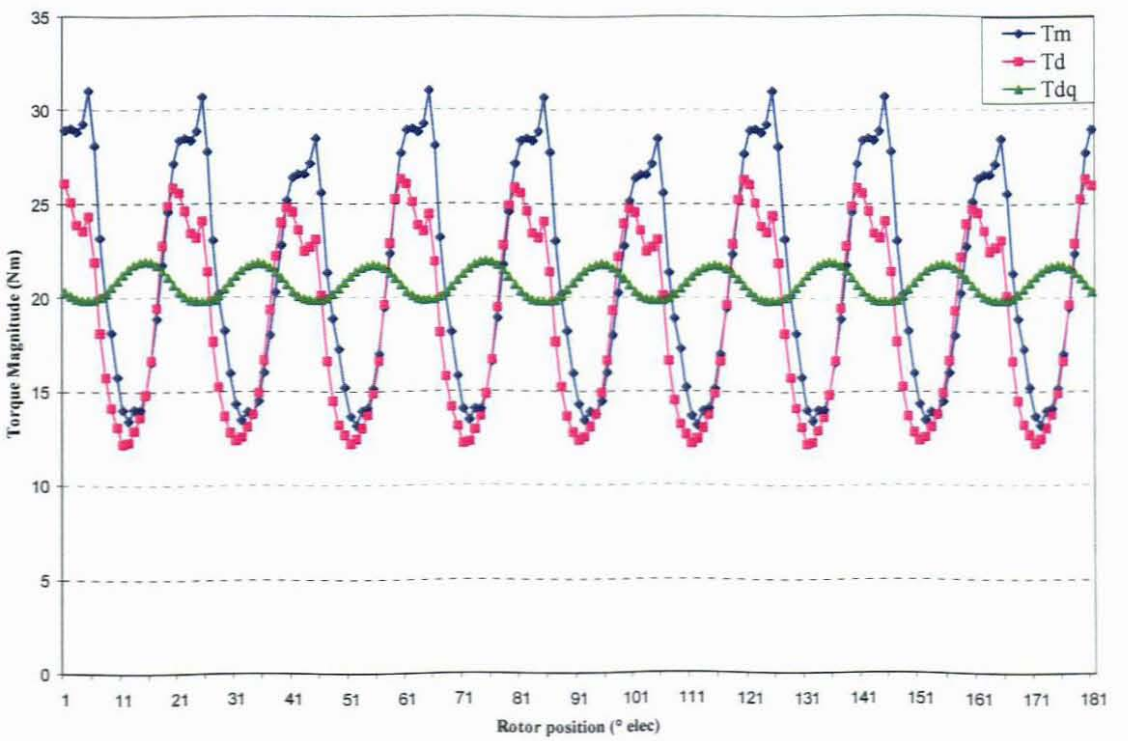

Fig 2.1.6 Comparison between different proposed torque calculation techniques

From Fig 2.1.6 it can be seen that the development of torque can be presented in numerous ways but all with a different outcome. The method presented by eq (2.1.34) compared exceptional good with the well established Maxwell's stress tensor method (eq 2.1.38) even when numerous assumptions have been made. The T_{dq} method (eq 2.1.33) did not

represent the torque deviation as good as the latter but clearly produced comparable average torque values. Even though this method will be neglected for torque ripple calculation, conclusion will be derived for parameters in the following chapters. With this said the author wishes to choose the Maxwell stress tensor method as it is well established and integrated as part of the FE software package which will be used for the analysis of the RSM.

2.1.4 Calculation of the power factor

The RSM consists of a rotor structure of such a nature that the inductance of the stator windings varies sinusoidally from a maximum value of L_d to a minimum value of L_q as a function of the speed of the shaft. These inductances are calculated as follows

$$L_d = \frac{\lambda_d}{i_d} \tag{2.1.39}$$

$$L_q = \frac{\lambda_q}{i_q} \tag{2.1.40}$$

A figure of advantage for an RSM is the saliency ratio which is the ratio of the direct- to the quadrature inductance (Hofmann 2000). Calculating the power factor can be achieved by using different methods each depending on the chosen fundamentals used in the calculation. Kamper (1994) showed by ignoring the stator resistance and the iron loss the power factor $\cos\varphi$ as a function of the saliency ratio can be represented by the following equation

$$\cos\varphi = \cos\left(\tan^{-1}\left(\frac{\sigma\upsilon + \upsilon}{\sigma - 1}\right)\right) \tag{2.1.41}$$

where $\sigma = L_d/L_q$ is the saliency ratio and υ is given by i_q/i_d. This equation indicates that the stability of the power factor is highly dependent on the change in saliency ratio. Since the value of L_q is very small the power factor is very sensitive to the change of it. Another approach is given by Parasiliti (1995) where he expressed the latter as the ratio

between the projection of the voltage space phasor vector V_S and the current space phasor vector I_S (Fig 2.1.7).

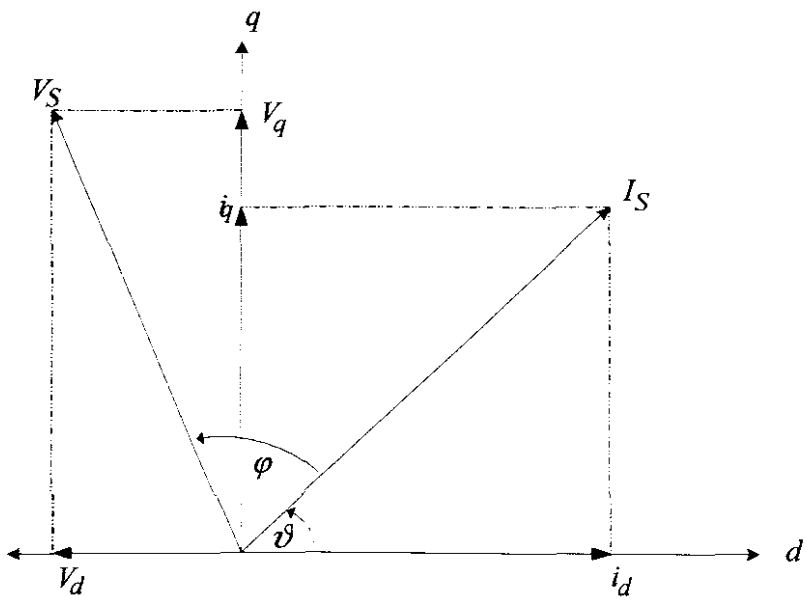

Fig 2.1.7 Space phasor diagram

This is done by substituting eq (2.1.6), (2.1.24) and (2.1.25) for ϑ, V_q and V_d into the following equation

$$\cos\varphi = \frac{V_d \cos\vartheta + V_q \sin\vartheta}{V_S} \tag{2.1.42}$$

where

$$V_S = \sqrt{V_d^{\,2} + V_q^{\,2}} \tag{2.1.43}$$

with V_S being the magnitude of the voltage space phasor vector. It must be made clear that power factor can expressed in numerous ways depending on the variables used. In this work the method presented in eq (2.1.41) will be used.

2.2 Investigated machine geometries

This similar rotor structure was originally used by Honsinger (1971) where he performed a study on the self-inductances L_d and L_q by derivation of the flux linkages of a reluctance machine with cut-outs and flux barriers. He found that calculated results were close to that of the measured ones, or at least tolerable, in most cases. Based on the last statement, he said that the whole machine performance could be calculated with knowledge of the machine's admittance. Later Kamper (1994, 1995) contributed with his findings on the steady state analysis where he studied what effect dimensional changes had on the cross magnetization and performance of the RSM. He later focused on the control of the RSM and produced optimized current angles for maximum torque, maximum torque per kVA and maximum efficiency. The proposed rotor based on the design given by Honsinger is given in Appendix B.2

In this study this rotor structure will be used as a foundation point where dimensional changes will be made with respect to the number- and pitch of the flux barriers and combine this machines with optimized cut-out dimensions. Optimization will be done where low torque ripple would be considered as primary factor, but bearing in mind the change of certain parameters like average torque, power factor, saliency ratio and the inductance difference of L_d and L_q. The rotor was situation in a standard 4-pole, 36-slot, 5.5 kW IM frame consisting of a 7/9 chorded double layer winding distribution which is detailed in Appendix B.1. The nominal frequency will be 50Hz with an rms input current of 10A.

Due to the nature and behaviour of the RSM with respect to its non-homogeneous and non-isotropic rotor and stator laminations, predicting the response of parameters with change in geometry was always a challenge for the engineer and has been a topic investigated for many years. Numerous indicated that when machine optimization with respect to geometrical changes in the rotor or stator were desired, it would be sensible to derive dimensional ratios inside the machine. To achieve this, the individual dimensional components must be identified as seen in Fig 2.2.1

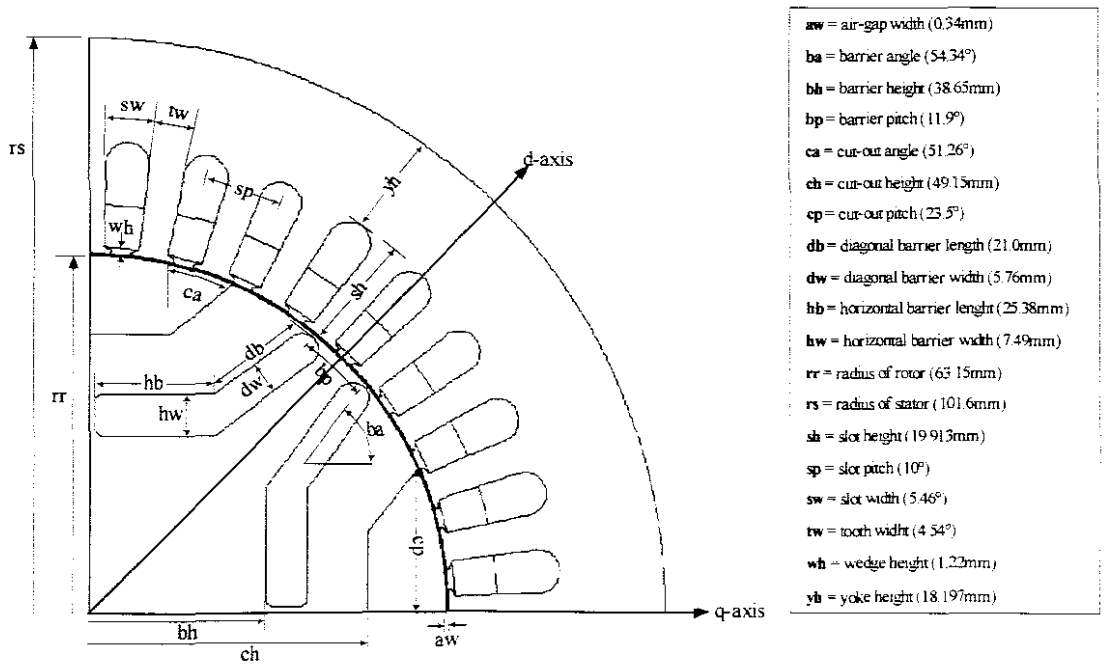

Fig 2.2.1 Cross-sectional view of original RSM with given dimensions

In this study there will be dimensional changes in the rotor as well as the stator each depending on the given criteria. It has been decided on that the change of the flux barrier pitch **bp** and the number of barriers present will be the focus point of the geometrical change in this thesis. From these optimized results the influence of cut-outs will be investigated where the pitch **cp** and height **ch** will be of interest. Consequently it would be relevant to identify the dimensional ratios which change for a specific optimization study and those who will stay constant. The following ratios will not change in analysis of the RSM in this thesis:

Stator: *rr/rs* (0.622) **Rotor:** *dw/hw* (0.769)

tw/sw (0.832) *bh/rr* (0.565)

yh/sh (0.914)

The changing ratios will be discussed in more detail in the following chapters. The original machine was modelled in a FE software simulation package with rotor movement simulated in steps of 0.5° mechanical. The results are presented in table 2.2.1

Table 2.2.1 Performance parameters of orginal RSM

Machine	T_{avg} (Nm)	T_{ripple} (%)	ΔL (mH)	cosφ	saliency σ	L_d (mH)	L_q (mH)
original	21.161	84.36	91.97	0.777	8.637	104.06	12.1

The performance of this machine at a current angle of $\vartheta = 65°$, presented good results for the overall parameters of the machine. Unfortunately the same statement could not be made for the torque ripple (see equation 2.3.1). The machine performed horribly in this region and suggested that much improvement is necessary to use such a machine in applications where high precision movement is essential. With i_d and i_q being constant (5.977A and 12.817A) during rotor movement the instantaneous torque may be deduced from λ_d and λ_q flux linkages according to eq (2.1.11) & (2.1.12).

$$i_d = \sqrt{2} \cdot I_{rms} \cos(\vartheta) \tag{2.2.1}$$

$$i_q = \sqrt{2} \cdot I_{rms} \sin(\vartheta) \tag{2.2.2}$$

With phase flux linkages calculated according to eq (2.1.8), (2.1.9) & (2.1.10) while taking the effect of cross-magnetization and saturation into account, these individual linkages presented a dominant 3rd with a less dominant 5th and 7th harmonic which was 5.15%, 0.17% and 0.37% of the fundamental. When these flux linkages were converted to the rotating reference frame both λ_d and λ_q linkages presented a dominant 9th harmonic as seen as seen in Fig 2.2.2.

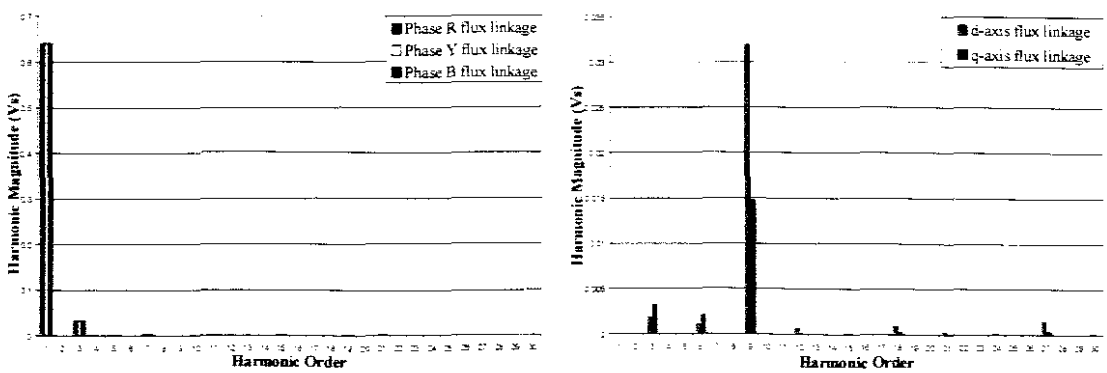

Fig 2.2.2 Dominant flux linkage harmonics for stationary- and rotating reference frame

Table 2.2.1 Performance parameters of orginal RSM

Machine	T_{avg} (Nm)	T_{ripple} (%)	ΔL (mH)	cosφ	saliency σ	L_d (mH)	L_q (mH)
original	21.161	84.36	91.97	0.777	8.637	104.06	12.1

The performance of this machine at a current angle of $\vartheta = 65°$, presented good results for the overall parameters of the machine. Unfortunately the same statement could not be made for the torque ripple (see equation 2.3.1). The machine performed horribly in this region and suggested that much improvement is necessary to use such a machine in applications where high precision movement is essential. With i_d and i_q being constant (5.977A and 12.817A) during rotor movement the instantaneous torque may be deduced from λ_d and λ_q flux linkages according to eq (2.1.11) & (2.1.12).

$$i_d = \sqrt{2} \cdot I_{rms} \cos(\vartheta) \tag{2.2.1}$$

$$i_q = \sqrt{2} \cdot I_{rms} \sin(\vartheta) \tag{2.2.2}$$

With phase flux linkages calculated according to eq (2.1.8), (2.1.9) & (2.1.10) while taking the effect of cross-magnetization and saturation into account, these individual linkages presented a dominant 3rd with a less dominant 5th and 7th harmonic which was 5.15%, 0.17% and 0.37% of the fundamental. When these flux linkages were converted to the rotating reference frame both λ_d and λ_q linkages presented a dominant 9th harmonic as seen as seen in Fig 2.2.2.

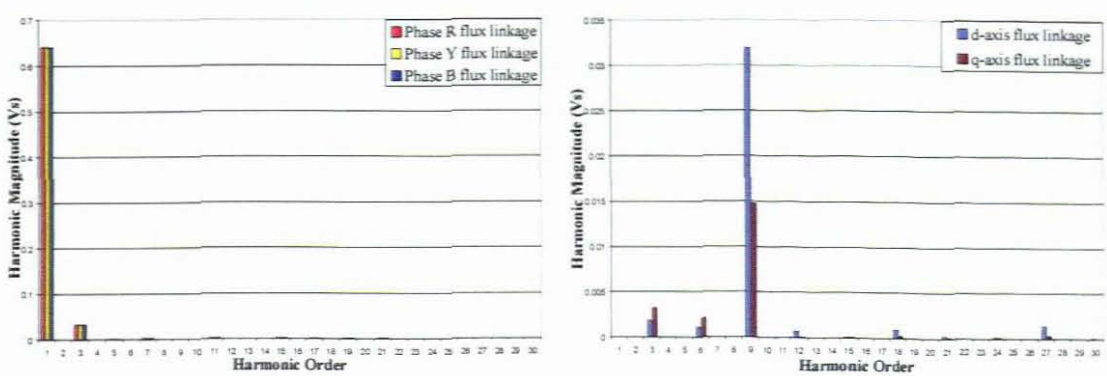

Fig 2.2.2 Dominant flux linkage harmonics for stationary- and rotating reference frame

With the 5th and 7th harmonic being minute it can be said that the 3rd harmonic is mostly responsible for the cogging of the torque. With the deviation of the instantaneous torque also presenting a dominant 9th harmonic (Fig 2.2.3) suggest that the quality of the torque can be derived from the behaviour of these linkages. The dominant 9th harmonic in the torque indicates that the slotted structure of the stator (9 slots per pole) in the RSM plays a large role in the torque behaviour.

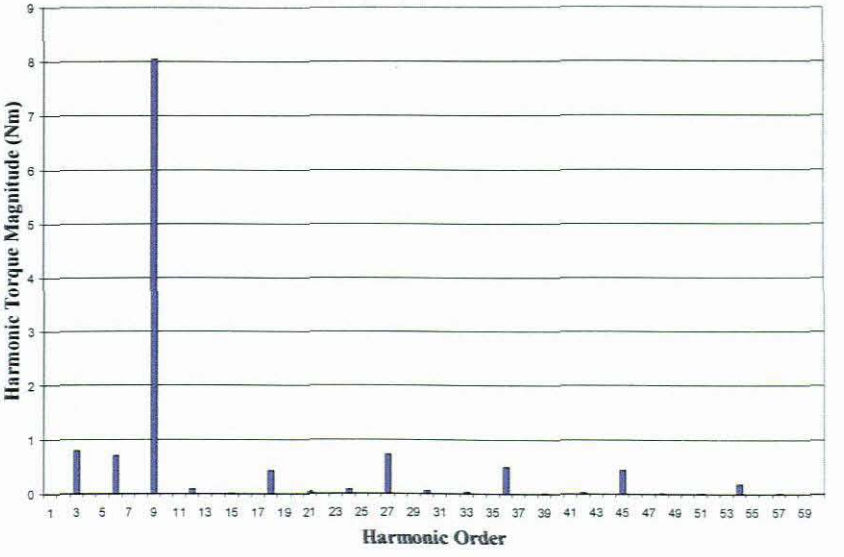

Fig 2.2.3 Fourier analysis of original machine torque

Possible methods to counteract the effect of these dominant harmonics will be discussed in the following chapters.

2.3 Discussion on torque ripple

When the Reluctance Synchronous Machine (RSM) is compared to the Induction Machine (IM) it present numerous advantages. It consist of a rugged rotor design, no rotor cage which consequently suggest no rotor copper losses (I^2R) which reduce the operating temperature dramatically and high efficiency with respect to minimal power losses. The stator of RSMs and IMs are exactly the same, meaning the one can be converted into the other which will save production costs given that most industrial machines are IMs. One specific performance area where the RSM lag the IM is high torque ripple. Torque ripple is

defined as the deviation of the minimum and maximum torque from the average value and presented accordingly.

$$T_{ripple} = \frac{T_{\max} - T_{\min}}{T_{avg}} \times 100\% \tag{2.3.1}$$

where $T_{\max}$, $T_{\min}$ and T_{avg} are defined as the maximum-, minimum- and average torque respectively. This fluctuating torque (Fig 2.3.1) is unwanted since it creates uneven directional pull on the rotor which partly causes its deformation, leading to audible noise and mechanical resonance especially in high speed applications.

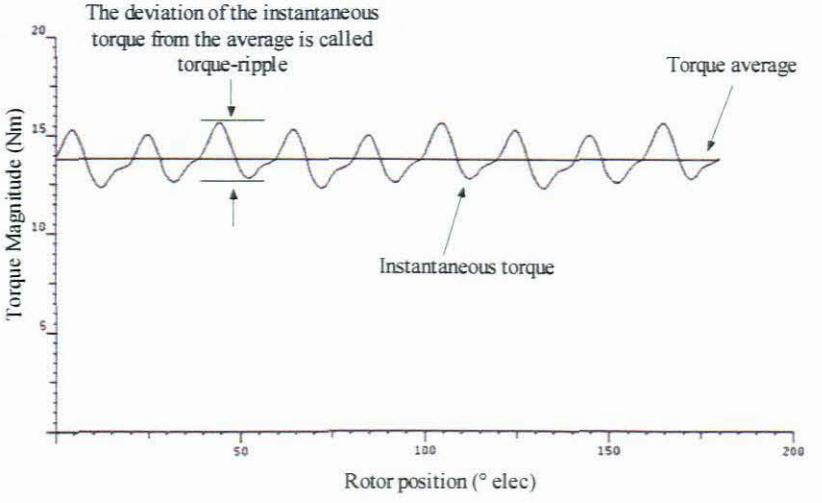

Fig 2.3.1 Torque as a function of the rotor position

Further disadvantages are poor power factor, low output power and unstable operation at open loop control. The torque ripple can be reduced by means of a fine motor design and an approximate choice of geometrical design parameters such as flux barrier-width, height, length, angle and location which present the same opportunities for cut-outs (Chiricozzi 1996). The ideal torque of a RSM (in fact of any machine) is constant which means it does not change with respect to the rotor position. However, reality shows that this is not the case since the torque fluctuates about an average value. For this reason the torque characteristics of the RSM with respect to the rotor and stator geometry was investigated.

2.3.1 Discussion on deformational forces

Due to the rotor asymmetry in a RSM, the machine itself suffers naturally from deformational forces on the rotor surface and consequently the stator. The machine's behaviour in generating vibrations and noise, due to cogging torques, is determined by the electromagnetic field in the air-gap and the mechanical structure of the machine. The link between magnetic and mechanical analysis is the electromagnetic force exerted by the magnetic field on the rotor and stator (Delaer 1999). Even if a machine design consists of a smooth torque, deformational forces will always be present in the machine itself.

Electromagnetic torque created by the magnetic field can be broken down into two components each playing a different role in mechanical deformation. For every rotational position the instantaneous torque is numerically determined by the force distribution on the rotor surface. This distribution known as the local force consist of a radial and tangential component each responsible for mechanical deformation of a specific area. The tangential forces created by the magnetic field in the air-gap are only responsible for rotor deformation and therefore single-handedly responsible for rotor movement by producing the measured output torque. To identify how this tangential force distribution changes with respect to different rotor positions the output torque (Fig 2.1.6) of the original machine (Fig 2.2.1) was subject to analysis.

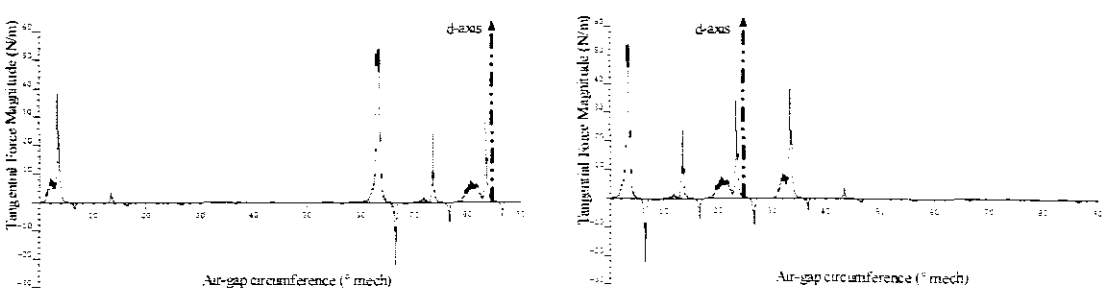

a) Tangential force at 4° elec b) Tangential force at 64° elec

Fig 2.3.2 Tangential force distribution at different rotor positions where instantaneous torque is at a maximum

With the air-gap taken as reference circumference the force distribution were chosen at rotational angles where the machine produced maximum instantaneous torque (Fig 2.1.5). It is clear that the force distribution pattern on the rotor circumference does not change

where the arithmetically calculated instantaneous torques is the same at different rotor positions. However when this instantaneous torque change to a minimum with rotor movement the force distribution do change as seen in Fig 2.3.3

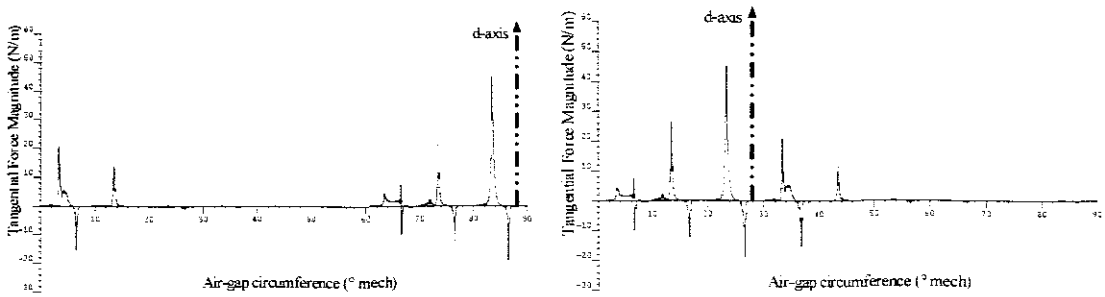

a) Tangential force at 11° elec b) Tangential force at 71° elec

Fig 2.3.3 Tangential force distribution at different rotor positions where instantaneous torque is at a minimum

Although the force distribution is not uniformly spread over the rotor circumference and at some places opposite to that of the rotational direction, the fact still remains that, when the instantaneous torques are equal the force distribution will be the same. Consequently it can be said that if the tangential deformation pattern between rotational angles is kept constant, vibrations and mechanical resonance can be suppressed to a minimum. The radial force component of the instantaneous torque is exclusively responsible for the deformation of the stator. To keep consistency in the investigation the same rotor positions were used for analysis and the findings are presented in Fig 2.3.4 & 2.3.5.

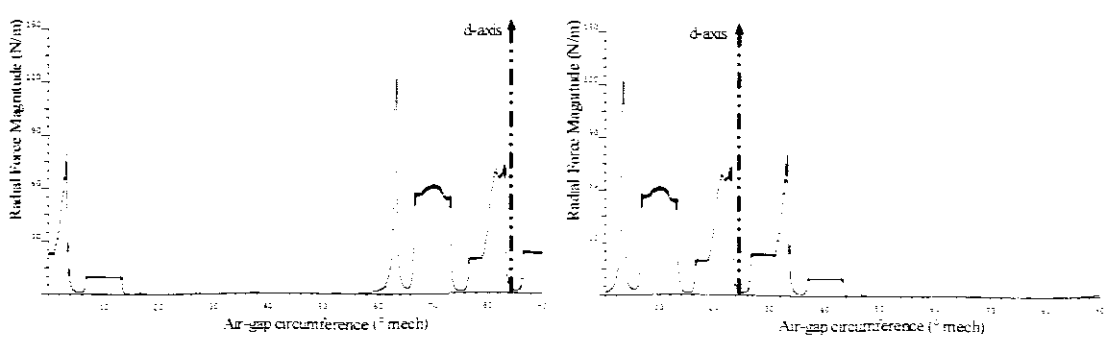

a) Radial force at 11° elec b) Radial force at 71° elec

Fig 2.3.4 Radial force distribution at different rotor positions where instantaneous torque is at a maximum

Again the same radial force pattern was sustained where the instantaneous torques were of equal magnitude. The deformational force will be experienced like a spatial wave through the circumference of the stator. However, the instantaneous torque does change and the analysis of the two minima's with respect to radial force distribution are indicated in Fig 2.3.5.

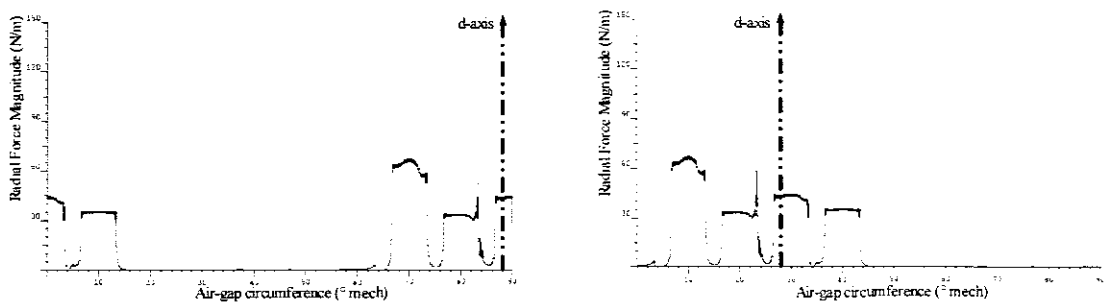

a) Radial force at 11° elec b) Radial force at 71° elec

Fig 2.3.5 Radial force distribution at different rotor positions where instantaneous torque is at a minimum

Another negative aspect of the radial components is the degree of the magnitude compared to that of the tangential one. Analysis indicated that the radial force at maximum and minimum instantaneous torque vary 10 to 30 times in magnitude to that of the tangential one. This indicates that when a machine has an output torque for example of 20 N, the radial force will put a pressure of 200 to 600 N on the stator circumference indicating how important mechanical stiffness of the stator, especially at the teeth, is. The fact still remains that in electrical machines, or any magnetic device for that matter, the magnetic materials are subjected to an elastic deformation under the action of magnetic forces. Inversely, the magnetic field as well as the force distribution is more or less influenced by this elastic deformation (Ren 1995).

2.3.2 Torque sensitivity to rotor position

In section 2.2 the geometry of the machine has been broken down into certain dimensions which resulted into dimensional ratios. Observing the change of these ratios enables the engineer to analyze the link between geometry and performance. Let us consider the actual torque produced by the machine presented in Fig 2.2.1.

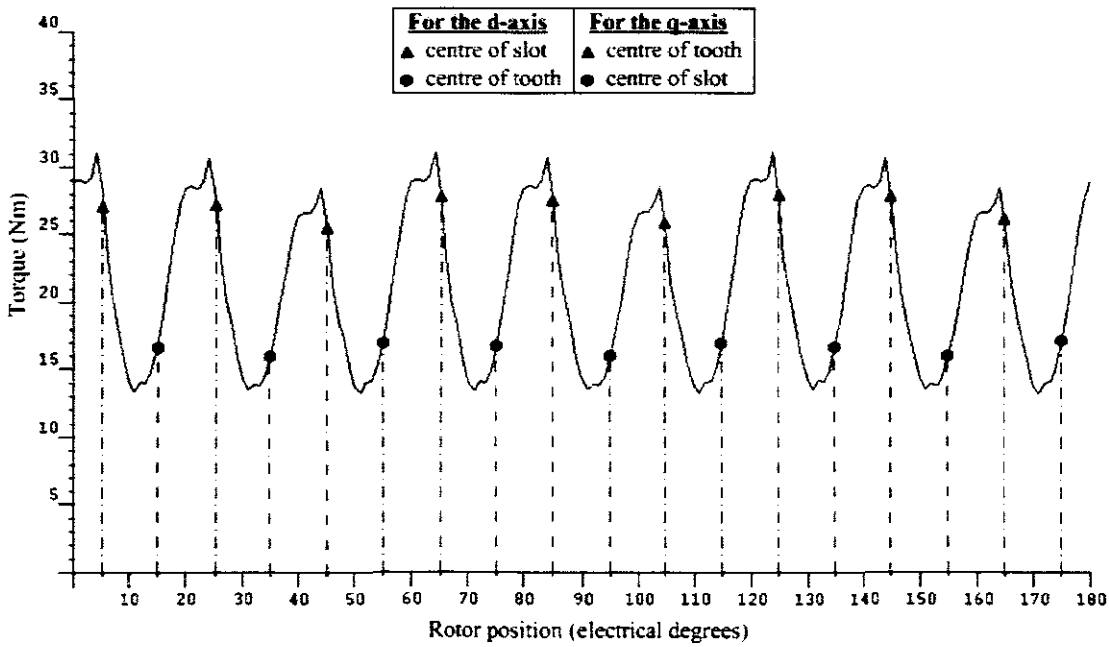

Fig 2.3.6 Torque as a function of the rotor position for different d- and q-axis positions

In Fig 2.3.6 the actual torque created in the machine is being referred to a stationary stator reference frame while the position of the d- and q-axis in the rotating rotor frame have been changed. It is clear that the machine is sensitive to the actual position of the rotor and indicates that when the d-axis is in the centre of a slot while the q-axis is in the middle of a tooth more torque is created then when the opposite is true. These d-and q-axis positions also indicate that the centre of a slot or tooth is not the absolute position for maximum or minimum instantaneous torque. A further analysis indicates that when the d-axis is situated at the edge of a tooth maximum instantaneous torque is obtained. As the rotor turns and the d-axis passes through the slotted region (semi-closed slots in this case) a decay of instantaneous torque occurs. This decay in torque continues until the slot is passed and a minimum instantaneous torque is reached at the start of the next tooth. When the d-axis is shifted from the edge of the tooth's left side to the edge of the tooth's right side the instantaneous torque again changes from a minimum of 14.05 Nm to a maximum of 30.7 Nm as seen below in Fig 2.3.7.

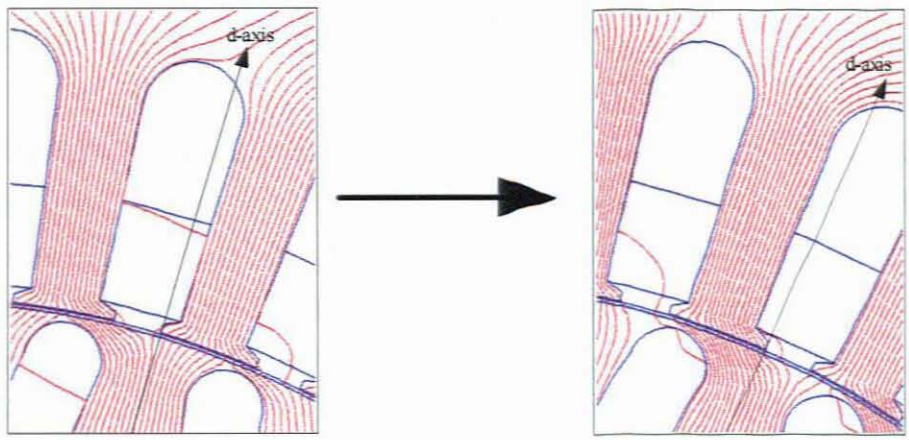

a) Rotor position at 10° elec b) Rotor position at 24° elec

Fig 2.3.7 Change of rotor position between the edges of a tooth

The above pictures show how the directions of the tangential forces change from the edge of the left side of the tooth to the right side of it. In Fig 2.3.7 a) the tangential forces in clockwise and anti-clock wise direction are almost equal while in Fig 2.3.7 b) they are almost all clockwise. The question is will the change of the tangential forces from equal to almost uni-directional always be taking place at the same rotor d-axis position (i.e. will the maximum tangential force always be on the right side of the tooth edge as in the figures above)?

In order to draw conclusive findings on how the geometry of the rotor is responsible for torque ripple, flux barriers and cut-outs will be changed gradually, but only either one at a time. The exact changes will be explained in the next chapters in detail.

3. Changing Parameter of the Rotor

An existing 5.5 kW reluctance machine (Fig 2.2.1) from Honsinger (1971) was used in this investigation to establish how the performance characteristics were altered if certain dimensional variables were changed. In this study only geometrical changes in the rotor will be done with respect to the pitch difference of single- and double flux barriers to each other and the further optimization introduction of different cut-out pitches and heights. The stator dimension will be kept constant with a 7/9 chorded double layer winding distribution fed by a sinusoidal input current with a magnitude of 10A rms.

3.1 Investigating single flux barriers

In this analysis the machine in Fig 3.1.1 is used for simulation where the pitch of the flux barriers **bp** with respect to the d-axis will be changed each in 1° steps from 8° to 34° presenting 14 different machine prototypes. The rotor will be turned clock wise (due to winding distribution) through one pole pitch in steps of 0.5° mechanical. The reason for such small increments is to obtain sufficiently accurate results.

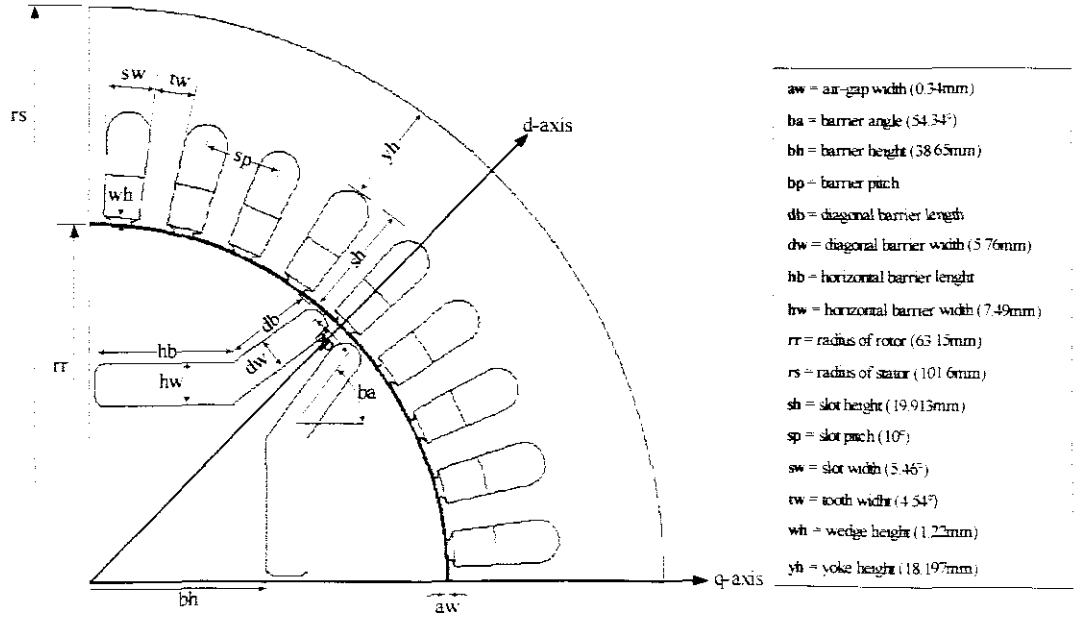

Fig 3.1.1 Cross-sectional view of single flux barrier RSM used for analysis

In this analysis the stator dimensions **sh**, **sp**, **sw**, **tw**, **wh** and **yh** are kept constant. The rotor diameter will not be changed through out the analysis keeping the optimized air-gap width **aw** constant at 0.34 mm. A study done by Kamper (1995) indicated that for maximum torque per ampere, using the rotor design proposed by Honsinger (1971), the current angle must lie between 60° and 65°. Even though the focus point of this thesis is on obtaining minimal torque ripple the possibility of a high average torque should not be neglected and therefore choosing an angle from this optimized range is justified. Consequently the author chose a fixed current angle of $\vartheta = 65°$ for this analysis. The current angle will be discussed in more detail in the following chapter. The results are shown in Fig 3.1.2 & 3.1.3 and the numerical values of all parameters are given in Table B.3.1 of Appendix B.3.

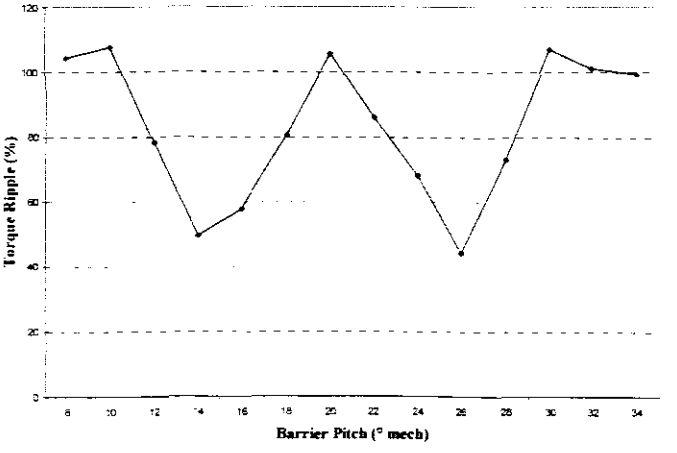

Fig 3.1.2 Torque ripple as a function of the barrier pitch

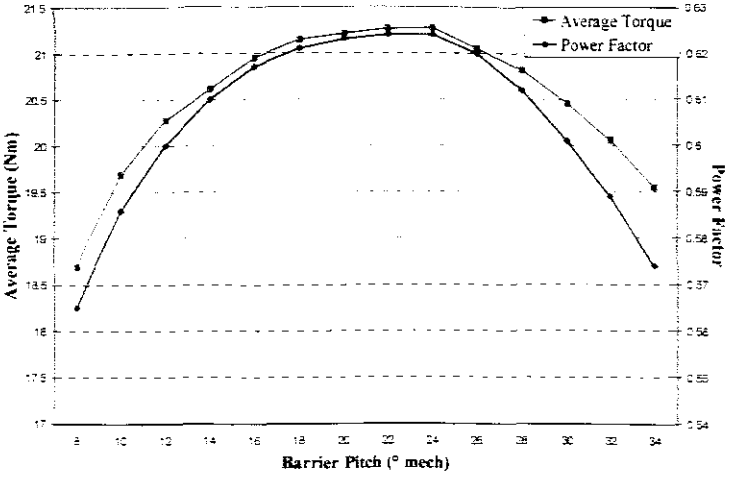

Fig 3.1.3 Average torque and power factor as a function of the barrier pitch

In this analysis the stator dimensions **sh**, **sp**, **sw**, **tw**, **wh** and **yh** are kept constant. The rotor diameter will not be changed through out the analysis keeping the optimized air-gap width **aw** constant at 0.34 mm. A study done by Kamper (1995) indicated that for maximum torque per ampere, using the rotor design proposed by Honsinger (1971), the current angle must lie between 60° and 65°. Even though the focus point of this thesis is on obtaining minimal torque ripple the possibility of a high average torque should not be neglected and therefore choosing an angle from this optimized range is justified. Consequently the author chose a fixed current angle of $\hat{v} = 65°$ for this analysis. The current angle will be discussed in more detail in the following chapter. The results are shown in Fig 3.1.2 & 3.1.3 and the numerical values of all parameters are given in Table B.3.1 of Appendix B.3.

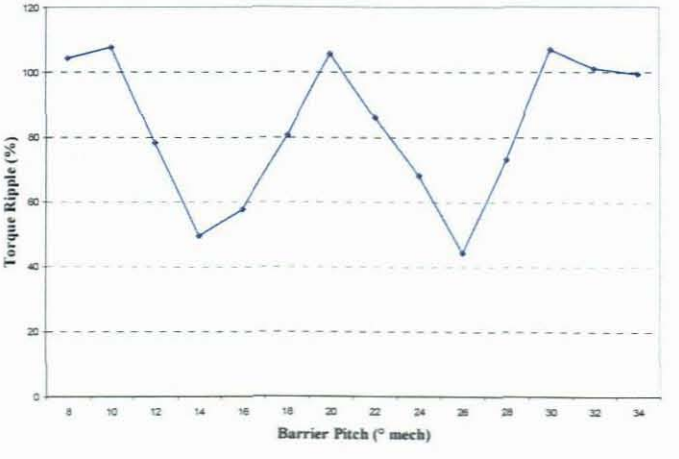

Fig 3.1.2 Torque ripple as a function of the barrier pitch

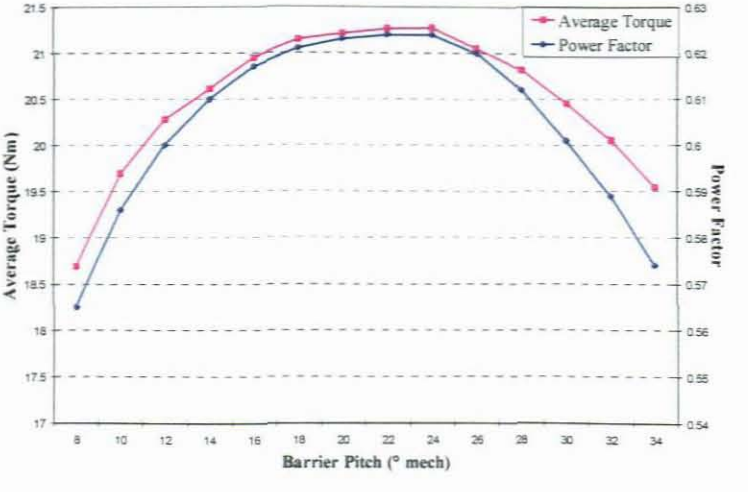

Fig 3.1.3 Average torque and power factor as a function of the barrier pitch

When the flux barriers were increased with respect to the d-axis a distinct pattern can be derived from the parameters. For the inductance difference ΔL, the power factor $\cos\varphi$ and the saliency ratio σ the average value have been taken as a function of the barrier pitch. From the results it is clear that the position of flux barriers in the rotor have a fundamental effect on the overall performance of the machine. With the barrier pitch increasing an incline in average torque T_{avg}, ΔL, $\cos\varphi$ and σ was achieved until a maximum was reached, which happened at a barrier pitch of 24°. From here the latter declined accordingly until the maximum barrier pitch of 34° was reached. What is more of interest is the way or the ratio these parameters change with respect to each other, especially between T_{avg} and ΔL. Through out this analysis the ratio between the latter varied between 229.7 and 230.7 which clearly indicate consistency and verify that the one can be derived from the other. Let us consider the equation for torque (eq 2.1.33) given by

$$T = \frac{3}{4} p\left(\lambda_d i_q - \lambda_q i_d\right) \tag{3.1.1}$$

By definition the d- and q-axis inductances L_d and L_q can be expressed as the ratio between the d- and q-axis stator flux linkage components λ_d and λ_q and the d- and q-axis stator current components i_d and i_q. Bearing in mind eq (2.1.5) & (2.1.6) the torque can be expressed in terms of the inductance difference of L_d and L_q and given by

$$T = \frac{3}{2} p \cdot \Delta L \cdot I_S \sin(2\vartheta) \tag{3.1.2}$$

This clearly indicates that ratio between the average torque and the inductance difference is a function of the input variables such as supply current and the current space phasor angle. Although this equation suggests that for maximum torque the current angle should be 45° it should be noted that the latter will alter the individual d- and q-axis inductances and therefore not produce maximum torque (Kamper 1996). However, eq (3.1.2) suggest that the fluctuating L_d and L_q inductances between rotor positions are partly responsible for the cogging of the torque.

The fact of the matter is that the torque ripple does not seem to follow the same pattern as the rest of the parameters as it seem to fluctuate between the different flux barrier pitches. With all the ratios starting at a maximum or minimum and change almost linearly to the opposite throughout the analysis indicates that deriving optimum dimensional ratios would be difficult especially when a new rotor design is to be proposed. However this study indicated that when using a flux barrier pitch of 26° the torque ripple would be decreased by almost half of that of the original design (84.36%) while the decline in average torque was only 0.1 Nm. Due to the rotor saliency (presents of cut-outs) of the original machine the new design could not match its relative good power factor of $\cos\varphi = 0.78$. The new proposed design is shown below

Fig 3.1.4 Cross-sectional view of best performing single flux barrier RSM

Even though the above machine indicted an improved design the possibility still presented itself geometrically to develop a rotor structure where torque ripple could be reduced. With dimensional ratios not giving concluding facts about rotor design improvement the decision have been made to include another set of flux barriers in the rotor with more or less the same features. The approach will be revealed in the next section.

3.2 Investigating double flux barriers

In this analysis the rotor will consist of double flux barriers where all possible combinations of different flux barrier pitches to be simulated. For the inner barrier the pitch will vary from 8° to 14° with respect to each other while the outer barrier will vary from 22° to 34° giving 22 possible combinations if no flux barriers where to overlap each other. The stator dimensions will stay the same as the previous analysis keeping the rotor radius the same. For consistency a current angle of $\delta = 65°$ with the same input currents will be used in this analysis. The introduction of an extra set of flux barriers increased the possibility of different dimensional ratios and will be discussed shortly. A possible prototype is given below in Fig 3.2.1 where new dimensions are described.

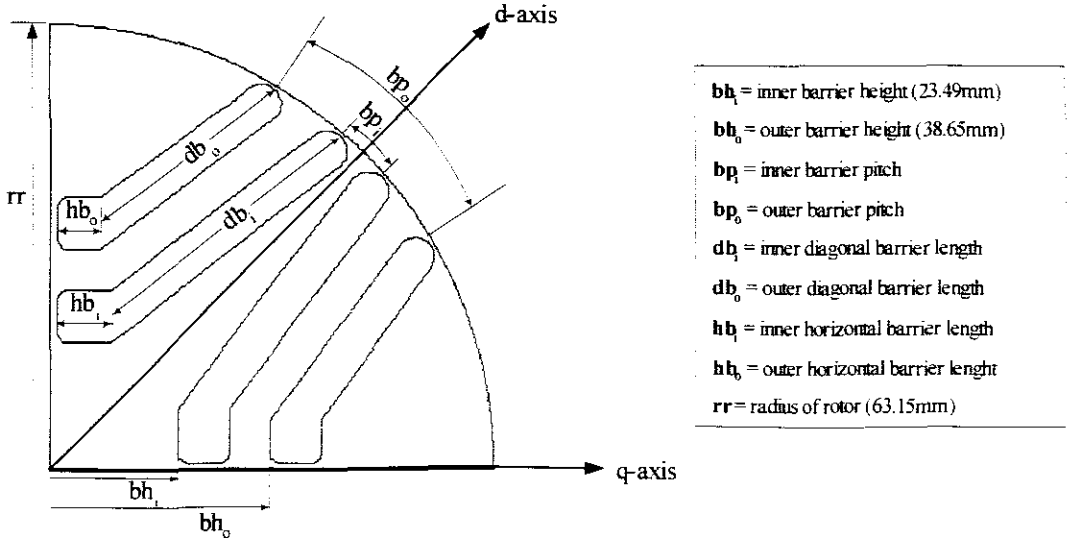

Fig 3.2.1 Cross-sectional view of double flux barrier RSM used for analysis

The height of outer horizontal flux barrier $\mathbf{hb_o}$ will be kept the same as in the previous study while the new set of barriers nearest to the d-axis will have an inner horizontal barrier height $\mathbf{hb_i}$ of 23.49mm. The width of the horizontal and diagonal part of both sets of barriers will be kept constant. With this said the possibility of new dimensional ratios have increased and will be showed accordingly. The results are shown in Fig 3.2.2 & 3.2.3 and the numerical values of all parameters are given in Table B.3.2 of Appendix B.3.

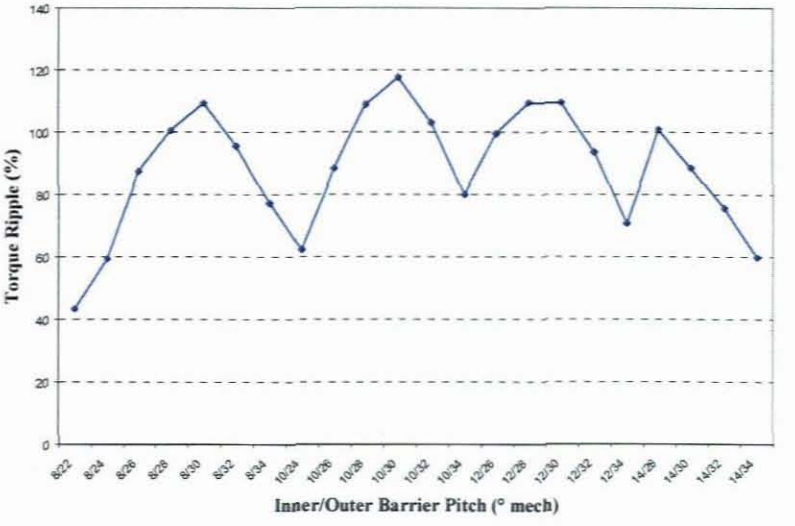

Fig 3.2.2 Torque ripple as a function of the barrier pitch

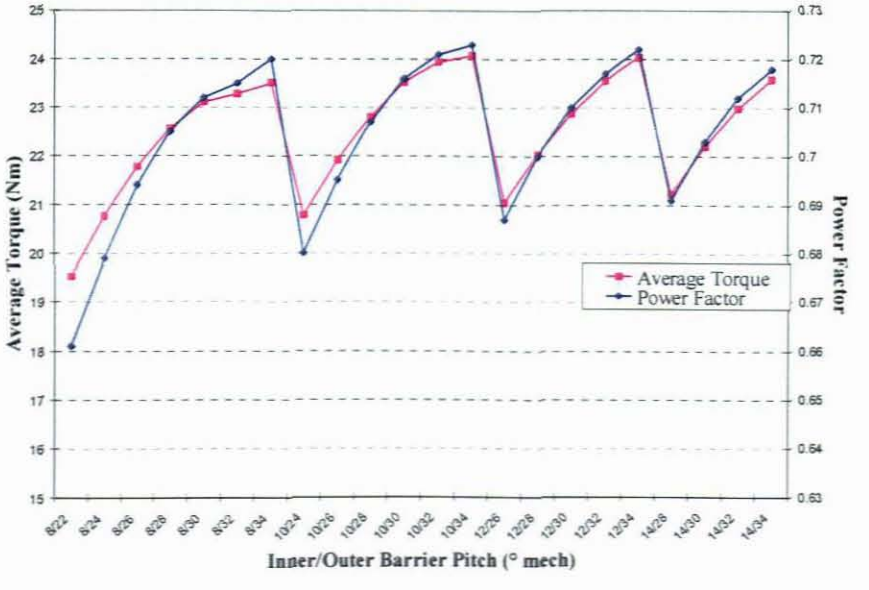

Fig 3.2.3 Average torque and power factor as a function of the barrier pitch

The introduction of an extra set of flux barriers has surely indicated positive results to that of the previous analysis. With respect to the power factor the worst performing machine in this analysis maintained a higher value than that of the best performing machine in the previous study. With the torque to power factor ratio declining from an average of 33.92 (for single barrier machines) to 31.93 (for double barrier machines) surely indicates that multiple barriers should be considered for machine optimization when a higher power

factor with same output torque is wanted. When the inner flux barrier was kept stationary and the outer one being increased the average torque increased until the outer barrier was at a maximum pitch. This indicates that maximum average torque can be obtained when the ratio between the inner and outer flux barrier $\mathbf{bp_i/bp_o}$ is at a maximum. Consequently for parameters such as the power factor $\cos\varphi$, the saliency ratio σ and the dq-inductance difference ΔL, the same statement could be made. This indicates that when machine optimization with respect to the latter is wanted only one of these parameters have to be calculated in a study to indicate the most favourable machine.

However, for optimal torque ripple the same statement as above can not be made. Not even the dimensional ratios indicated a clear pattern to how the machine will perform with a given dimension. The physical placement of the flux barriers in the rotor presented different scenarios to where the best position should be. The study indicated that when the inner flux barrier is close to the d-axis the outer barrier pitch should be at a minimum pitch to obtain lowest torque ripple. On the contrary when this inner flux barrier is moved away from the d-axis lower torque ripple will be obtained when the outer barrier is at a maximum pitch. This again signifies how difficult design specifications with respect to dimensional ratios can be when low torque ripple is the primary objective.

Further investigation indicated that the change in the d-axis inductance L_d was minimal while a more rapid reduction of q-axis inductance L_q was achieved when compared to the previous study. In both cases an increase in L_d resulted in a decline in L_q when the pitch of the flux barrier was changed. Consequently in both cases the machine which shown peak average torque was the one with the highest L_d and lowest L_q and conclusively indicate that the best performing machine (excluding lowest torque ripple) can be deduced from the dq-inductances. Although the double barrier machines indicate an improvement for average torque, designing for low torque ripple rely on the steady-state stability of these inductances, especially for L_q. Further investigation indicated that the deviation of L_d was in most cases 5 times that of L_q. The suppression of q-axis linkage fluctuations are therefore a necessity in search for low torque ripple.

The machine which presented the lowest torque ripple has been identified as the one where the inner barrier pitch was 8° and the outer one 22°. The proposed design is shown below in Fig 3.2.4

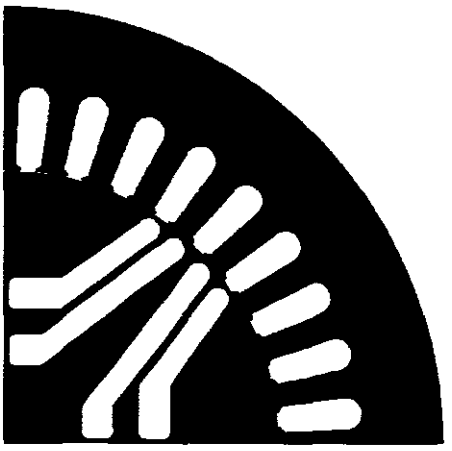

Fig 3.2.4 Cross-sectional view of best performing double flux barrier RSM

With analysis done on certain dimensional changes with respect to the flux barrier pitch the final component needs to be investigated namely the cut-outs from the original design. The geometrical dimension of the later will be discussed in the following section.

3.3 Investigating cut-outs with best flux barrier positions

In this study the two best performing machines from section 3.1 & 3.2 (BP26 and BP8/22) with respect to low torque ripple will be subjected to analysis. These machines will undergo geometrical changes by adding cut-outs to the rotor where the pitch and height of the latter will be the focus point. The geometry of the cut-outs is based on that of the original design presented in Fig 2.2.1. The cut-out angle **ca** will stay constant at 51.26° for the first part of the analysis and consequently change when the height of the cut-out is increased. The first section of this analysis will introduce the machine to a cut-out pitch **cp** which will vary from 62° to 74° in steps of 2° giving a total of 14 possible prototypes for single- and double flux barrier machines. Once the most optimum span is found the horizontal height of this cut-out **ch** will be increased from 2 mm to 12 mm in steps of 2 mm giving 12 possible prototypes. From these simulations the best performing machines for

single- and double flux barriers will be presented. A possible prototype for a single flux barrier machine is shown below in Fig 3.3.1 with given dimensions.

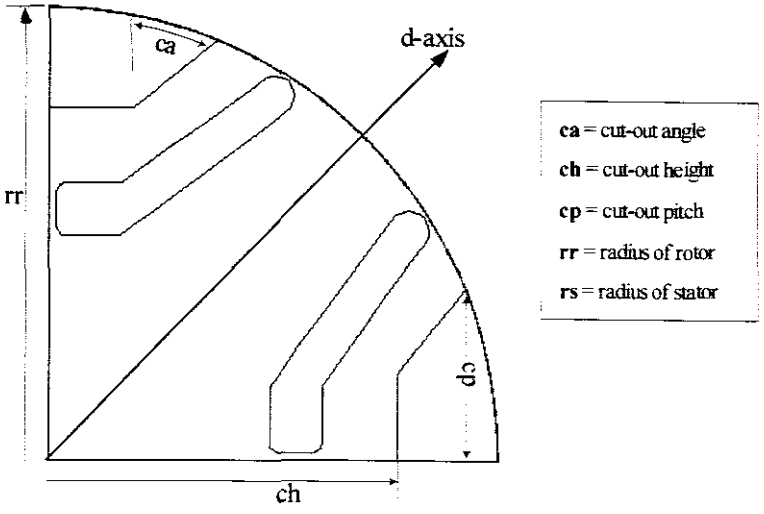

Fig 3.3.1 Cross-sectional view of a RSM with cut-outs used for analysis

For consistency the stator dimensions (Fig 3.1.1) will stay the same as in the previous analysis keeping the optimized rotor radius **rr** the same. Again a current angle of $\delta = 65°$ with the same input currents will be used in this analysis.

3.3.1 Changing the cut-out pitch

In the original design (Fig 2.2.2) the presents of cut-outs was mostly responsible for the high saliency ratio σ. According to the eq (2.1.41), the magnitude of these saliency ratios are directly accountable for the power factor magnitude of a given current angle. Most authors chooses a d-axis pole span of 0.5 but in this analysis the whole spectrum will be subject to analysis with no cut-out and flux barrier interception. The idea is to identify how these cut-outs relate to the parameters when single and double flux barriers are present in the rotor. The results are shown in Fig 3.3.2 to 3.1.4 and the numerical values of all parameters are given in Table B.3.3 of Appendix B.3.

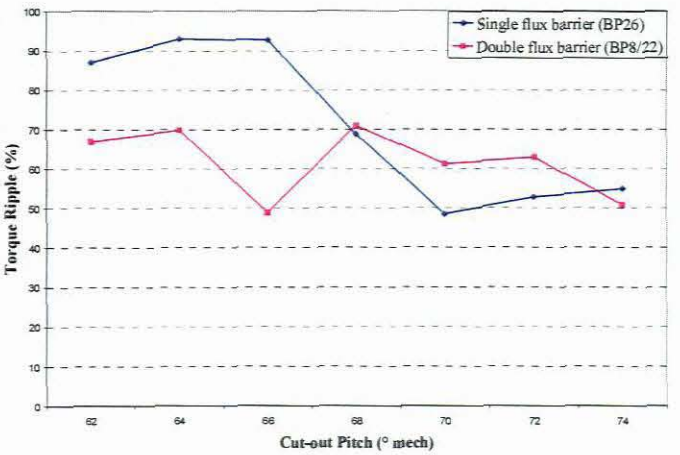

Fig 3.3.2 Torque ripple as a function of the cut-out pitch

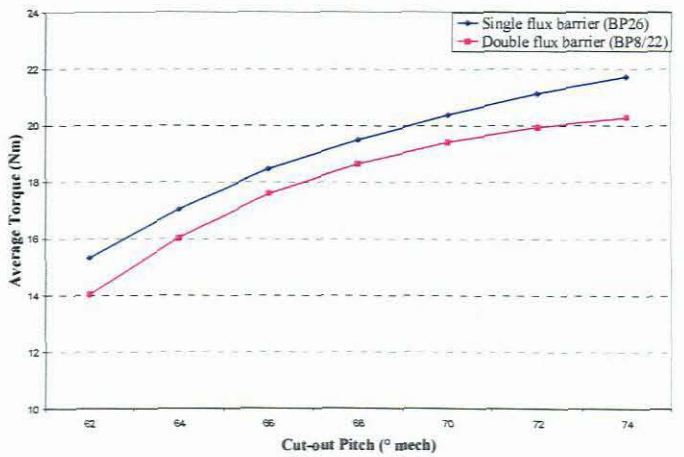

Fig 3.3.3 Average torque as a function of the cut-out pitch

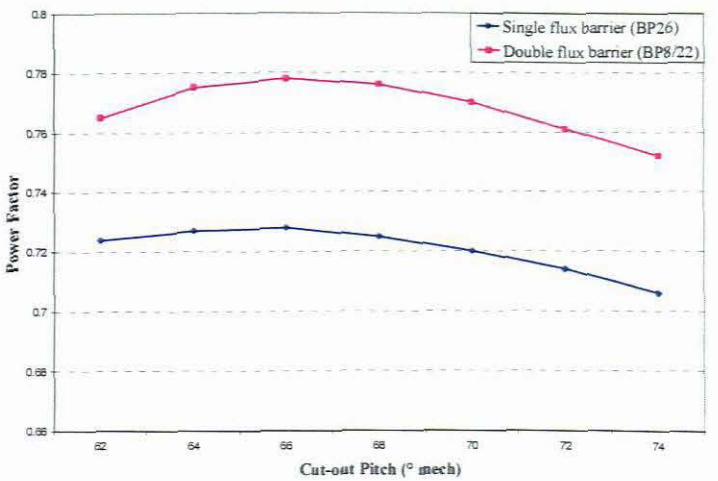

Fig 3.3.4 Power factor as a function of the cut-out pitch

From the results it is clear that the position of cut-outs in the rotor have a fundamental effect on the overall performance of the machine. The behaviour of the d- and q-axis inductance L_d and L_q showed a different pattern than in the previous analysis for single and double flux barriers. The increase in **cp** resulted in an incline for both L_d and L_q while in the previous analyses with flux barrier positional changes the magnitude of L_d increased while the one of L_q decreased. With L_d being relatively low and L_q increasing with each **cp** the average torque is sure to be suppressed.

However, the average torque seems to favour a high pitching angle of the cut-outs. In both cases the highest **cp** presented the best average torque indicating that high d-axis pole spans should be considered for machine refinement. Although both L_d and L_q amplify with the **cp** increasing, it is their rate of change with respect to each other that is of importants. The fact that the single flux barrier machine indicated a higher average torque than the double layer one was as such before the addition of cut-outs. Therefore it must not me misinterpreted that the cut-outs are necessary more influential on the torque performance of the single barrier machines.

The saliency ratio revealed a different anecdote in this analysis than in section 3.1 & 3.2. Previously an increase in saliency indicated an increase in average torque or any other parameter (except torque ripple) for that matter. The average torque to saliency ratio (T_{avg}/σ) for the single flux barrier machines was in the region of 5.03 while the one for double flux barrier machines was approximately 3.86. In this study the exact opposite is true where high saliencies are responsible for low average torques and vice versa. For the single barrier and cut-out analysis the T_{avg}/σ ratio vary from 2.39 to 3.7 while the double barrier and cut-out combination revealed a change from 1.76 to 2.63. Thus the statement can be made: When only flux barriers are present in the rotor high saliency ratios would result in high average torque while for machines with flux barriers and cut-outs the opposite is true.

With respect to the power factor $\cos\varphi$ the machines with cut-outs out performed the ones with only flux barriers in the rotor. Although an increase in **cp** resulted in a reduction of the

power factor, the rate of change was minimal and suggested that optimization with respect to cut-out can be done without affecting the latter excessively. The fact still remain that the saliency is a very important factor in the outcome of the power factor. With small powered RSMs (build for low cogging torques) having a saliency ratio hardly above 20 a power factor comparable to that of induction machines would be hard to accomplish. Fig 3.3.5 presents possible power factors for a given saliency at a current angle of $\vartheta = 65°$.

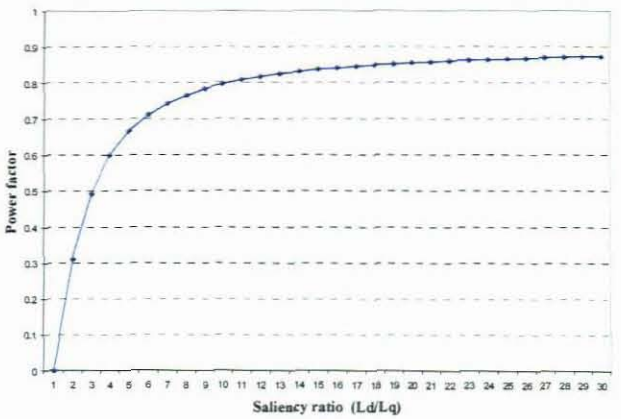

Fig 3.3.5 Power factor as a function of the saliency ratio for $\vartheta = 65°$

Although the influence of saliency seems extraordinary, the influence of the magnitude of the input currents and the current angle should not be neglected. This however will be discussed in the following chapter.

With the increased torque ripple compared to the rotor with only flux barriers, the idea of cut-outs does not seem to be a good approach to torque ripple reduction. With an increasing **cp** the fluctuating torque ripple indicates its sensitivity to the actual position of cut-out itself. Although the torque fluctuates with different pitches, there tend to be a decay towards higher pitching angles suggesting that the size of the cut-out geometry plays a role in the latter. With the increasing L_q for higher pitching angles imply that the stability of the q-axis linkage has increased and consequently indicate that cut-outs itself should not necessarily be neglected (Table B.3.3). Therefore the cut-outs would be subjected to a geometrical transformation where the horizontal height **ch** would be the object of transformation and is explained next.

3.3.2 Changing the height of optimized cut-out pitch

The previous section suggests that the position and geometry of the cut-out plays an enormous role in the behaviour of the parameters. While broad d-axis pole spans suggest good saliency and consequently high power factor a lower pole span indicate high average torque and low torque ripple. Accordingly the latter has been chosen for optimization where the geometrical dimensions of the cut-out are changed by increasing the cut-out height **ch** and therefore reducing the saliency. The two machines subject to analysis will be the single flux barrier machine with a cut-out pitch of 70° and the double flux barrier machine with a pitch of 66°. The results are indicated in Fig 3.3.6 to 3.3.8 with actual values of all parameters indicated in Table B.3.4 of Appendix B.3.

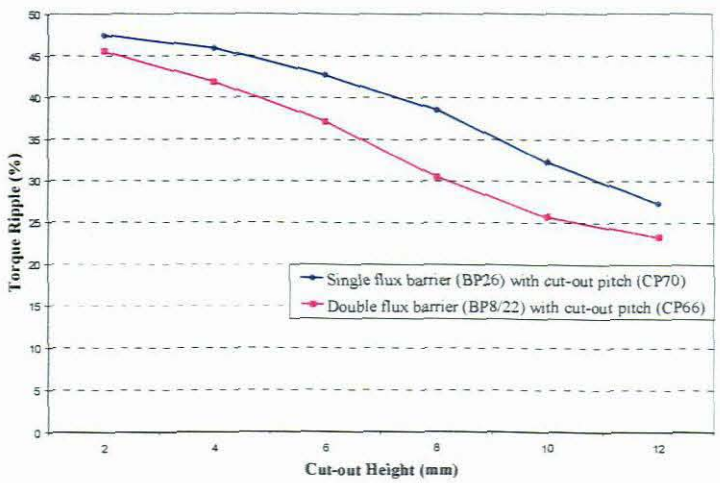

Fig 3.3.6 Torque ripple as a function of the cut-out height

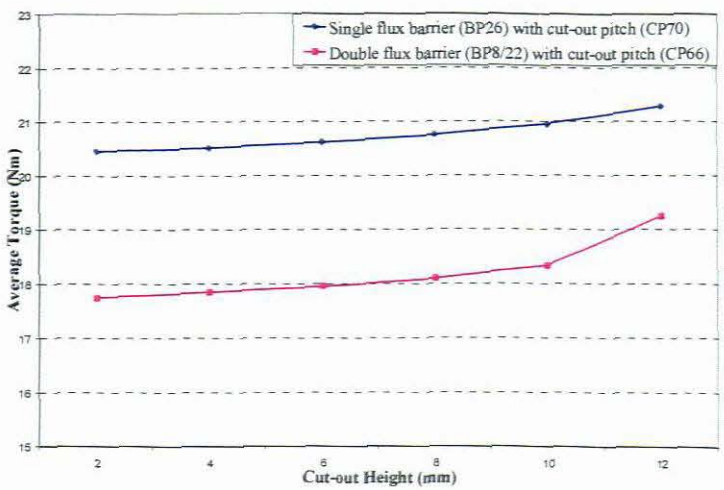

Fig 3.3.7 Average torque as a function of the cut-out height

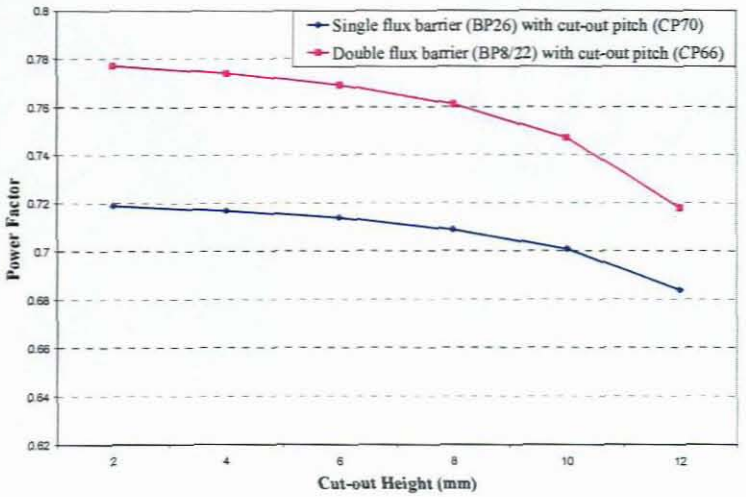

Fig 3.3.8 Power factor as a function of the cut-out height

In this analysis the cut-out has gone through a vast geometrical change. The increase of the cut-out height has surely presented its advantages and disadvantages over the previous analysis. The torque ripple was significantly deduced where the latter dropped almost by half between the minimum and maximum **ch**. With the increase of average torque for the single- and double flux barrier machines being about 4% and 6% indicate that the increase of the **ch** was a good approach.

This suggests that the ratio of cut-out height to rotor radius **ch/rr** should be as high as possible and considered essential when rotor optimization with respect to low torque ripple and high average torque is wanted (Fig 3.3.6 & 3.6.7).

With the saliency decreasing, the power factor could unfortunately not match the high values in the previous analysis. However with the new improved cut-out geometry the obtained power factor was still higher for each machine when only single- and double flux barriers was present in the rotor. The two best performing machines with respect to low torque have been identified and shown in Fig 3.3.9.

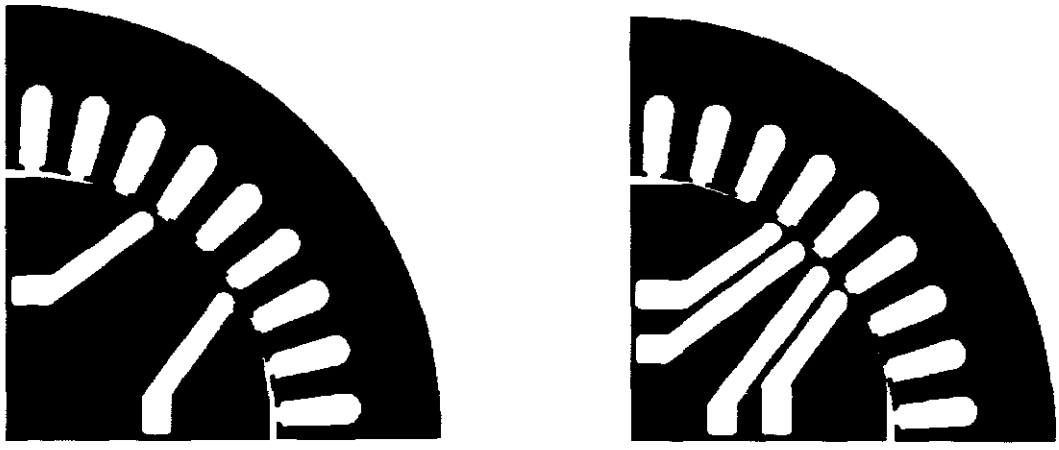

a) SBP26 with CO70 and CH12 b) SBP8/22 with CO66 and CH12

Fig 3.3.9 Cross-sectional view of best performing single- and double flux barrier RSMs with cut-outs

3.4 Summary of findings

The parameters have surely indicated that the performance of an RSM can be influenced in many ways when geometrical changes were made to the rotor. Each section indicated different results and contributed to the understanding of how such a design should be approached.

In the first analysis for machines with only a single set of flux barrier present in the rotor the torque ripple seems to fluctuate between the different barrier pitches **bp**. With the highest cogging torques achieved at 10°, 20° and 30° and the lowest values in between these maxims (14° and 26°) indicates that the pitch of the barriers have an immense influence on the steady state stability of the q-inductance. This also suggests that the actual ratio of **bp** should not coincide with slot pitches **sp** when low torque ripple is wanted. With the latter changing with up to 34% between different barrier pitches indicate that smaller increments should be considered for future optimization. The change of **bp** with respect to the other parameters such as T_{avg}, ΔL, $\cos\varphi$ and σ revealed a different story. The results indicate that these parameters behave arithmetically the same and that the optimization can be obtained for the same **bp**. The optimum **bp** for these parameters was at 24° and indicated the physical position of these barriers should be more or less between the d- and q-axis for optimum results.

In the second analysis the behaviour of machines with double sets of flux barriers revealed different results. With the inner barrier pitch $\mathbf{bp_i}$ kept stationary and the outer barrier pitch $\mathbf{bp_o}$ increased, lower torque ripple seems to be achieved where the distance between these barriers is either at a minimum or a maximum i.e. the inner flux barriers close to the d-axis suggests that $\mathbf{bp_o}$ should be at a minimum, while for $\mathbf{bp_i}$ being increased $\mathbf{bp_o}$ should be at a maximum. This illustrates that the ratio of the barrier pitches $\mathbf{bp_i/bp_o}$ indicates no clear tendency of what barrier pitch combination should be used (Fig 3.2.2). The same does not hold true for the average torque and the power factor. In this case the distance between the inner and outer flux barrier should be at a maximum to obtain optimized results. The addition of the extra set of flux barriers improved the overall average torque and power factor compared with single flux barrier machines and should be considered a design improvement if these two quantities are wanted.

The third analysis combined the best performing machines from section 3.1 and 3.2 with respect to low torque ripple and inserted cut-outs to the rotor with geometries similar to that of the original design. With the pitch of the cut-out **cp** being changed, the torque ripple again fluctuated between minimum and maximum angles. The machines' overall performance (except for power factor and saliency) could not be compared to that of only flux barriers present and suggested that cut-outs was not a good approach to counter torque ripple. With an increased air-gap length the saliency increased dramatically which resulted in an incline of the power factor. However with a higher **cp** the torque ripple tend to decay while the average torque increased indicated that a smaller cut-out geometry would be more appropriate. Therefore the height of the cut-out **ch** was increased to a maximum and improved results were obtained. For the first time optimization with respect to low torque ripple and high average torque was achieved for the same dimensions. Although with the decreased air-gap length resulting in a decreased saliency and power factor, the torque ripple decreased significantly while the average torque increased. In each case (single and double flux barrier machines) the maximum **ch** presented the best results to the latter and out performed the machines with only flux barriers present in the rotor.

4. Changing Parameters of the Stator

The focus point of this Chapter is to keep stator geometrical changes to a minimum to keep the structure of the original stator frame the same therefore presenting the possibility of interchangeable rotors for existing induction motors of this given power range. The introduction of magnetic wedges will be discussed, especially die physical height of the wedge itself, and conclusions drawn on how they affect the parameters of an RSM. The top performing machines from Chapter 3 will be subject to analysis with current angle optimization for both machines with- or without magnetic wedges. Consequently the physical nature and behaviour of the current angle have to be understood first and is described next.

4.1 Influence of current angle

The current angle (given in electrical degrees) is one of the most important input variables when machine optimization is required. Numerous research has been conducted towards finding the optimum current angle for RSMs and consequently different results where published. Some has found that the optimum angle must be between $45° < \delta < 90°$ while Kamper (1995) shows that the current angle for maximum torque-per-ampere must be between 60° and 65°. Mostly only mathematical derivations for these angles was publishes which made the understanding of the physical results slightly complex. Vagati (1992) said that when machine optimization is wanted the machine as a whole have to be 'revamped' which justified a further investigation in this matter. The idea of this study is to see how the average torque, torque ripple and power factor change with different current angles and present findings.

Before such an analysis can be conducted two key parameters should be identified namely the position of the rotor d-axis and the location of the current space phasor I_s. The physical location of the current space phasor relies on the nature of the winding distribution and the time displacement of the input currents while the rotor can be shifted physically. In this analysis a 7/9 chorded winding distribution was used while the red phase was chosen as reference. This caused the current space phasor to lay between slot 5 and 6 for $\omega t = 0°$ and can be seen below in Fig 4.1.1

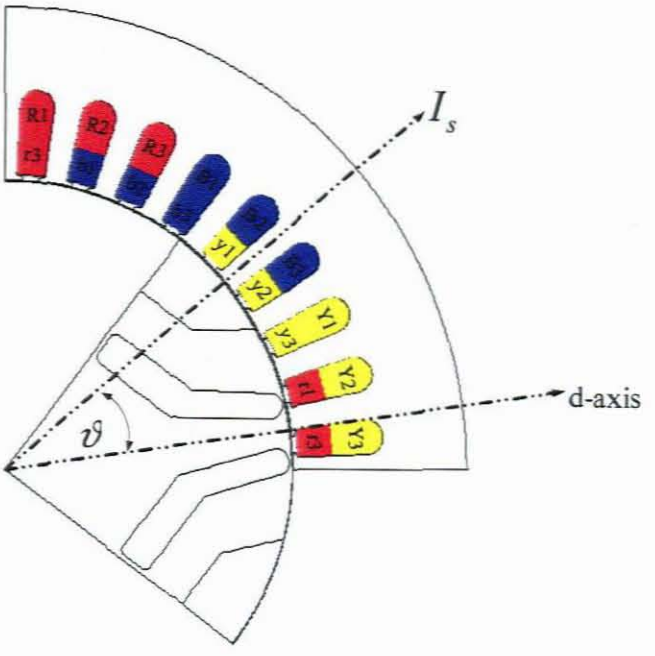

Fig 4.1.1 Physical position of the current angle

Before analysis can be conducted the given range of different current angles should be decided on. Let us consider the equation for torque (eq 3.2.1) given by

$$T = \frac{3}{2} p \cdot \Delta L \cdot I_S \sin(2\vartheta) \tag{4.1.1}$$

According to this the current angle is an important factor for the development of instantaneous torque. The equation suggests that a current angle of 0°, where the d-axis of the rotor aligns with the axis of the current space phasor in the stator, the developed torque would be zero. When this angle is shifted to 90°, meaning the q-axis of the rotor aligns the current space phasor of the stator, again the torque would be zero. This indicates that between these minima's a maximum must occur. Although this equation suggest for a current angle of 45° maximum torque would be obtained, the value of ΔL, from L_d and L_q, is very much a function of this angle. Therefore the range of the current was chosen between 0° and 90° elec. and will be simulated in steps of 1° to present accurate results. The two extreme positions are indicated in Fig 4.1.2 below.

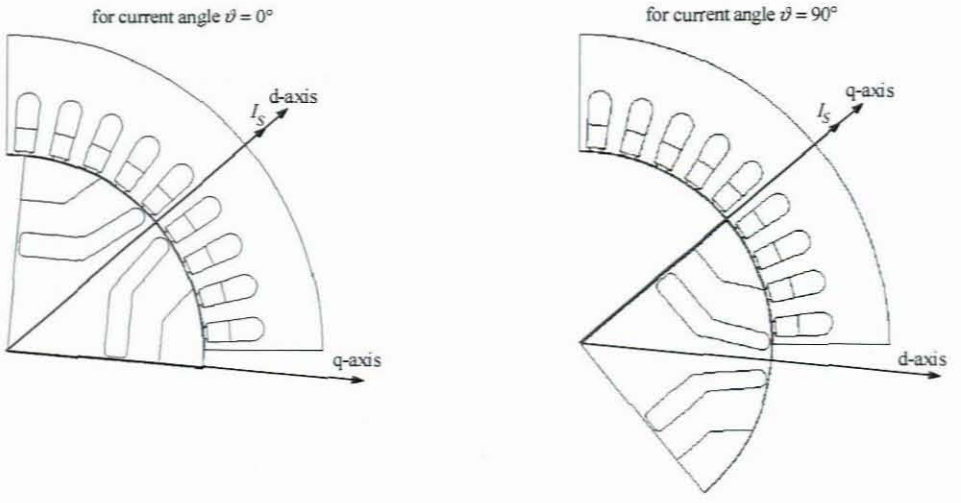

Fig 4.1.2 Rotor starting angles for maximum and minimum current angles if red phase was chosen as reference

Apart from the fact that eq (4.1.1) suggests that these current angles would produce no torque, the physical picture behind this equation should be clear. Let us consider the magnetic field distribution of these current angles for a given point in time as shown in Fig 4.1.3.

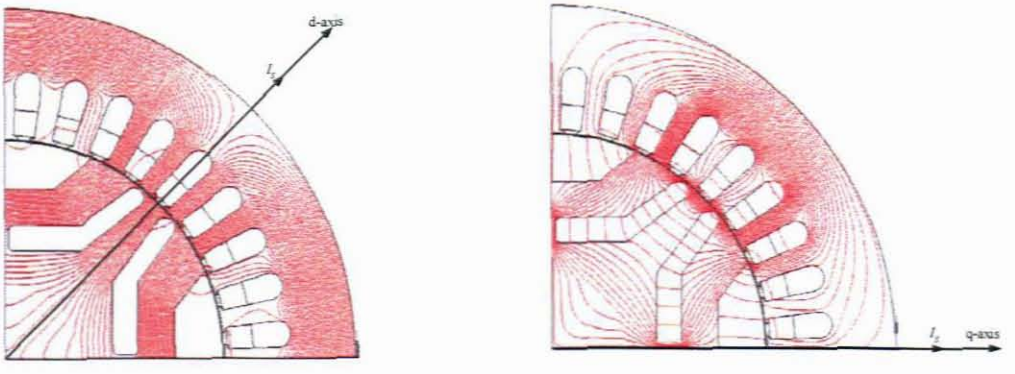

a) D-field where $\vartheta = 0°$ b) Q-field where $\vartheta = 90°$

Fig 4.1.3 D-and Q-magnetic field for two extreme current angles at a given point in time

It can be seen that there is a distinct difference between the patterns of the magnetic field distribution for these two situations. The D-field shows a clean flow of magnetic flux between the centre of the flux barrier in the direction of the d-axis while the Q-field indicates a saturated flow of flux perpendicular to the flux barriers and cut-outs in the

direction of the q-axis. However, in these types of RSMs rotor symmetry is obtained when a mirror image is taken from either the rotor d- or q-axis. In both cases the magnetic field was symmetrically distributed throughout the machine. The question is why does such a symmetrical field not produce any torque? Since the tangential force distribution was responsible for rotor movement, both D- and Q-fields were subjected to analysis for force patterns in the air-gap. The results are indicated below in Fig 4.1.4 & 4.1.5.

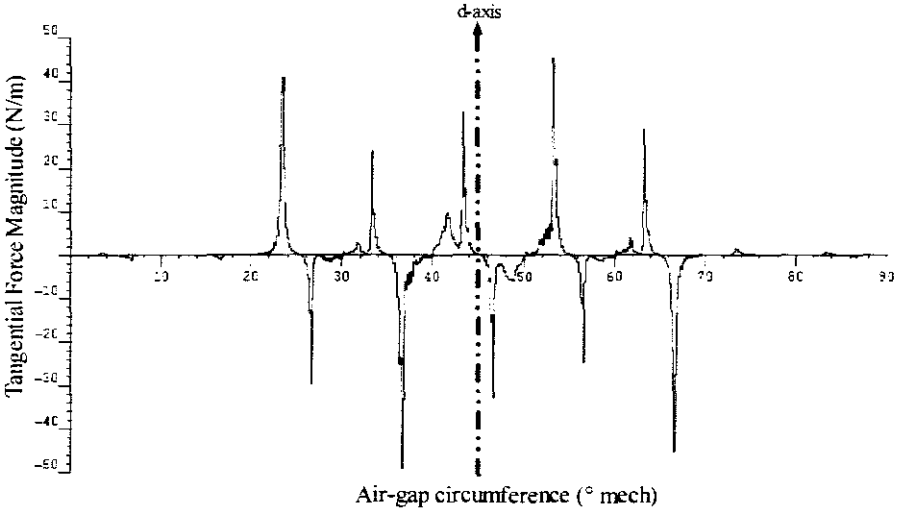

Fig 4.1.4 Tangential force distribution in the middle of the air-gap for the D-field

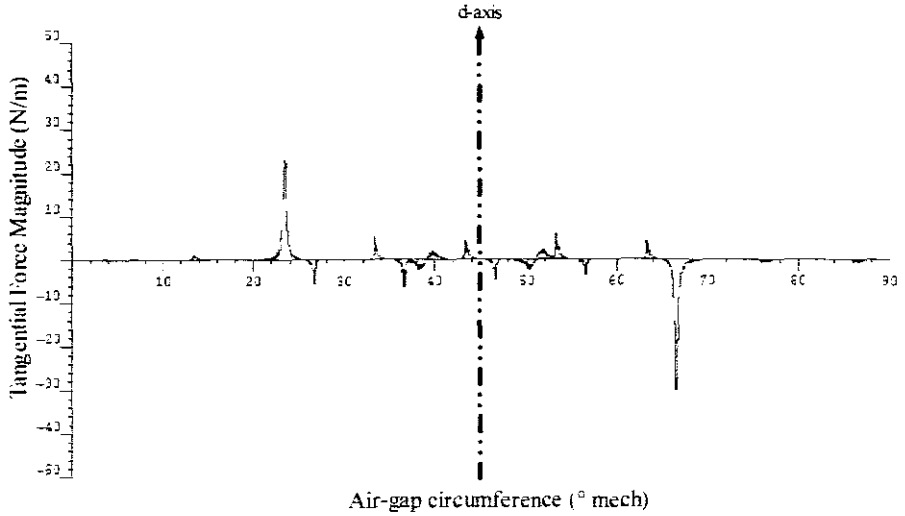

Fig 4.1.5 Tangential force distribution in the middle of the air-gap for the Q-field

It can be seen in both Fig 4.1.4 & 4.1.5 that the actual distribution of the tangential force is both a periodical and symmetrical mirror image, with d-axis as reference, of each other.

This indicates that when a force on the rotor circumference at a certain point is experienced, the same force, but opposite in direction will, occur on the opposite side of the reference axis. Due to the slotted geometry of the RSM these force patterns will change, but they will always cancel each other out independent of rotor position.

The best performing machines from chapter 3 with respect to lowest torque ripple was subjected to current angle transformation. For easy machine identification the following statements are made.

i. Machine 1: Single set of flux barriers present in rotor with barrier pitch of 26° and no cut-outs.
ii. Machine 2: Double set of flux barriers present in rotor where inner flux barrier pitch was 8° and outer pitch 22° with no cut-outs.
iii. Machine 3: Single set of flux barriers with 26° barrier pitch where cut-outs have a pitch of 70° and height of 12mm.
iv. Machine 4: Double set of flux barriers with inner and outer pitch being 8° and 22° where cut-outs have a pitch of 66° and height of 12mm.

Although numerous research have been conducted towards current angle optimization, the fact that torque ripple has only been a topic mentioned recently justified the study. In this analysis the behaviour of machines with different flux barrier and cut-out geometries will be explained and conclusions drawn for optimum current angles. It must be made clear that the stator geometries of each machine is the same and dimensional geometries is given in Fig 2.2.2 of section 2.2. The current angle will be presented in electrical degrees where 2° electrical = 1° mechanical. The results are shown in Fig 4.1.6 to 4.1.8.

Machine 1: Bearing torque ripple in mind, this single set flux barrier machine reacted remarkably different than the other machines. With an increased δ the torque ripple reduced exponentially to roughly 10° where an equilibrium was reached. This stability continued until δ = 70° was reached where the torque ripple inclined exponentially. This indicates that such a machine is open to optimization towards other parameters such as average torque and power factor provided that their optimized angles fall between the

equilibrium range. With the absolute minimum T_{ripple} of 36.21% occurring at 45° indicate that single flux barrier machines favour the current space phasor I_S to be exactly between the d- and q-axis. The increase in T_{avg} occurred fairly linear towards the peak of 22.26 Nm at 57° and compared well against the other machines. The power factor $\cos\varphi$ on the other hand did not contrasted a good performance and was only able to reach a maximum of 0.62 at ϑ = 66° indicating that the saliency ratio σ of these machines was relatively poor.

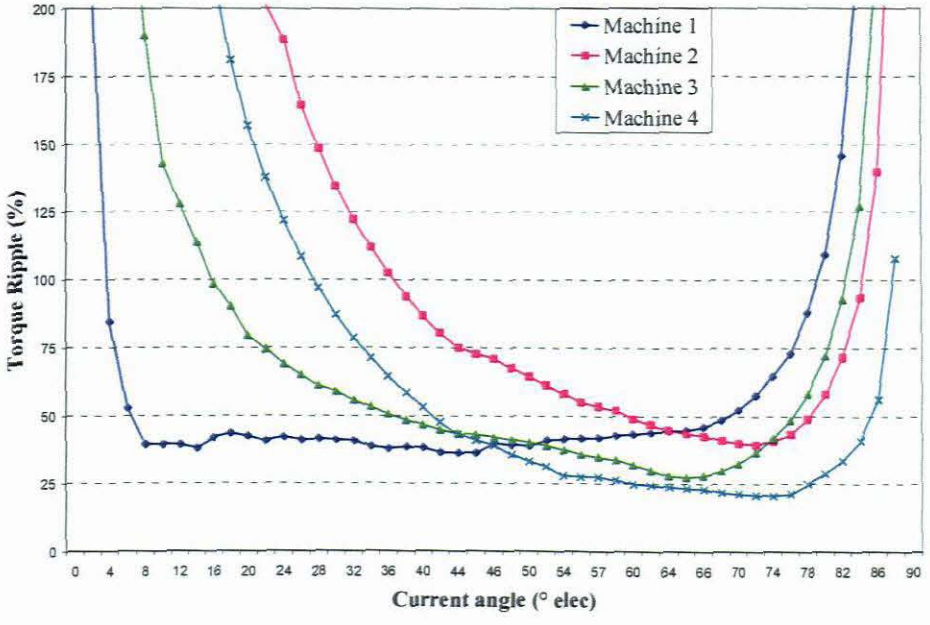

Fig 4.1.6 Torque ripple for a given current angle

Machine 2: With double sets of flux barriers in the rotor the torque ripple surely behave different compared to that of the previous analysis. Although the minimum of 39.42% compared reasonability the same against the single flux barrier machine, the angle (72°) at which the minimum was obtained was very different. The study indicated that these machines do not favour I_S being in the region closest to the d-axis but rather near the q-axis. With dramatic incline and decline of T_{ripple} for given ϑ indicate that optimization for all parameters would be hard to achieve. With maximum T_{avg} of 20.79 Nm occurring at $\vartheta = 56°$ indicate that maximum torque-per-ampere for single and double flux barrier machines can be achieved with the same current angle. With the overall $\cos\varphi$ being higher

and consequently a higher σ than in the previous analysis, suggest that the number of flux barriers in the rotor have a direct affect on the latter. Compared to the other machines with respect to the parameters, the overall impression of these machines did not seem good. However, from the results in Chapter 3, the double flux barrier machines produced the highest T_{avg}, an improved $\cos\varphi$ towards the single flux barrier machine and a reasonable T_{ripple}. The fact the most optimum machine, with respect to lowest torque ripple, was taken from this range does not indicate that these machine are incapable of delivering good results for high T_{avg} and $\cos\varphi$. This analysis only indicates that machines do not produce low T_{ripple} when compared to the other machines.

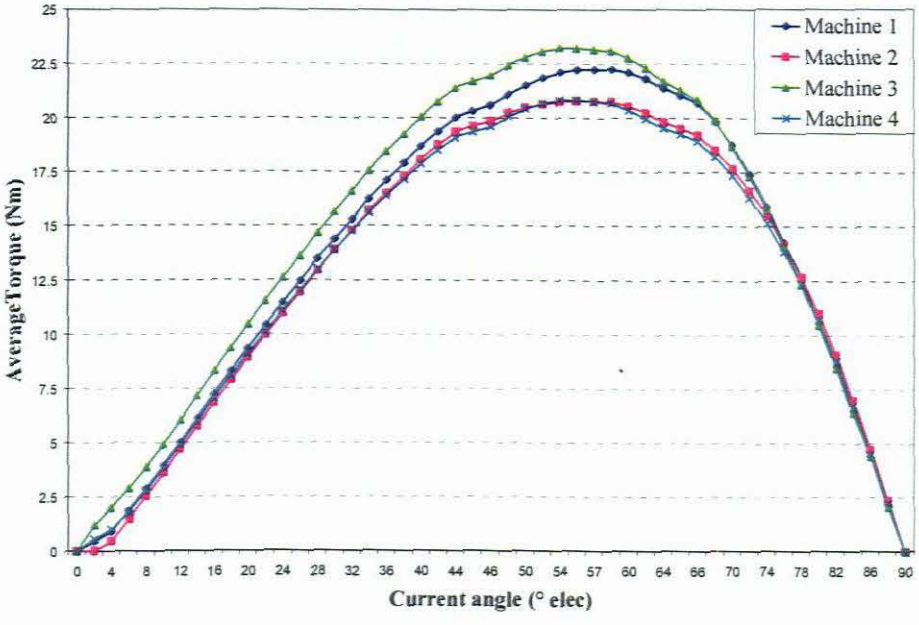

Fig 4.1.7 Average torque for a given current angle

Machine 3: With the introduction of optimized cut-outs to *Machine 1* an overall improvement was achieved for the given parameters. Compared to the single flux barrier machine, the T_{ripple} of this machine did not compare good in the range where $0° \geq \vartheta \geq 51°$. This was due to the overall good stability that the single barrier machine presented. However, beyond this range where $\vartheta \geq 51°$ the T_{ripple} did improved and declined to 27.33% at 65° indicating that cut-outs was a good approach to lower the latter. An overall

improved T_{avg} was achieved with a maximum of 23.22 Nm at 54° indicating a shift of 3° in ϑ for optimized results. With the geometry of the cut-out increasing the air-gap length and consequently the σ, an improved $\cos\varphi$ of roughly 10% was achieved. The cut-outs surely presented an improved performance towards that of single and double flux barrier machines thus indicating that this geometrical dimension should not be neglected in rotor design for RSMs in this power range.

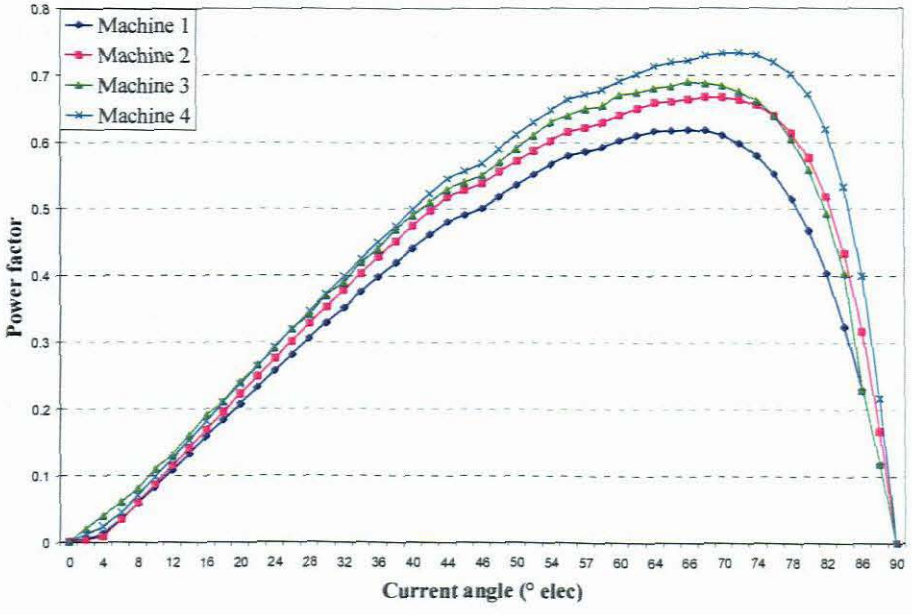

Fig 4.1.8 Power factor for a given current angle

Machine 4: With the introduction of optimized cut-outs to *Machine 2* again an overall improvement was achieved for the given parameters. With *Machine 2* being very sensitive to the value of ϕ the opportunity presented itself to improve on the overall performance of T_{ripple}. The latter improved compared to *Machine 2* and indicated an optimization of between 32% and 60% for $0° \geq \vartheta \geq 90°$. The most optimum results were found at 74° and had a ripple magnitude of 22.92% indicating the machine having the lowest T_{ripple} compared to the *Machine 1, 2 & 3*. With the optimum angle being close to that of *Machine 2* indicates that the double flux barriers influence the optimum position for ϑ more than the cut-outs. The T_{avg}, however, did not compare well against the other machines and again indicate that double flux barriers influence this parameter in magnitude more than cut-outs.

With the maximum value of 20.84 Nm obtained at 54°, which was the same as for *Machine 3*, indicate that the cut-outs was responsible for the optimized current angle. The $\cos\varphi$ of this machine was the highest compared to the other machines and indicate that both cut-outs and double flux barriers are essential for the optimization of this parameter. The maximum power factor of 0.73 occurred at angle of 72°.

The significance of current angle optimization has been presented and surely indicated the importants of it. With an original ϑ being 65° chosen for the analysis in Chapter 3, indicated that the approach was a good choice since most of the parameters favoured the current space phasor I_S to be closer to the q-axis. However, the study did indicate that presenting beforehand an optimal current angle for any given parameter depends on the nature of the rotor geometry and its dimensional ratios. The study indicated that maximizing all parameters at the same time would not be possible. The optimum current angle range for each parameter is given below

- Minimum torque ripple: $45° \geq \vartheta \geq 74°$
- Maximum average torque: $54° \geq \vartheta \geq 57°$
- Maximum power factor: $66° \geq \vartheta \geq 70°$

The optimized current angle spectrum for low T_{ripple} suggests its sensitivity to machine geometry. This range of optimum angles for the latter can be reduced to $65° \geq \vartheta \geq 74°$ if single flux barriers (without cut-out) in the rotor were not to be modelled. These machines clearly indicate that lowest torque ripple would always appear where the current space phasor I_S lies exactly between the d- and q-axis. The rest of the parameters (T_{avg} and $\cos\varphi$) signified a more narrow spectrum for optimized current angles, even for single flux barrier machines, indicating its unresponsiveness to rotor geometry. Furthermore optimized machines with appropriate current angles have been identified for given parameters. The next step will be to change the geometry of the stator by means of magnetic wedges and will be explained in the next section.

4.2 Magnetic wedges

From theory it is known that a machine with closed slots will produce little or no torque, but the geometry of the wedge itself has not been discussed with respect to the latter. The use of magnetic wedges has not been a topic investigated for many years, especially it's affect on torque ripple, and only recently made its introduction. Voss (2002) did an analysis on the effect of magnetic wedges where the magnetic material of the rotor and stator was assumed linear. Later Hanekom (2004) contributed with his findings on how single layer winding machines modelled with non linear material react to the closure of the slots by means of magnetic wedges. Both concluded that the use of these wedges present positive results with respect to torque ripple reduction. The geometry of the wedge can be seen in Fig 4.2.1

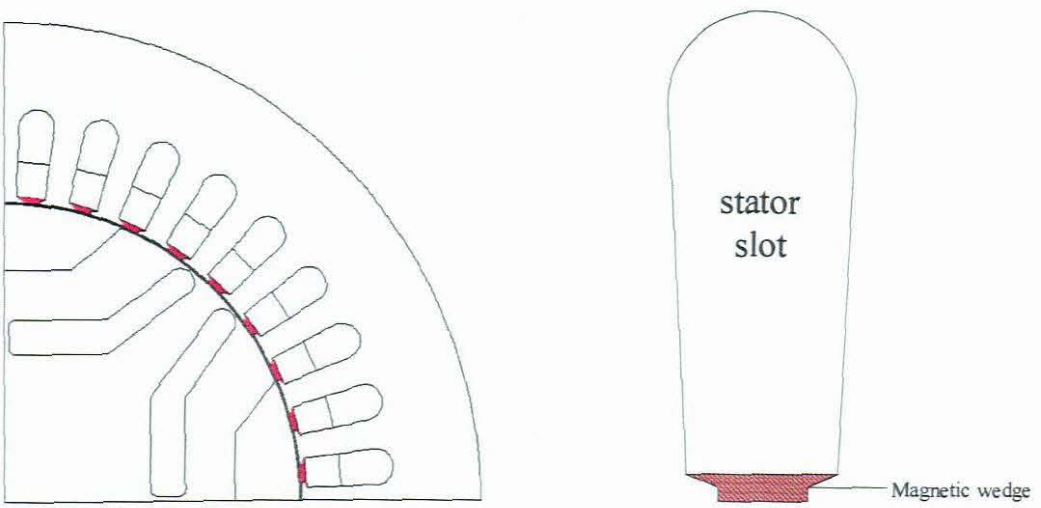

Fig 4.2.1 Stator slot with magnetic wedge

The author therefore wishes to introduce the use of magnetic wedges, with permeability the same as that of the back iron, in the slot region to make the air-gap magnetically smooth.

4.2.1 Introduction of magnetic wedges

The magnetic wedges are used to make the air-gap permeance function more uniform since more flux is led under the stator opening than without wedges. This reduces the change of radial forces on the stator circumference between rotor movements. Choosing the material of the wedge is a question of optimization between the power factor of the machine and the

harmonic losses on the rotor surfaces which reduces the average torque (Haataja 2003). The question is why it has a negative effect on these parameters? Let us consider the flux distribution in an electrical machine as seen in Fig 4.2.1.

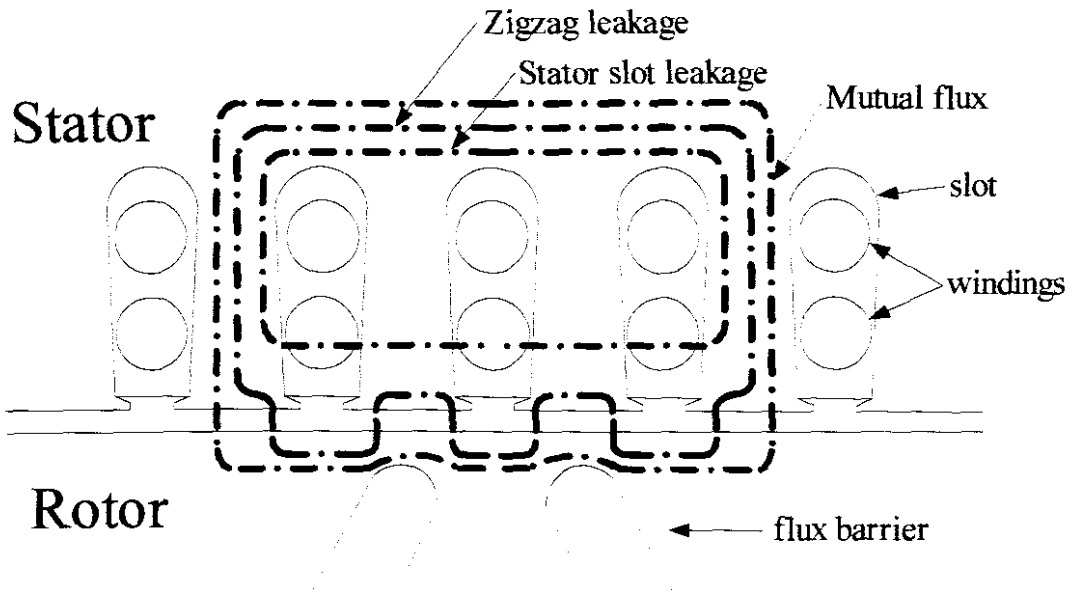

Fig 4.2.2 Different fluxes produced by the windings in an RSM

It can be seen that the two fluxes responsible for rotor movement are the zigzag leakage flux (also known as differential leakage flux) and the mutual flux. If the slots where to be closed both fluxes would be force to take this path of lower reluctance. With this flux passing rather through the stator and not through the rotor would surely affect the outcome of the output torque. If the height of the wedges was to be increased, the magnitude of the mutual flux, passing through the rotor, would also be reduced and again reducing the torque. However the aim of this study is to reduce the torque ripple of the RSM, but keeping in mind the change of the average torque and power factor. Therefore the machines used in Chapter 3 would be subject to stator transformation by addition of magnetic wedges to compare how these wedges affect the parameters. Although improved current angles per parameter have been investigated, for consistency an angle of $\psi = 65°$ will be chosen for this analysis. The results are indicted as shown in Fig 4.2.3 to 4.2.11.

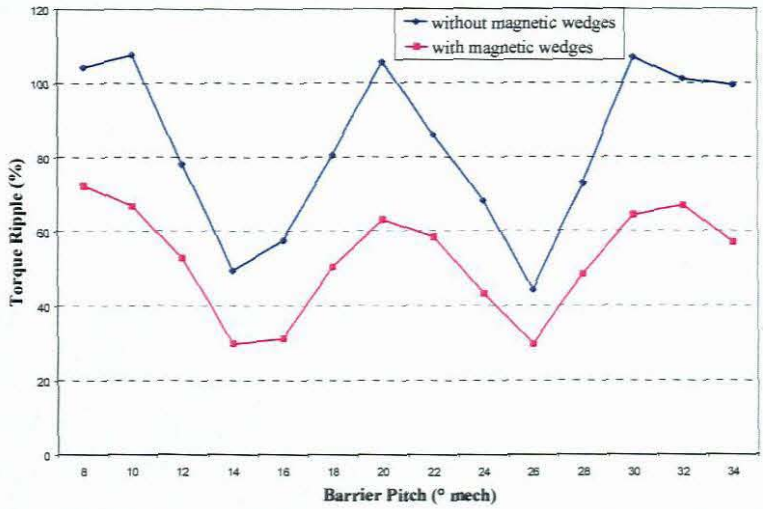

Fig 4.2.3 Torque ripple for single flux barrier machines with- and without magnetic wedges

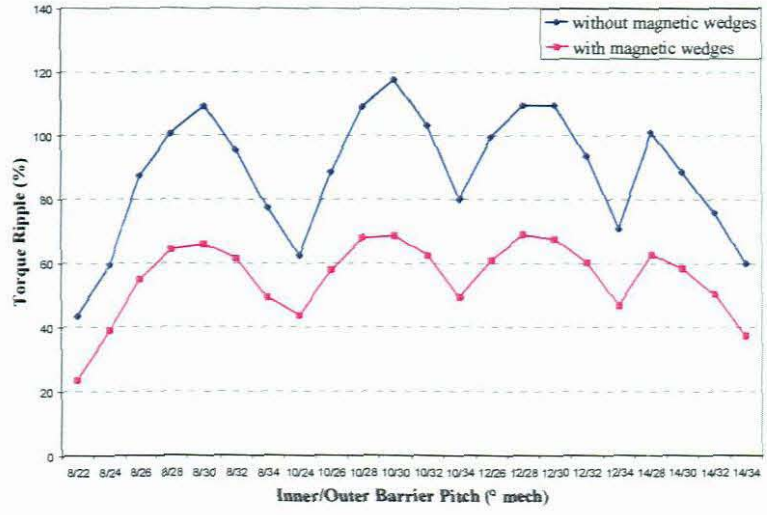

Fig 4.2.4 Torque ripple for double flux barrier machines with- and without magnetic wedges

Torque ripple: It can be seen (Fig 4.2.3 & 4.2.4) that the introduction of these magnetic wedges surely presented positive results to the reduction of torque ripple for both single- and double flux barrier machines. For every flux barrier pitch, the magnetic wedges out perform semi-closed slots with fluctuations between different barrier pitches being the same in each case study. For the single flux barrier machine T_{ripple} was reduced between 30.7% and 45.8% while the reduction in the double barrier machines were between 30%

and 46.2%. Further investigation indicated that the increase of L_q (percentage wise) was more than L_d for machines with magnetic wedges compared to semi-closed slots per given barrier pitch as seen below.

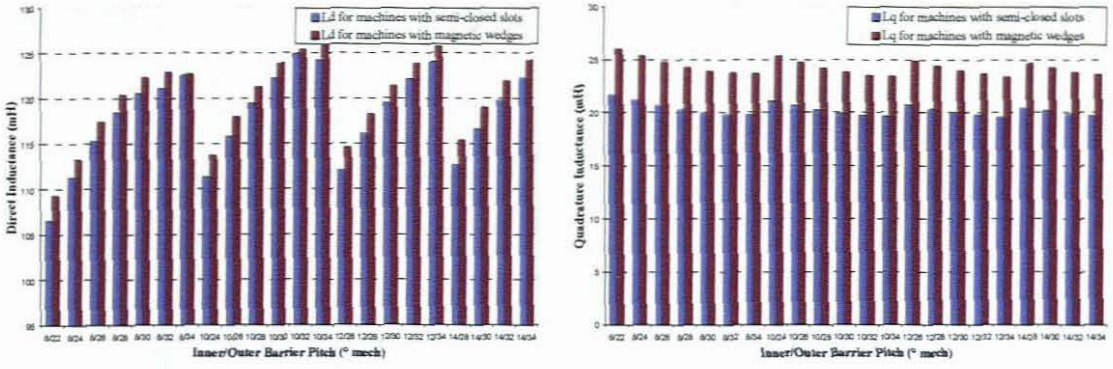

Fig 4.2.5 Direct –and quadrature inductance for machines with semi-closed slots and magnetic wedges as a function of the barrier pitch

However, the stability (change in magnitude between minimum and maximum) of these individual inductances did not change. The question would be why a decline in torque ripple was achieved? Taking equation (2.3.1) into consideration the stability of the flux linkage, which is the variable in the calculation of L_d and L_q, can be calculated the same and given by

$$\lambda_{ripple} = \frac{\lambda_{\max} - \lambda_{\min}}{\lambda_{avg}} \tag{4.2.1}$$

According to analysis the change in magnitude between $\lambda_{\min}$ and $\lambda_{\max}$ for machines with semi-closed and closed slots were in most cases the same. With λ_{avg} being higher for machines with wedges surely indicate that a reduction in λ_{ripple} was achieved. With flux linkages being smoother, percentage wise, the change fluctuating torque would certainly be reduced. The machines with magnetic wedges which presented the best results were the same as those with semi-closed slots namely 26° (reduced from 44.3% to 29.7%) for single- and 8°/22° (reduced from 43.5% to 23.4%) for double flux barrier machines. Therefore the statement can be made that machine optimization for different flux barrier

pitches, and only flux barriers present in the rotor, are the same for closed or semi-closed slots when low torque ripple is desired.

Average Torque: With magnetic wedges added to the stator slots the average torque decayed in both, single and double flux barrier machines for all barrier pitches as seen in Fig 4.2.6 & 4.2.7.

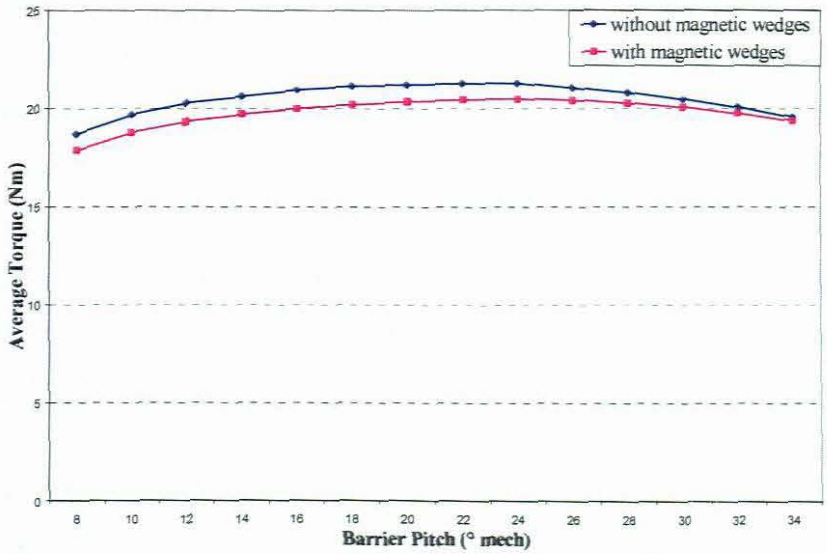

Fig 4.2.6 Average torque for single flux barrier machines with- and without magnetic wedges

Fig 4.2.7 Average torque for double flux barrier machines with- and without magnetic wedges

Due to the increase of L_q, and L_d being minor with magnetic wedges, the inductance difference ΔL was affected negatively and consequently reduced the average torque. This decay of T_{avg} was minimal and varied for single flux barrier machines between 0.8% and 4.7% while for double barrier machines the variation were between 1.8% and 3.3%. With the vast reduction of T_{ripple} for both types of machines the reduction of the average torque can be considered negligible (for these medium power machines) when machine optimization with respect to these parameters where to be considered. Again the machines with magnetic wedges which presented the best T_{avg} were the same as those with semi-closed slots namely 24° (reduced from 21.27 Nm to 20.48 Nm) for single- and 10°/34° (reduced from 24.07 Nm to 23.53 Nm) for double flux barrier machines. Therefore the statement can be made that machine optimization for different flux barrier pitches, and only flux barriers present in the rotor, are the same for closed or semi-closed slots when high average torque is desired.

Power factor: Although minimization of torque ripple, with minor changes to the average torque, was achieved that fact that the reduction of the power factor for both single- and double barrier machines was a reality (Fig 4.2.8 & 4.2.9).

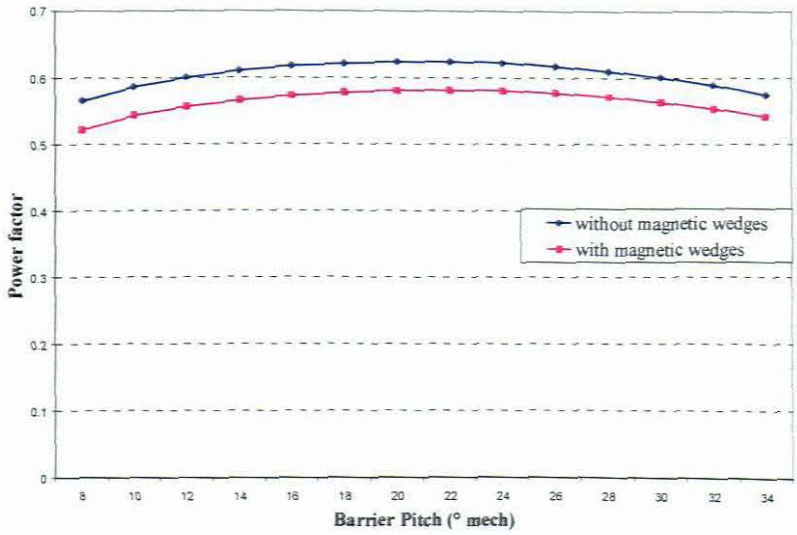

Fig 4.2.8 Power factor for single flux barrier machines with- and without magnetic wedges

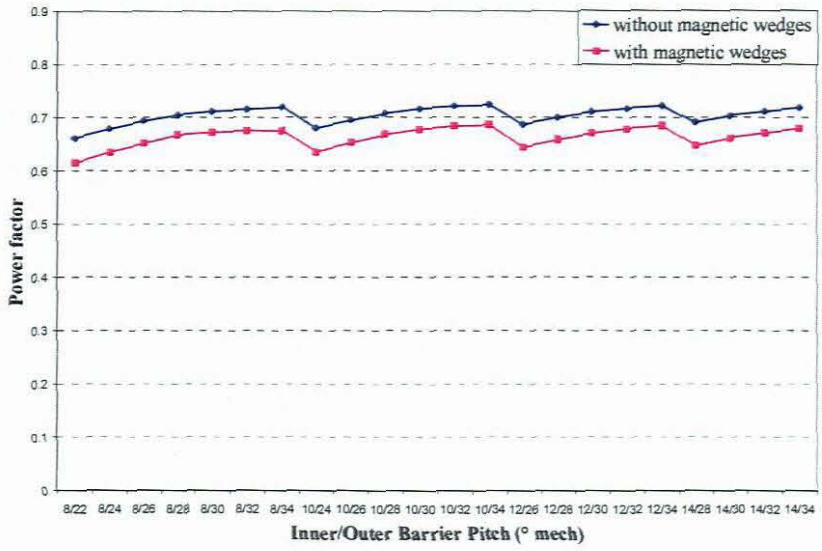

Fig 4.2.9 Power factor for double flux barrier machines with- and without magnetic wedges

The reduction of $\cos\varphi$ for single flux barrier machines varied between 5.8% and 7.8%, while for double barrier machines the deviation was between 5.4% and 7%. Although these changes percentage wise seem small, the nature in magnitude of $\cos\varphi$ indicates that this is not true. The closure of the stator slots increased L_q while the change in L_d were minimal which decreases the saliency of the machine. From eq (2.1.41) it can be seen that the saliency of the machine is directly responsible for the outcome of $\cos\varphi$ if the magnitude of input currents and the current angle is kept constant. For single- and double flux barrier machines the best saliency and therefore best power factor were found at 22° (reduced from 0.62 to 0.58) and 10°/34° (reduced from 0.72 to 0.69). With the addition of magnetic wedges not changing the optimum flux barrier pitch for each individual parameter it can be said that that an optimized machine, with respect to flux barrier configuration, would be the same for closed or semi-closed slots and only a change in magnitude of these parameters would occur. The effect of different magnetic wedge materials on the parameters, especially the power factor, is beyond the scope of this thesis and should be considered for future investigation. After identifying the two best machines as in section 3.3 the cut-out-pitch and height are evaluated. The results are shown below.

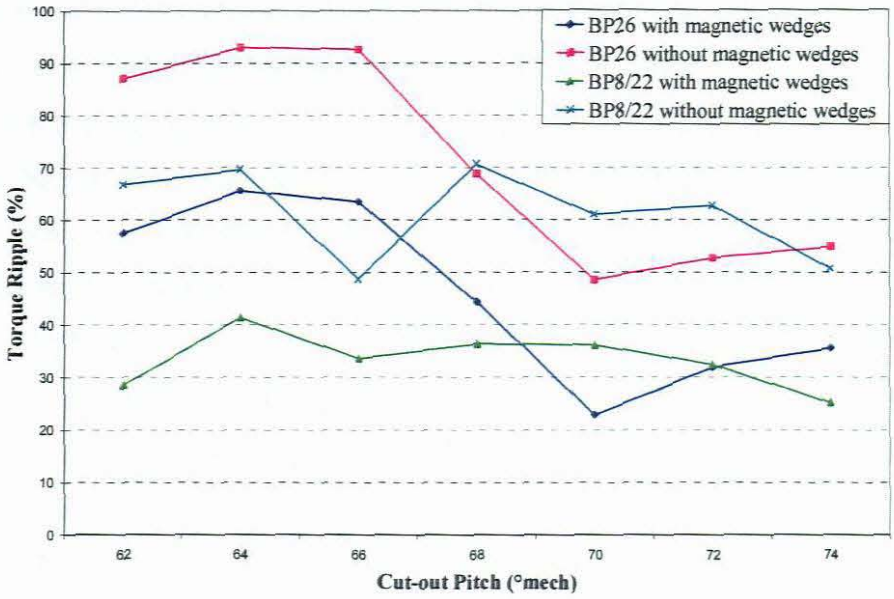

Fig 4.2.10 Torque ripple for the change in cut-out pitch with optimum single- and double flux barrier machines

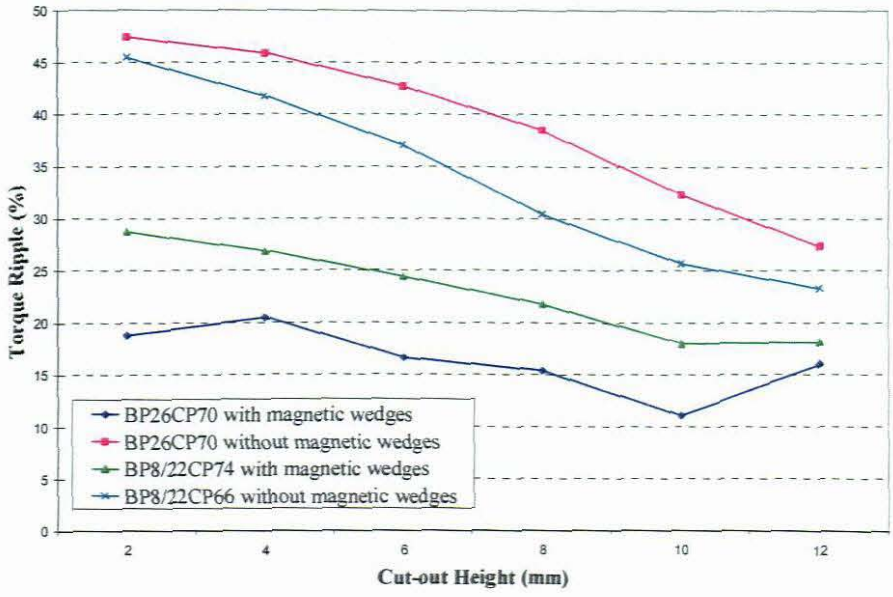

Fig 4.2.11 Torque ripple for the change in cut-out height with optimum single- and double flux barrier machines

Torque ripple: Again a decline in torque ripple was achieved with introduction of magnetic wedges to the machines as seen in Fig. 4.2.10 & 4.2.11. With the pitch of the cut-out

changing, the same fluctuations occurred in the machine with single flux barriers while the one with double barriers displayed a different result. Using magnetic wedges T_{ripple} in the single flux barrier machine was reduced between 29.4% and 52.8%, while the reduction in the double barrier machine was between 31% and 57.2%. Combination of the optimum cut-out pitch with single barrier machine stayed the same when magnetic wedges was introduced which were at a pitch of 70° reducing torque ripple from 48.5% to 22.9%. The optimum cut-out pitch for the double barrier machines shifted to a higher angle of 74° where the torque ripple were reduced from 50.8% to 25.2%. Again with L_q increasing, its stability increased as explained previously. When the height of these optimized cut-outs pitches were increased analysis presented a different result with the addition of magnetic wedges than in chapter 3. When the machines were modelled with semi-closed slots the double flux barrier machines were superior to those with single barriers with respect to low torque ripple (Fig 4.2.11). With magnetic wedges present and a change in cut-out height the reduction in T_{ripple} for single barrier machines varied between 41.4% and 65.8% while for double barrier machines only a reduction variation of between 22% and 36.8% were achieved. Previously the lowest T_{ripple} for semi-closed slots were achieved with a cut-out height of 12mm for both types of flux barrier machines while with magnetic wedges the optimum height changed to 10mm. With this said optimized machines with respect to rotor geometry and modelled with semi-closed slot doesn't necessarily mean the same rotor structure will produce the best machine for lowest torque ripple when magnetic wedges are added to the stator. However the addition of these wedges showed an overall improvement and should be considered as a necessity for low torque ripple machines.

Average Torque: In contrast to the machines modelled with only flux barriers present in the rotor the machines with magnetic wedges strangely increased the average torque (Fig 4.2.12 & 4.2.13). It seems that the wedges introduced dimensionality in the "equation" for high saliency equal high torque. This however can only be confirmed with a further indept investigation, which is not part of this study. For both types of barrier machines, the T_{avg} increased with the increasing cut-out pitch. Therefore optimized machines, with respect to the latter, will be the same for those where the stators either have closed or semi-closed slots. The increase of T_{avg} was rather small and were between 3.4% and 4% for single

barrier machine while the increase varied between 2% and 3.3% for double barrier machines when the cut-out pitch were increased.

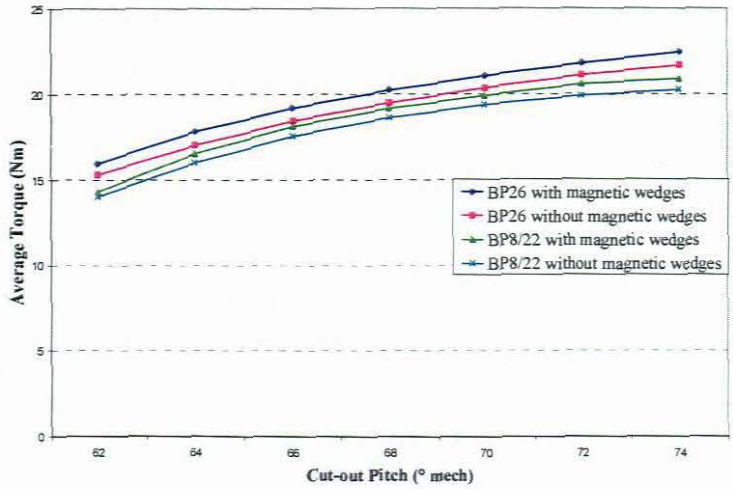

Fig 4.2.12 Average Torque for the change in cut-out pitch with optimum single- and double flux barrier machines

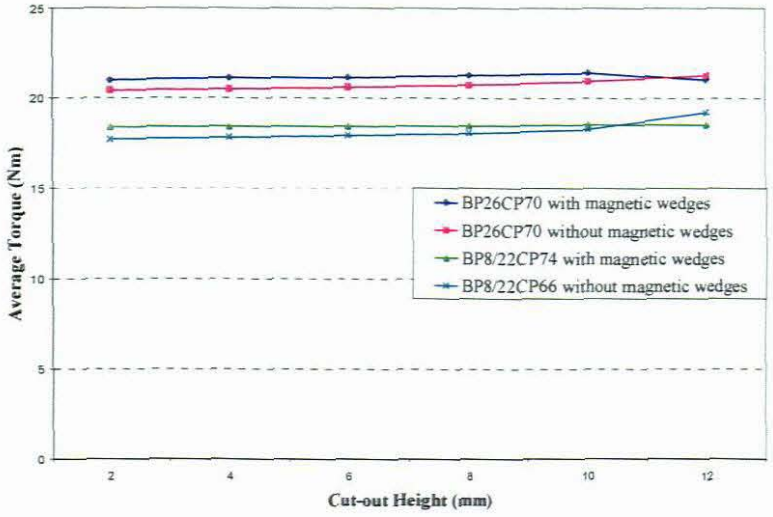

Fig 4.2.13 Average Torque for the change in cut-out height with optimum single- and double flux barrier machines

A further increase of the latter was achieved with increasing cut-out height which varied between 2.2% and 2.9% for single barrier machine while the variation for the double barrier machines was between 1.1% and 3.6% (excluding the cut-out height of 12mm in both cases). Due to the increase of both L_d and L_q (but increase of d-inductance the most

with magnetic wedges), the inductance difference ΔL was affected positively and consequently increased the average torque. Again the machines with magnetic wedges and increasing cut-out pitch which presented the best T_{avg} were the same as those with semi-closed slots namely 74° (increased from 21.71 Nm to 22.47 Nm) for single- and (reduced from 20.28 Nm to 20.91 Nm) for double flux barrier machines. With the increase of the cut-out height and T_{avg} being more sensitive to the addition of magnetic wedges the optimum height in both cases reduced to 10mm which increased the latter from 20.95 Nm to 21.43 Nm for single barrier machine while the increase for the double barrier machine was from 18.33 Nm to 18.56 Nm. Therefore the statement can be made that machine optimization for different flux barrier pitches, with increased cut-outs, are the same for closed or semi-closed slots when high average torque is desired. With increased height of cut-outs the machines' performance are more sensitive to these geometrical changes and therefore the same statement could not be made. However, with these increased cut-out heights in all the cases the best average torque were obtained at the same height where the lowest torque ripple occurred.

Power factor: Although minimization of torque ripple and maximized average torque were achieved the saliency suffered with introduction of magnetic wedges (Fig 4.2.14 & 4.2.15).

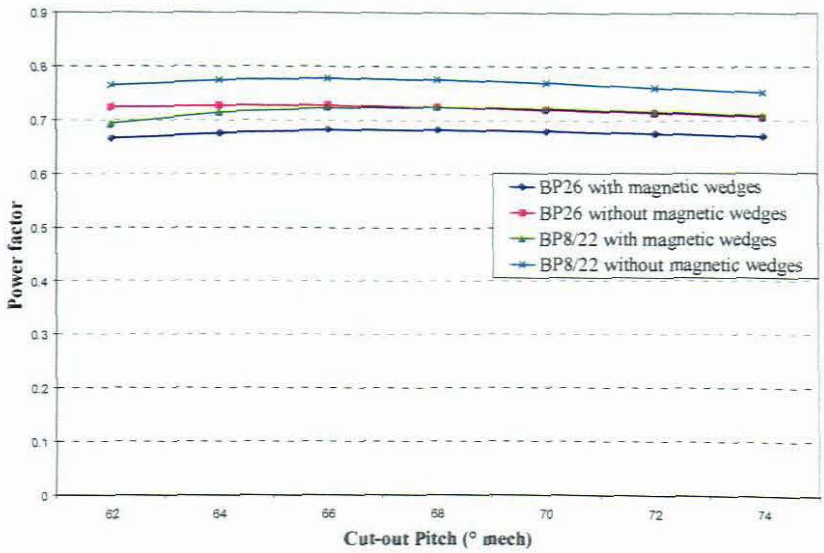

Fig 4.2.14 Power factor as a function of change in cut-out pitch with optimum single- and double flux barrier machines

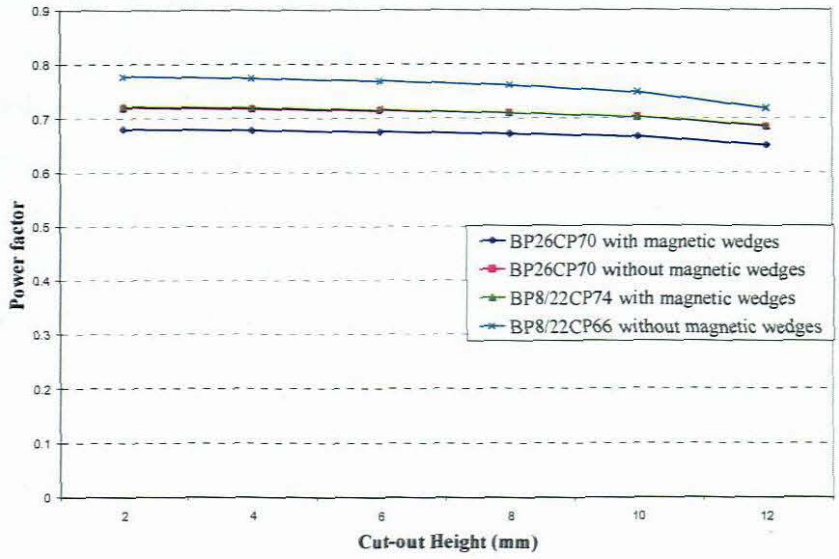

Fig 4.2.15 Power factor as a function of change in cut-out height with optimum single- and double flux barrier machines

The reduction of $\cos\varphi$ when the pitch of the cut-outs were changed for single flux barrier machines varied between 5.1% and 8% while with double barrier machines the deviation was between 5.7% and 9.4%. With the cut-out height being increased a further reduction for the later was between 5% and 5.4% for single barrier machine and between 4.6% and 7.2% for double barrier machine. With the presents of magnetic wedges resulted in an incline of L_q which reduced the saliency ratio and consequently had a negative effect on $\cos\varphi$. The importants of the magnetic wedge material should be considered as top priority for improvement of this parameter.

The closure of the stator slot by means of magnetic wedges have shown positive results toward minimizing torque ripple and in some cases the increase of the average torque. It now needs to be established how the physical height of these magnetic wedges influence the parameters.

4.2.2 Different magnetic wedge heights

The addition of magnetic wedges indicated positive results towards the reduction of cogging torque in the RSM for varies rotor structures. In the previous case study the wedge area was filled with magnetic material which consisted of a height of 1.22mm and the

wedge permeability the same as that of the rotor and stator. This height, however, was decided on empirically and therefore justifies a further investigation towards optimizing magnetic wedge heights. In this analysis the wedge height will be varied from 1mm to 5mm in steps of 1mm. The idea of magnetic wedges is to apply it to existing machines which indicate that the height of the wedge is restricted to the slot size and consequently the winding distribution inside the slot of the motor. The maximum magnetic wedge height chosen in this analysis will be considered as the maximum for the given 5.5 kW machine used in the study.

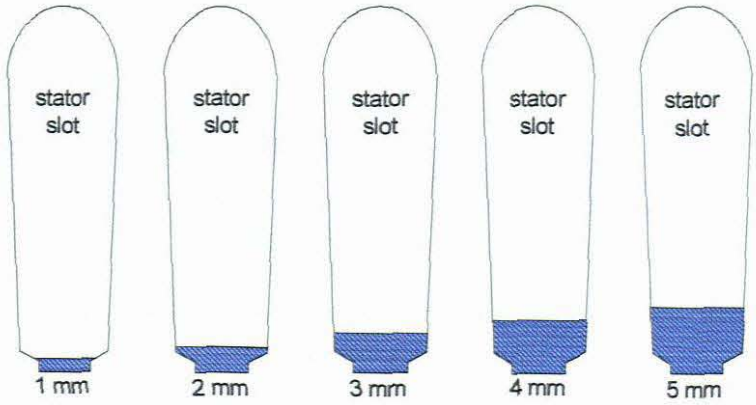

Fig 4.2.16 Different magnetic wedge heights used for simulation

The increase of the magnetic wedges will shift the mutual and differential leakage flux as indicated in Fig 4.2.2 towards the stator area. The shifts of these fluxes occur due to lower reluctance paths to the magnetic field through the stator rather than through the rotor. Due to the latter these fluxes responsible for rotor movement will decrease and consequently reduce the average torque. The magnetically "smooth" air-gap reduces the saliency of the machine and therefore would have an affect on the power factor as seen from eq (2.1.41). However the torque ripple has reacted positive to these wedges and the machine which gave the best results from the previous analysis is be subjected to stator slot changes. This single flux barrier machine had a rotor structure which consisted of a single set of flux barriers with a pitch of 26°, while the cut-outs had a pitch of 70° with a cut-out height of 10mm. In section 4.1 optimized current angles have been investigated for these types of machines but with semi-closed slots. The fact that rotor geometry played a huge role in the optimization of these angles for different parameters surely indicates that the same have to be done for machines with magnetic wedges with main objection function of obtaining low

torque ripple. This machine performed the best at a current angle of $\vartheta = 65°$ when semi-closed slots were used. The best approach would be to use a current angle spectrum where the previous optimum angle was in the middle of this range to assure that if a shift of the latter where to occur, it would be seen. Therefore the chosen current angle range would be $60° \geq \vartheta \geq 70°$. The results are indicated next in Fig 4.2.17 & 4.2.18

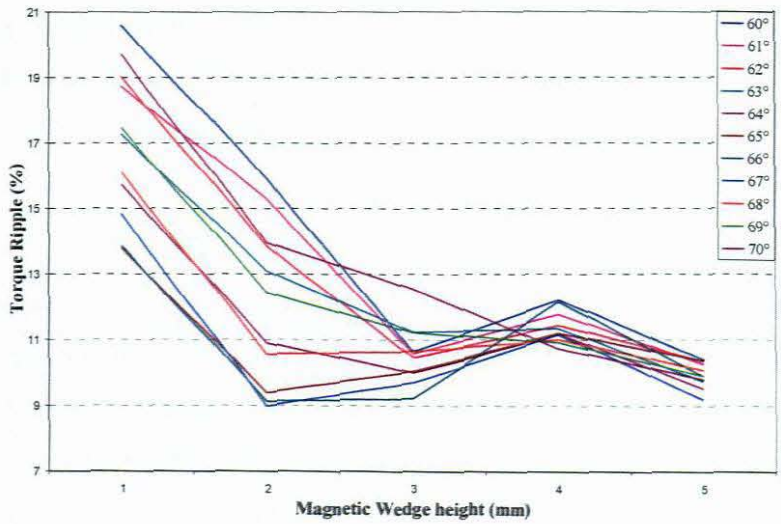

Fig 4.2.17 Torque ripple with an increased magnetic wedge height for different current angles

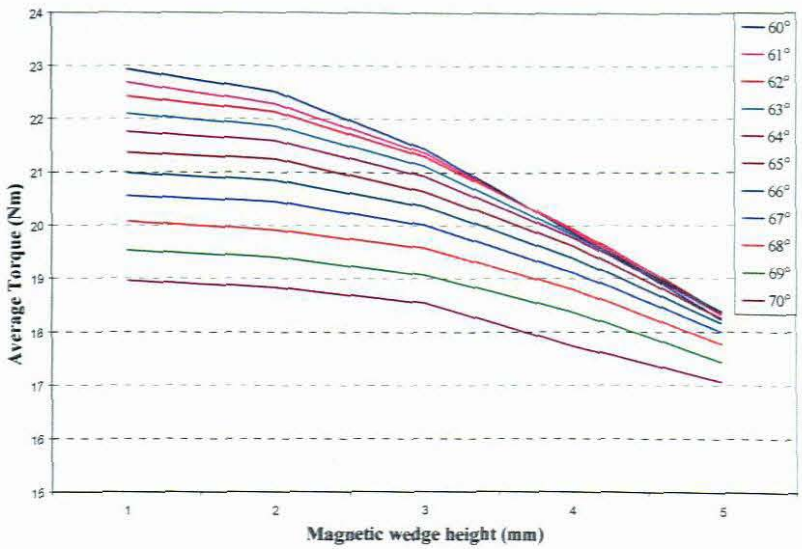

Fig 4.2.18 Average torque with an increased magnetic wedge height for different current angles

The change in magnetic wedge height has surely indicted different responses at different current angles. For every current angle the torque ripple fluctuated between the increased magnetic wedge heights and indicated different optimized heights at different current angles. With the current angle changing from 60° to 64° the lowest torque ripple were obtain at a height of 5mm indicating maximum height equals minimum torque ripple. When the current angle changed from 65° to 67° the minimum T_{ripple} occurred at a wedge height of 2mm. From here the optimum height again increased to 5mm for the remaining part of the current angle spectrum. The fact is that the lowest torque ripple (8.98 %) was obtained at $\vartheta = 67°$ (with 2mm wedge height) indicated a shift of optimized current angle of 2° compared to that of the machine with same rotor geometry but with semi-closed slots. In most cases the T_{ripple} of 2mm compared well to those with 5mm heights. The fact that the average torque decreases exponentially with increased magnetic wedge height certainly suggest that 2mm should be considered as the optimum wedge height for these machine, independent of the current angle. The negative affect of the increased wedge height on the power factor was more severely than the average torque. Analysis indicated that a decline of between 5% and 7% per mm of the latter occurred for varies current angles. This suggest that these wedges should not be considered for machine optimization when high saliency and power factor is wanted. If the necessity should exist to obtain high power factor and minimized torque ripple with the use of magnetic wedges, the focus point should rely on how the permeability of the wedge could be altered to obtain desired results. This however is beyond the scope of this work and should be considered for future research.

4.3 Summary of findings

With the most favourable rotor structures from section 3.1, 3.2 & 3.3 used in this analysis, a further optimization was achieved with selected current angles and minor changes to the stator geometry. The main objective function was to reduce the torque ripple but bearing in mind the change of certain parameters such as the average torque and the power factor. The selection of different rotor geometries with respect to single- or double flux barriers with- or without cut-outs each revealed a diverse response to the changes made to the geometry and input of the stator.

Torque ripple: The single flux barrier machines indicated it's favourability for the current space phasor to lie exactly between the d- and q-axis. Even though this was true, the given current angle spectrum revealed that these machines are open to optimization towards other parameters by maintaining a relative steady torque ripple between $10° \geq \delta \geq 70°$ compared to the other machines. Previously, the double barrier machines compared good to that of the single barrier ones in Chapter 3, but this study indicated that these machines are extremely sensitive the value of the current angle. Therefore these machines should not be used where optimization of more than one parameter is wanted. With these machines obtaining the highest torque ripple at optimum δ it can be said that double flux barriers should not even be (bearing in mind the nature of the stator construction) used when low torque ripple is wanted. The addition of optimized cut-out dimensions to the different barrier type machines indicated a further improvement with optimum current angles. When cut-outs were inserted to the single flux barrier rotor with the optimum current angle shifted with 20° indicating that these cut-out influence the latter the most. For the machine with double flux barriers and cut-outs present in the rotor the optimized current angle only shifted with 2° indicating in this case that the double flux barrier are mostly responsible for optimization of the latter.

Average Torque: Machines with single flux barriers with- or without cut-outs present in the rotor indicated the best average torque results for this study. However, since the optimum double flux barrier machine with respect to lowest torque ripple was chosen the previous statement can only be made if the latter was chosen as objective function. Chapter 3 indicated that these machine are very much capable of producing high average torques but at the cost of high cogging torques. The optimum current angle for maximum average torque in this study was between $54° \geq \delta \geq 57°$ and indicated that rotor geometry containing the dimensions described in fact have little affect on the latter. Therefore the statement can be made that for high torque-per-current ratios the above range should be chosen for machine operation.

Power factor: Maximum saliency and therefore maximum power factor were obtained where the current space phasor was close to the q-axis. The optimum current angle range for these types of machines is $66° \geq \delta \geq 72°$. Unfortunately in most cases the optimization

of the power factor resulted in low average- and high cogging torques. With the saliency playing a large role in the outcome of the power factor it should be mentioned that to obtain acceptable results the magnitude of L_d should be between 8 and 10 times to that of L_q. The change of the current angle indicated that the ratio between i_q and i_d also play a role in the outcome of the latter. When the saliency ratio versus power factor was investigated (Fig 4.3.1), it can be seen that for very low saliencies the best power factor was achieved for low current angles. With the increase in saliency the power factor increased more where higher current angle was used.

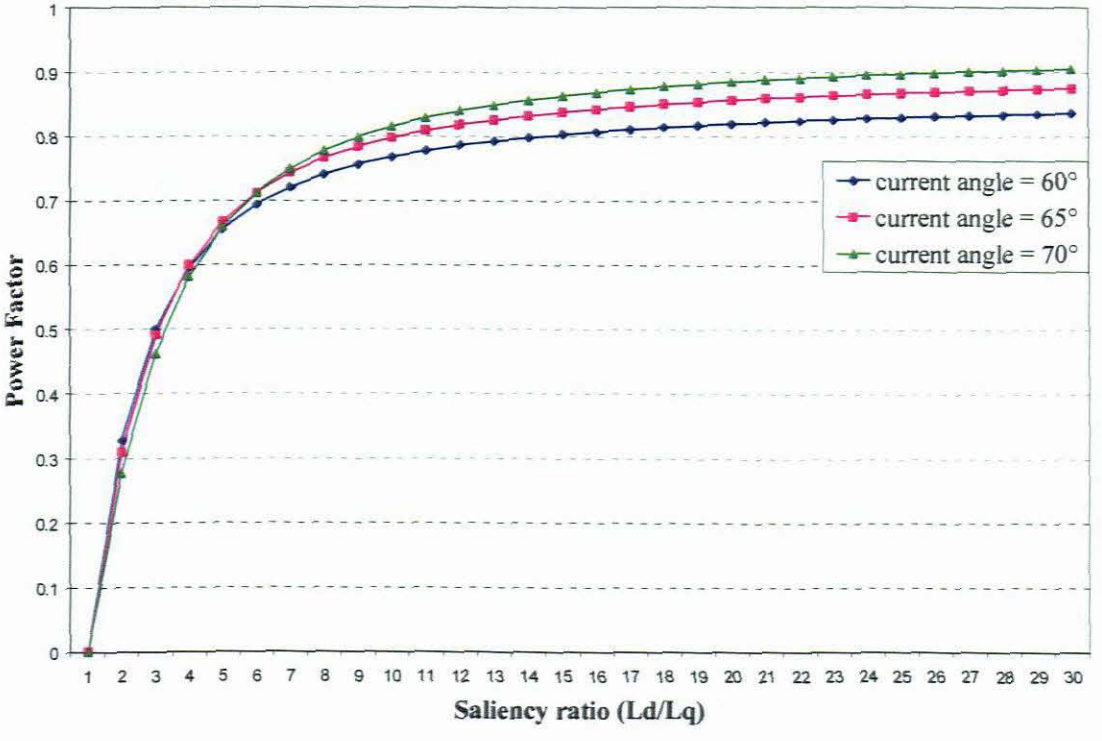

Fig 4.3.1 Power factor versus saliency ratio for different current angles

The addition of magnetic wedges have surely presented its positive influence on the reduction of torque ripple as seen in Fig 4.3.3 & 4.3.4. Optimum results for each parameter are indicated next for different rotor and stator geometries.

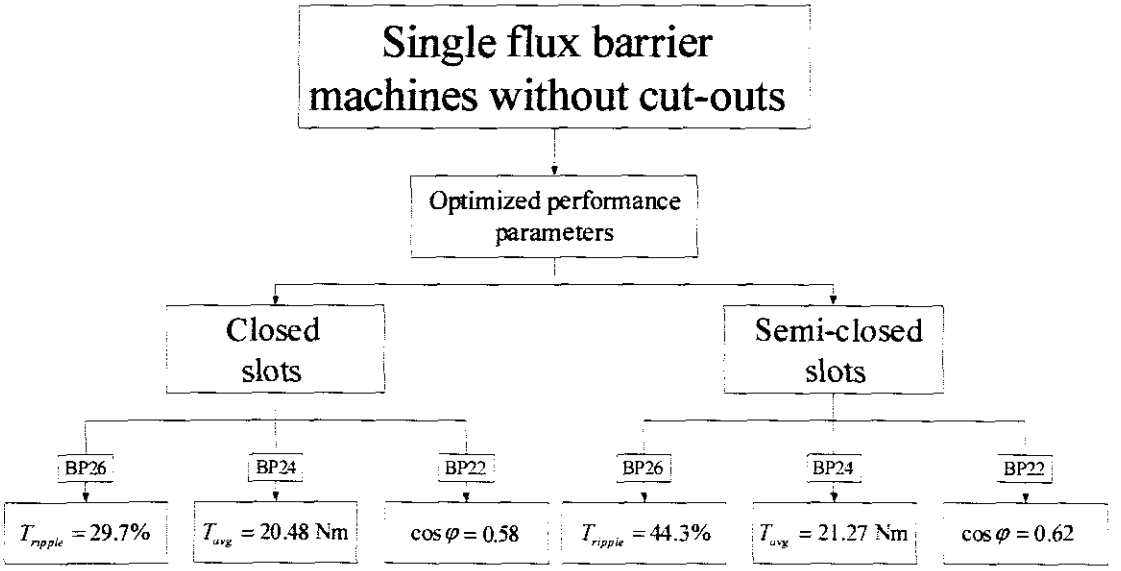

Fig 4.3.2 Optimized parameters for a given rotor and stator geometry with single flux barriers and no cut-outs

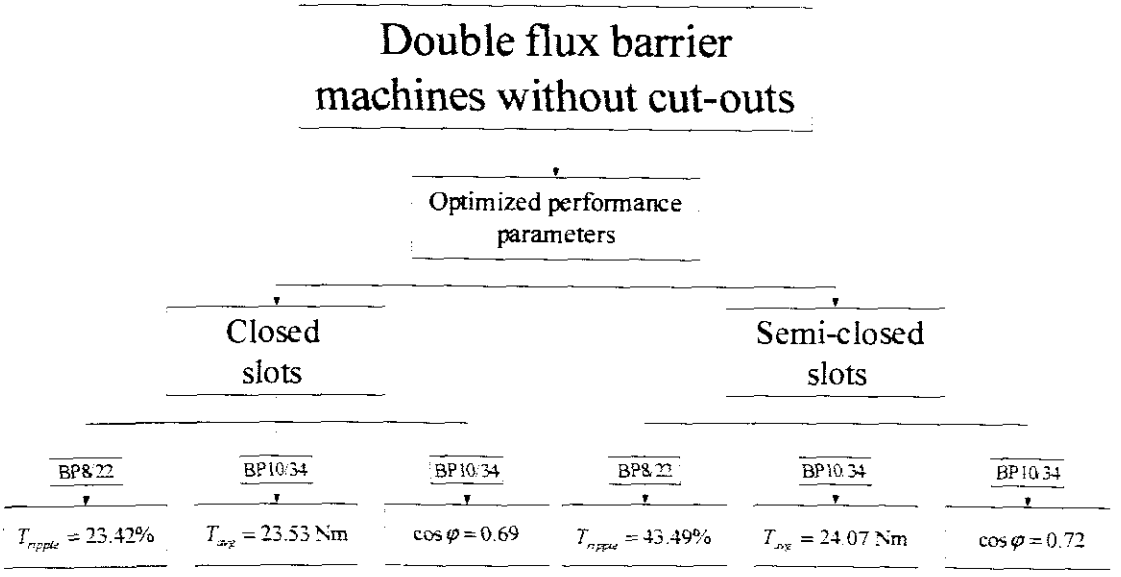

Fig 4.3.3 Optimized parameters for a given rotor and stator geometry with double flux barriers and no cut-outs

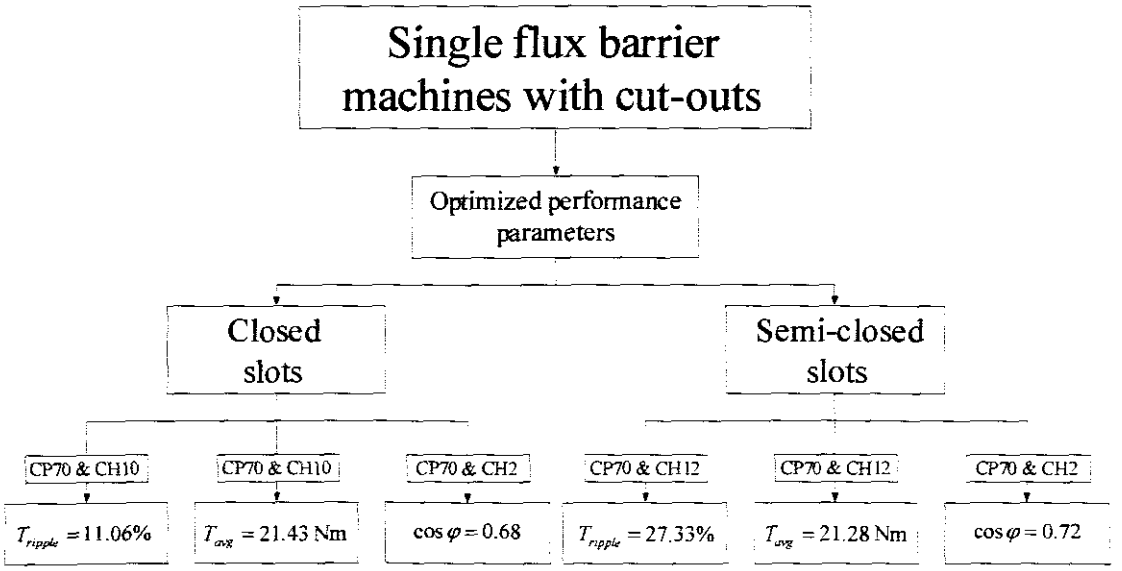

Fig 4.3.4 Optimized parameters for a given rotor and stator geometry with single flux barriers and cut-outs

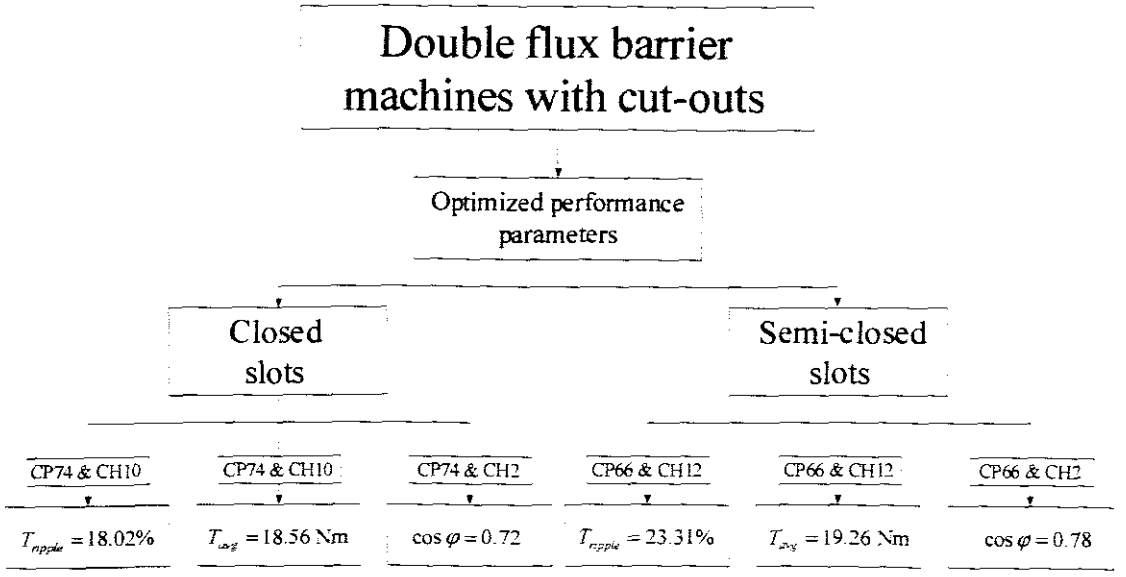

Fig 4.3.5 Optimized parameters for a given rotor and stator geometry with double flux barriers and cut-outs

Where machines with only single- or double flux barriers present in the rotor the addition of these magnetic wedges reduced the torque ripple dramatically while still presenting the same optimum rotor structures per given parameter. When cut-outs were introduced to the rotor, the magnetic wedges indicated different results for single- and double barrier machines with respect to lowest torque ripple. The single barrier machine indicated no change for the optimum cut-out pitch while the double barrier machine revealed a different anecdote. In both barrier type machines the magnetic wedges reduced the optimal cut-out height from 12mm to 10mm and therefore improved the saliency of the machine.

The negative effect on the average torque was minimal in most cases and can be assumed negligible in contrast to the significant reduction of the torque ripple. The power factor however suffered more and indicated that this method of torque ripple reduction reduced the saliency as well and should not be considered for machine where a high power factor is desired. The affect of the magnetic wedge material must be scrutinized but it's beyond the scope of this work and should be considered for future investigation. The optimum current angle for highest average torque and power factor with magnetic wedges present indicated almost no change compared to machines with semi-closed slots. The optimum current angle for lowest torque ripple for machines with magnetic wedges did change for machines with double barriers:

- Machine 1 Single barriers without cut-outs → from 45° to 45° (same)
- Machine 2 Double barriers without cut-outs → from 72° to 65°
- Machine 3 Single barriers with cut-outs → from 65° to 65° (same)
- Machine 4 Double barriers with cut-outs → from 74° to 68°

With the optimum current angle for lowest torque ripple reduced and the best angle for highest average torque being the same, the optimization range between these parameters decreased, meaning higher average torques can be obtained with current angle optimized for low torque ripple (Fig 4.1.6 & 4.1.7). The power factor revealed the same story. This optimization range are indicated in Fig 4.3.6 for an arbitrary machine modelled with semi-closed slots and magnetic wedges.

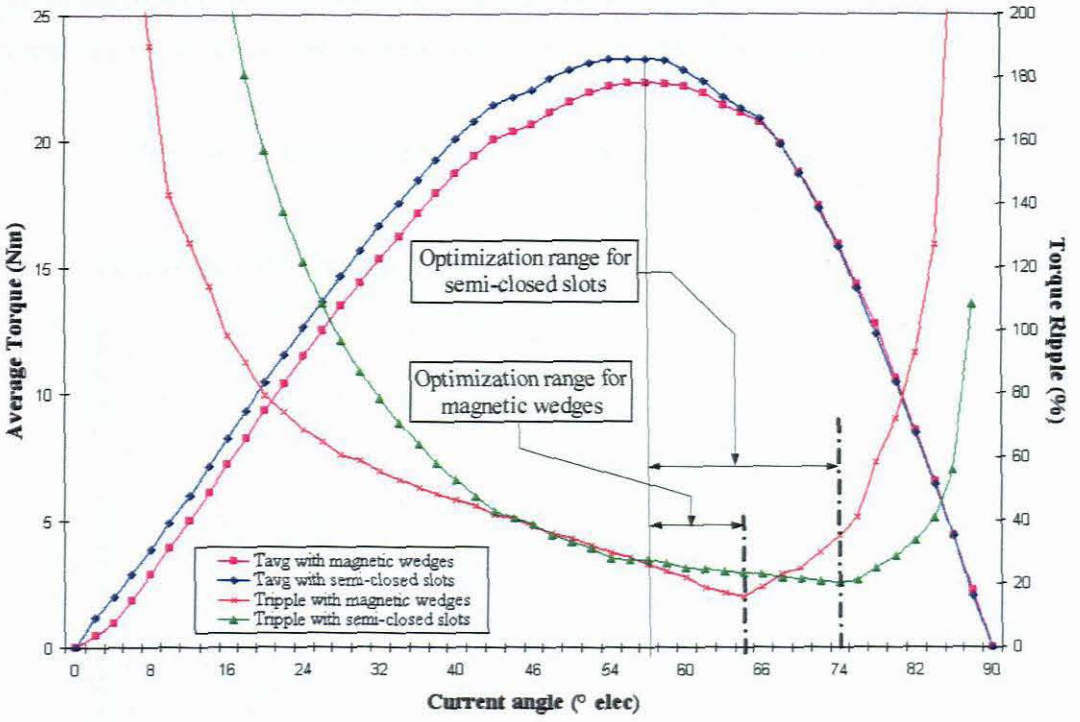

Fig 4.3.6 Optimization range for machines with different slots geometries

The best performing machine from this chapter, having single flux barriers (BP26) with a cut-out- pitch and height of 70° and 10mm, was used where the height of the magnetic wedge was changed. The analysis indicated that a height of 2mm produced the lowest torque ripple but shifted the optimum current angle by 2°. The average torque and power factor suffered with the increase of these wedges and indicated that reduction in torque ripple did not conciliate the reduction of average torque and power factor.

The same analysis was conducted with best performing machines from each rotor geometry category (with optimum current angles) and revealed the following results. In each case the lowest torque ripple was obtained at different magnetic wedge heights, for each rotor geometry (identified in red in Table 4.3.1). This indicates that optimized wedge heights can not be decided upon before hand and should be considered for individual machines with different rotor geometries. The average torque and power factor indicated above are not the optimum ones, but purely shown on how the increased wedge height decreases them. Up to now torque ripple reduction with respect to rotor and stator geometrical changes have been

accomplished without rotor skewing. The fact that the output torque of these machines still consist of a harmonic content will be dealt with in the following chapter.

Table 4.3.1 Magnetic wedge height changes for optimum machines

		Magnetic wedge height				
Performance Parameter		*1mm*	*2mm*	*3mm*	*4mm*	*5mm*
Machine 1	T_{avg} (Nm)	19.62	18.22	16.52	14.82	13.17
	T_{ripple} (%)	18.34	9.89	**9.42**	12.82	14.43
	$cos\varphi$	0.47	0.43	0.38	0.34	0.30
Machine 2	T_{avg} (Nm)	19.44	18.60	17.70	16.62	15.55
	T_{ripple} (%)	26.87	20.26	17.67	14.89	**13.63**
	$cos\varphi$	0.63	0.57	0.52	0.47	0.43
Machine 3	T_{avg} (Nm)	20.55	20.44	20.01	19.11	18.00
	T_{ripple} (%)	14.83	**8.98**	9.69	11.16	9.18
	$cos\varphi$	0.68	0.63	0.58	0.52	0.47
Machine 4	T_{avg} (Nm)	17.43	17.17	16.94	16.56	16.13
	T_{ripple} (%)	19.58	14.08	9.96	**9.12**	9.74
	$cos\varphi$	0.72	0.65	0.59	0.54	0.49

5. Cancellation of Torque Harmonics

The presents of singular dominant harmonics seems to be a problem in RSMs (Fig 2.2.3). The fact that changes to the rotor geometry adjust the outcome of the instantaneous torque and justifies the investigation of the harmonic content of it, with the aim of cancellation of certain torque harmonics. This will present the possibility of harmonic cancellation to a certain extend. The output torque per given rotor and stator structure for machines used in Chapter 3 (with semi-closed slots and magnetic wedges) will be subjected to a Fourier analysis (FA) to identify its harmonic content and present possible combinations.

5.1 Problem description

From the evaluation in section 2.2 it can be seen that the original machine presented a dominant 9th harmonic which was responsible for most of the torque deviation. This dominant harmonic even presented itself when the rotor and stator changed geometrically. By elimination, or reduction, of this harmonic the quality of the output torque can be significantly improved as seen in Fig 5.1.1

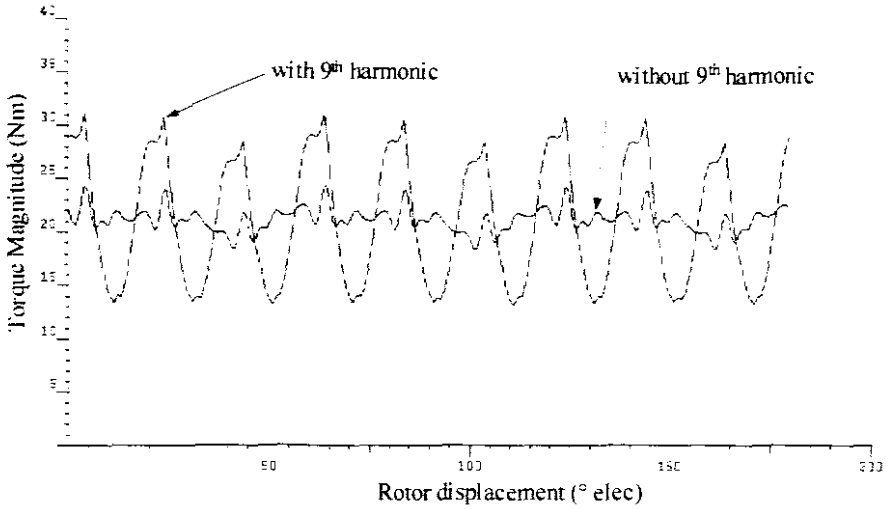

Fig 5.1.1 Output torque of original machine with- and without dominant 9th harmonic

In order to eliminate these dominant harmonics by means of combination of different rotor structures, the magnitude of the harmonics must be the same while their angles be 180° apart from each other. Consequently the output torques of these machines has to be subject

to a FA to identify the harmonic spectrum and the angle of them. Every periodic and monotonic function can be described by an infinite number of harmonic functions of different magnitudes and frequencies. With the torque being the objective function the series can be written as

$$T = T_{avg} + \sum_{n=1}^{\infty} [a_n \cos(n\delta) + b_n \sin(n\delta)] \tag{5.1.1}$$

or

$$T = T_{avg} + \sum_{n=1}^{\infty} [A_n \sin(n\delta + \varphi_n)] \tag{5.1.2}$$

where

$$A_n = \sqrt{a_n^{\,2} + b_n^{\,2}} \tag{5.1.3}$$

and

$$\varphi_n = \tan^{-1}\left(\frac{a_n}{b_n}\right) \tag{5.1.4}$$

where T_{avg} is the average torque, a_n & b_n are the magnitudes of the imaginary- and real parts of the n^{th} harmonic, δ the rotor angle (position), A_n the magnitude and φ_n the angle of the harmonic of order n. Fig 5.1.2 is the phasor representation of the above equations.

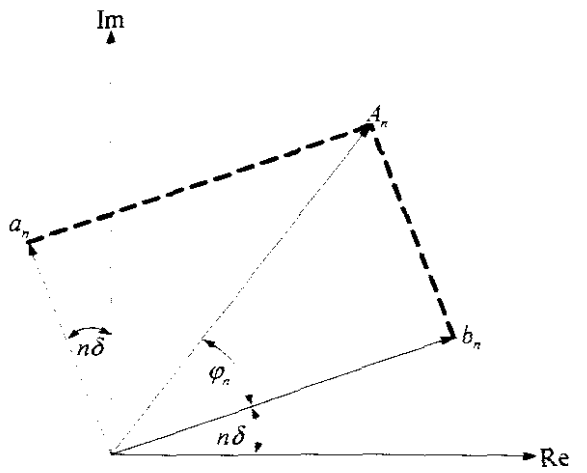

Fig 5.1.2 Phasor diagram of individual harmonic components

The output torque of machines from chapter 3 (with semi-closed slots and magnetic wedges) were subjected to a FA to identify, how magnitudes and angles of the dominant 9th harmonics changed, when dimensional ratios where altered. The results are shown in Fig 5.1.3 to 5.1.6.

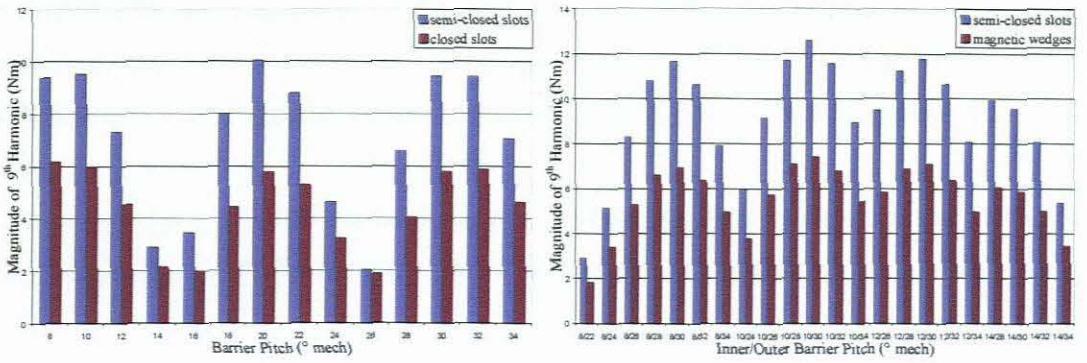

Fig 5.1.3 Magnitude of 9th harmonic for different single- and double flux barrier pitches without cut-outs

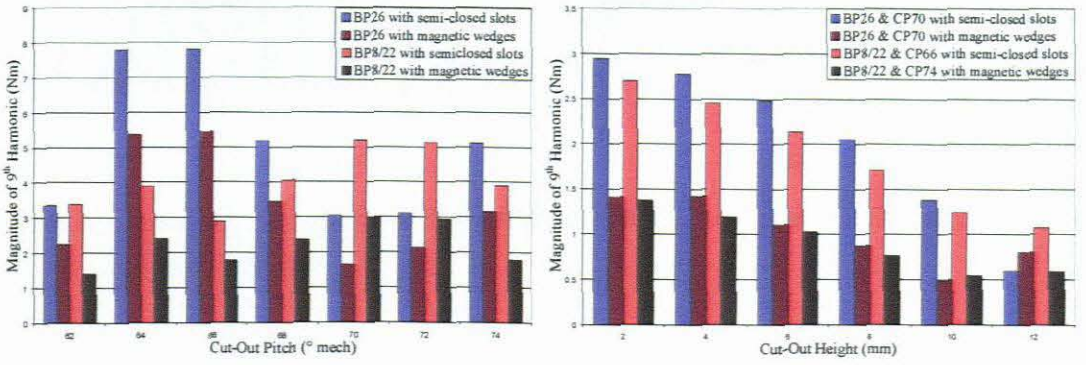

Fig 5.1.4 Magnitude of 9th harmonic for different cut-out pitches and heights for single- and double flux barriers

It can be seen that the addition of magnetic wedges to the stator slots reduced the dominant 9th harmonic dramatically. For single flux barrier machines without cut-outs the reduction of this harmonic was between 8% and 44% compared to the semi-closed slots while for double flux barrier machines a more steady reduction of between 34% and 41% were achieved. When cut-outs were added to the rotor the reduction was more prominent and indicated a decrease of between 30% and 38% for single flux barrier machines and 38% to 54% for double flux barrier machines when the pitch of the cut-out were changed. With

alterations made to the height of the cut-out again a reduction of between 49% and 64% for single barrier machines and 49% to 56% for double flux barrier machines. This comparison however was excluding the height of 12 mm. The reduction of the 9th harmonic for the top performing single flux barrier machine (BP26) was very small although the addition of magnetic wedges reduced the torque ripple from 44.3% to 29.7%. Further investigation indicated that the magnitude of the 18th harmonic was close to that of the 9th when modelled with semi-closed slots. The wedges reduced this 18th harmonic by 78% which indicates that these magnetic wedges are a good approach to harmonic suppression.

The way these dominant harmonic angles change revealed a different anecdote. The magnetic wedges indicated a rapid shift of these angles as indicated in Fig 5.1.5 & 5.1.6

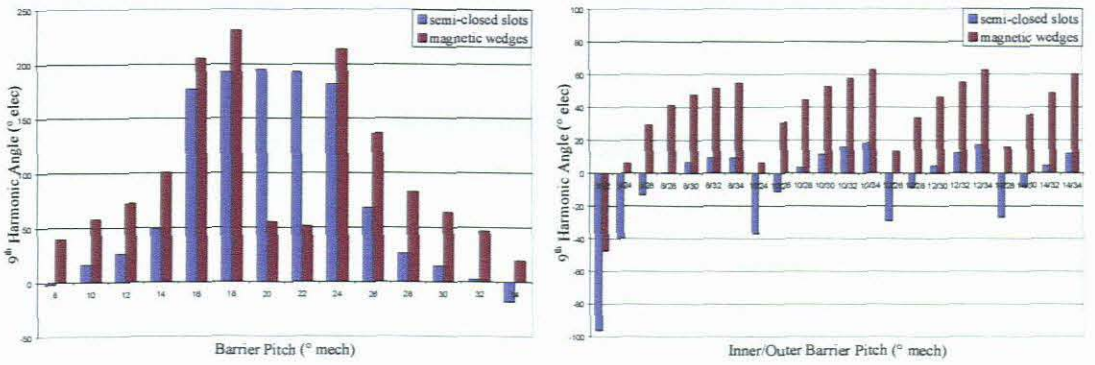

Fig 5.1.5 Angle of 9th harmonic for different single- and double flux barrier pitches without cut-outs

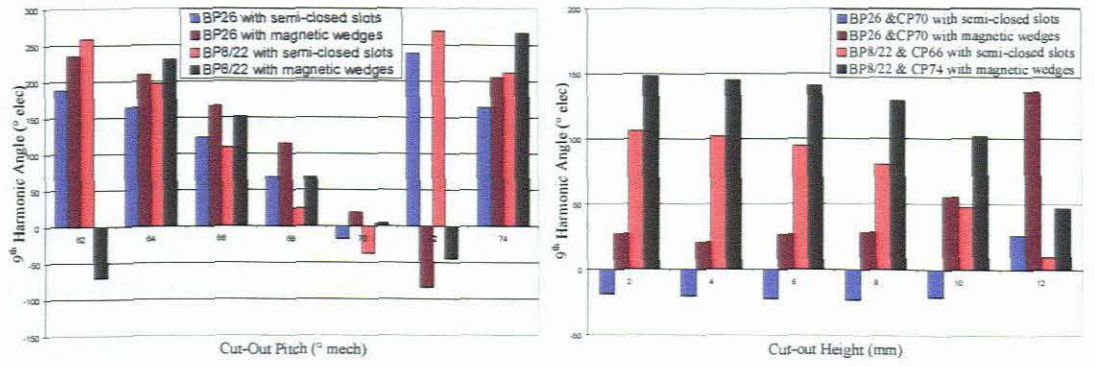

Fig 5.1.6 Angle of 9th harmonic for different cut-out pitches and heights for single- and double flux barriers

Although the double flux barrier machines, without cut-outs but with magnetic wedges indicated a coherent change in angles, for all other investigated machines the same statement could not be made. The results indicated that the prediction of these harmonic angles before hand would be a difficult task. With dominant harmonic magnitudes and angles identified the method of rotor combination of different rotor structures will now be investigated.

5.2 Rotor combinations without skewing

Fratta (1993) mentioned that the most straight forward way to compensate for one specific harmonic component in the torque ripple is to divide the rotor into two sections, shifted with respect to each other by the proper angle as seen in Fig 5.2.1.

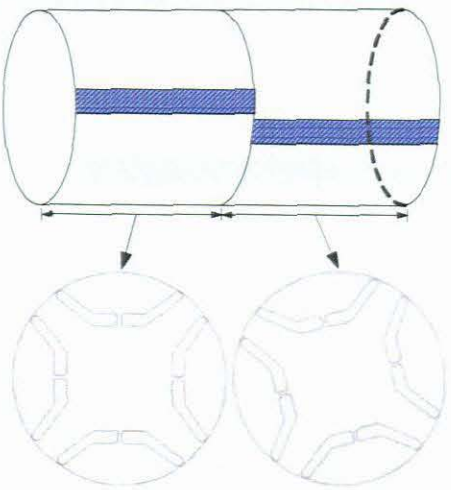

Fig 5.2.1 Rotor skewing be means of a multi-sliced method

He did however mention that complete compensation is not achievable, even if the whole rotor was skewed. This was due to the anisotropic behaviour of the magnetic material in the rotor. With geometrical changes made to the rotor in Chapter 3, the performance characteristics changed significantly in most cases, especially T_{ripple} , which indicated the most rapid change. With these geometrical changes made to the rotor, although the 9^{th} harmonic was reduced, it was not always the most dominant one. The magnitudes and angles of this harmonic, in fact, changed with each design and therefore related to the change of torque ripple. With the statement made by Fratta (1993) the question was: "If

skewing was done to compensate for harmonic cancellation can one combine different rotor structures where the dominant harmonics are equal in magnitude but shifted 180° apart?" From the FA done on the machines from Chapter 3 (Fig 5.1.3 to Fig 5.1.6) the possibility surely presented itself and justified a further investigation.

5.2.1 Problem approach

The idea behind this method is that the individual torque ripple magnitudes of each design are independent to the outcome of the combined rotor structure provided that their harmonic angles are 180° apart. This will enable the designing engineer to focus his attention on design models where parameters like average torque and power factor are more favourable while achieving torque harmonic cancellation at the same time. The rotor stack length will consist of two types of machines where the harmonic content of each design opposes each other. The method of rotor combination is indicated next in Fig 5.2.2.

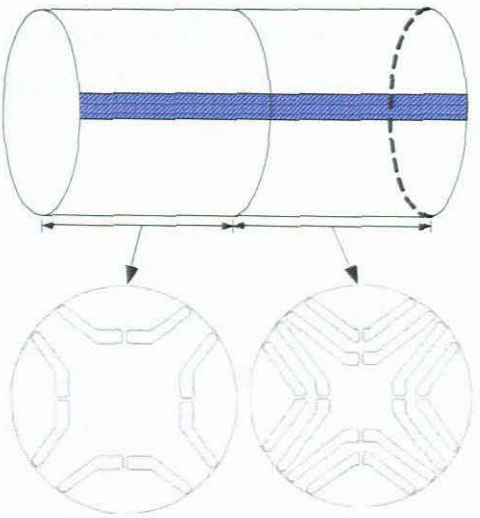

Fig 5.2.2 Rotor combination be means of a multi-sliced method

5.2.2 Combination model

Harmonic cancellation by combination of different rotor structures can be done in numerous ways depending on the harmonic content of each design, especially when more than one dominant harmonic are present. Identifying these harmonics by means of a FA, enable the engineer to decide how the problem should be approached in terms of the number of combinations and the respective length of each individual section. However,

with the increased number of individual sections and different rotor geometries the production cost will increase. In this study only two sections will be used to compensate for these costs.

In order to find the machines which are best suited for torque harmonic cancellation Fig 5.1.3 to 5.1.6 are investigated. It indicated that machines with equal 9^{th} harmonic magnitudes and angles 180° apart can be identified. However, only the significance of the 9^{th} harmonic was indicated and other harmonics neglected. In some cases the 3^{rd}, 6^{th}, 18^{th} and 27^{th} harmonic was dominant and therefore indicated that compensation for only one harmonic would not necessarily lead to the desired results. The torque data for all the modelled machines was accumulated and introduced to an algorithm topology where all possible rotor groupings (irrespective of their harmonic content) were analyzed. In the first study the rotor combinations used were divided into four sections according to the change of their geometries (section 3.1, 3.2, 3.3.1 and 3.3.2) and done for machines with semi-closed slots and magnetic wedges. The best combined machines, in terms of lowest torque ripple, were identified and indicated in Fig 5.2.3 & 5.2.4.

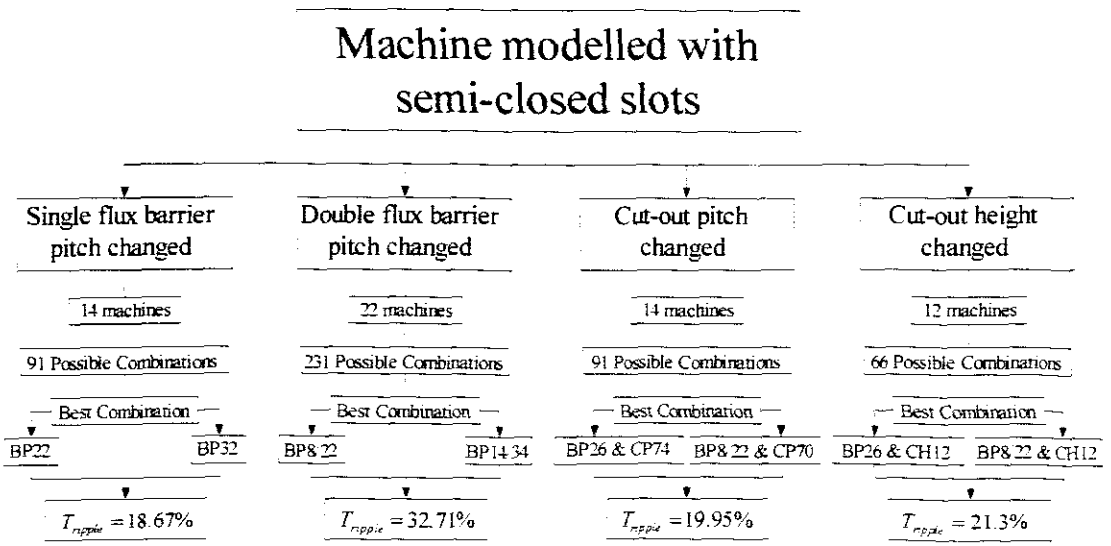

Fig 5.2.3 Best combinations per rotor geometry with semi-closed slots

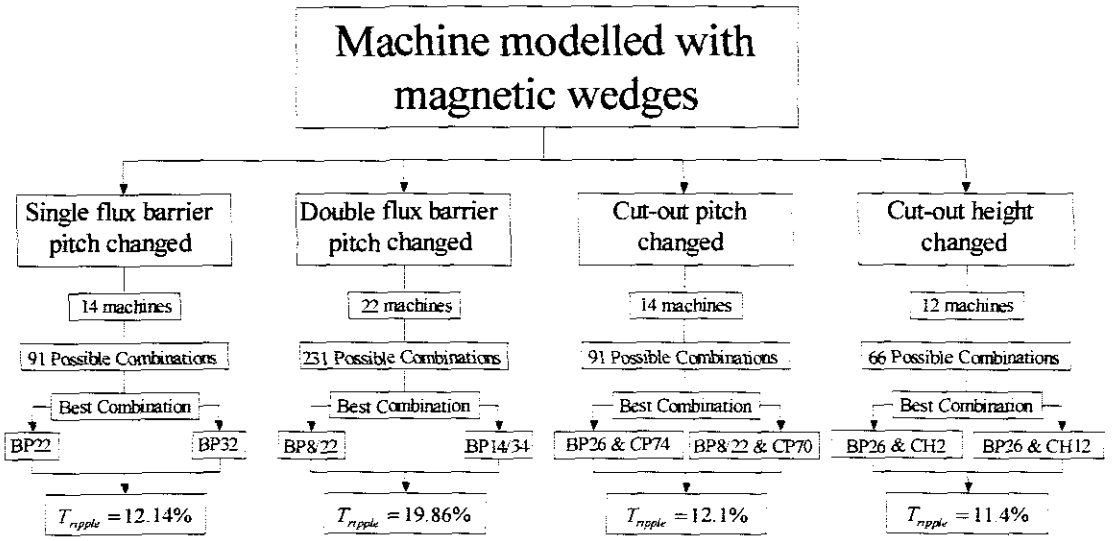

Fig 5.2.4 Best combinations per rotor geometry with magnetic wedges

With the possible combinations investigated for each individual section the possibility of combining rotor structures independent of its geometry description will now be investigated. The 62 possible rotor structures (modelled with semi-closed slots or magnetic wedges) yielded 1891 combinations and signified how important the use of a software algorithm topology is rather than individual FAs. The best combinations according to slot geometry are indicated below in Table 5.2.1

Table 5.2.1 Performance results for best possible rotor combinations

	Semi-closed slots			**Magnetic wedges**		
Parameter	BP18	BP8/34	Combination	BP18	BP8/34	Combination
T_{ripple} (%)	80.54	77.34	8.41	50.52	49.28	6.65
T_{avg} (Nm)	21.41	23.51	22.32	20.22	22.74	21.48
$cos\varphi$	0.62	0.72	0.67	0.58	0.68	0.63

With the combination of different rotor structures leading to the cancellation of dominant harmonics surely indicated a remarkable improvement with respect to the torque quality. The instantaneous torques of the individual machines and their resultant are shown in Fig 5.2.5 & 5.2.6

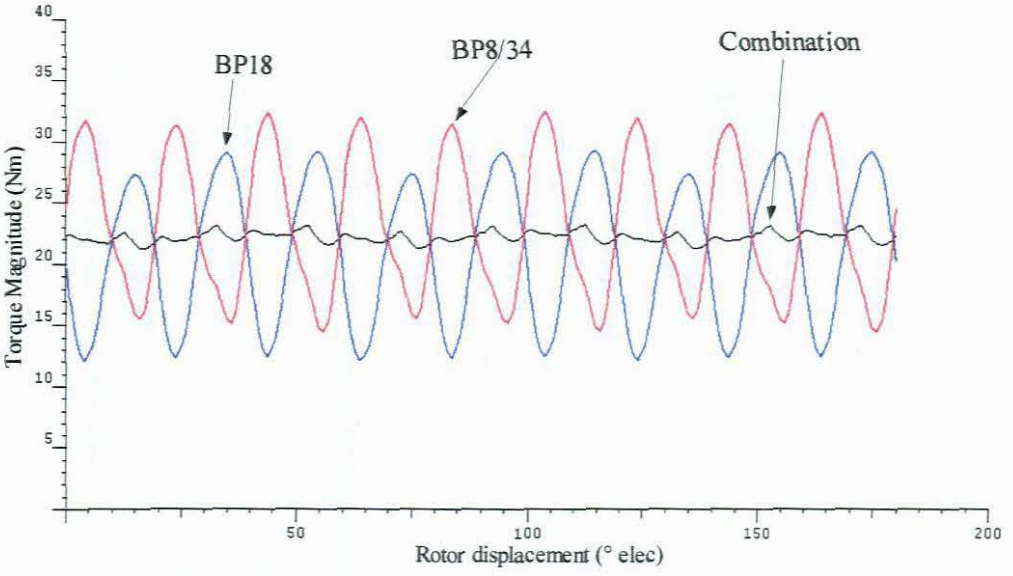

Fig 5.2.5 Instantaneous torque for best rotor combinations with semi-closed slots

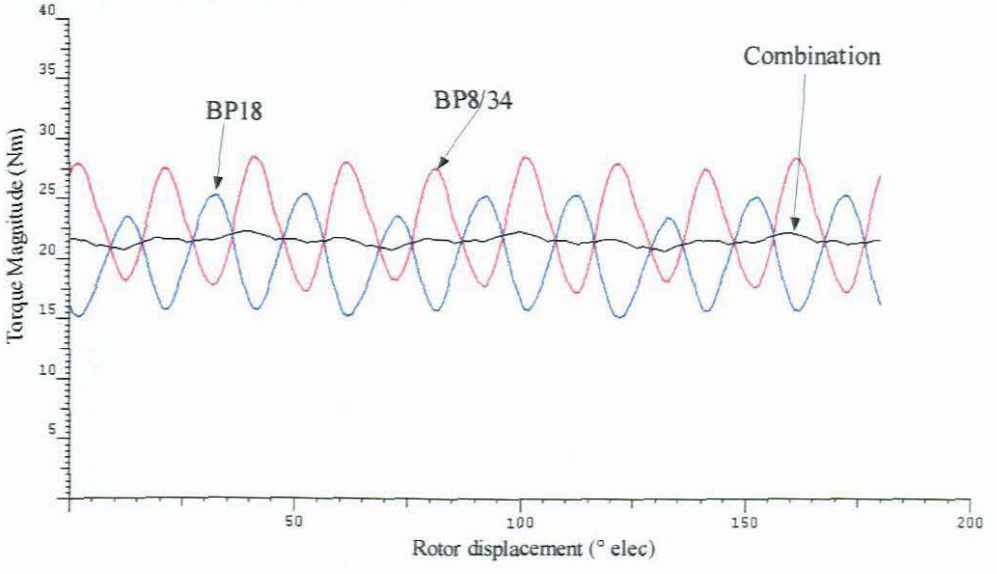

Fig 5.2.6 Instantaneous torque for best rotor combinations with magnetic wedges

In order to evaluate the change in harmonic content when different rotor geometries were combined, a FA was conducted on the instantaneous torque of the combined model. The dominant 9th harmonic was dramatically reduced in each case where the magnitude of less dominant harmonics reduced in addition. The results are indicated below in Fig 5.2.7 & 5.2.8.

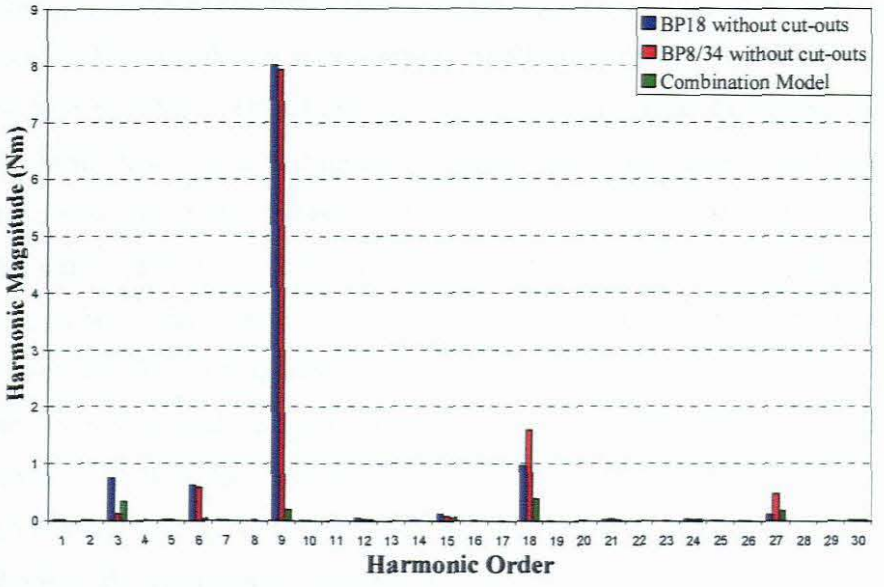

Fig 5.2.7 Fourier analysis of best performing machines with semi-closed slots

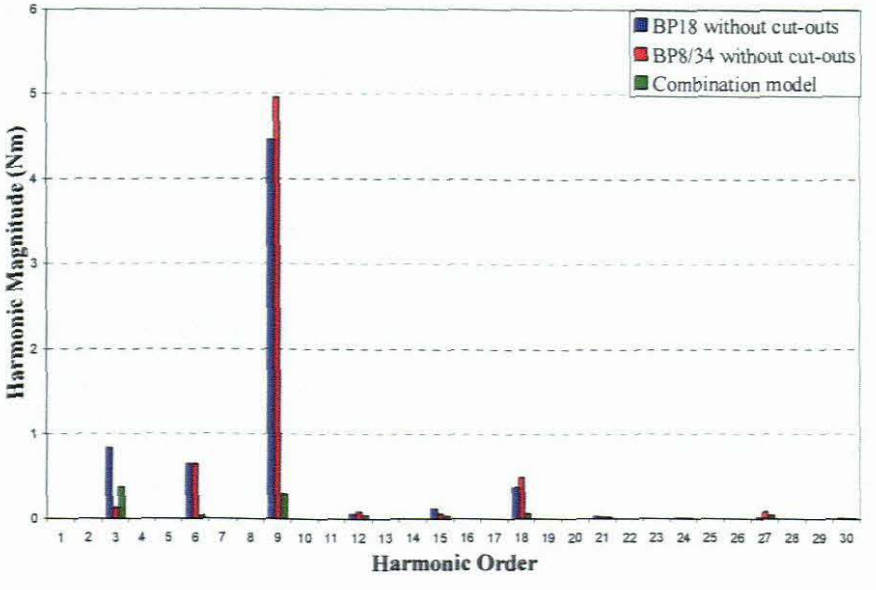

Fig 5.2.8 Fourier analysis of best performing machines with magnetic wedges

5.3 Summary of findings

Combining rotor structures with different layouts surely indicated favourable results with respect to low torque ripple. The following points were of interest:

- With the individual machines indicating good average torques and reasonably good power factors signify that improvement for all parameters are achievable.
- The best possible combinations per section were the same for machines modelled with semi-closed slots or magnetic wedges, except for section on cut-out heights which was due to the different optimum cut-out pitch per slot geometry chosen. This indicated that the best rotor combination is not affected by the nature of the slot geometry and therefore be the same when a machine is either modelled with semi-closed slots or magnetic wedges.
- The study indicated that although magnetic wedges change the magnitudes and angles of the harmonic content of one part of the rotor section, the change occurring on the other section will happen in the same way. However, this change will not influence the relationship between the opposing harmonics of each section but rather complement them as the combination of machine with magnetic wedges always presented the lowest torque ripple.
- The FA (Fig 5.2.6 & 5.2.7) indicate that the combination model compensate for all dominant harmonics and not necessarily for one.

With this said the cancellation of torque harmonic can be dealt with the combination of different rotor geometries. This method is therefore proposed as part of a design technique for the practising engineering with respect to lower torque ripple, while maintaining good results for other parameters at the same time. The author wishes to mention that the study was done for a chosen current angle. The same study can be done for any other current angle and the best rotor combinations might not necessarily be the same in all cases. This however is beyond the scope of this work and should be considered for future investigation.

6. Conclusions and Recommendations

This thesis presented the possibilities of torque ripple reduction by means geometrical changes made to rotor and the addition of magnetic wedges to the stator. With analysis made on different current angles per rotor geometry indicated that a further improvement on the performance characteristics was achievable. Combining rotor structures with opposing torque harmonics resulted in an additional improvement of torque ripple reduction.

This work indicated that a systematic approach, in terms of geometrical changes, should be considered in order to draw conclusive findings on how theses changes affect the outcome of the performance of the RSM. The fact that geometrical design improvements should not be neglected has been highlighted, rather than adding electronic controlling techniques. Some of the key statements and findings are highlighted next.

6.1 Important findings

In section 2.3.2 the sensitivity of the instantaneous torque towards rotor position was evaluated and indicated the following: "....when the d-axis is in the centre of a slot while the q-axis is in the middle of a tooth more torque is created then when the opposite is true." The question was: "Would this always be the case or do dimensional ratios play a role?" From Figs 5.2.5 & 5.2.6 it can be seen that the rotor structures consisting of a barrier pitch of 18° indicated a different result to the above statement. This concludes that the nature of the geometry is mainly responsible for the sensitivity of the instantaneous torque per rotor position.

With only single flux barriers in the rotor (section 3.1) highest cogging torques were achieved with barrier pitches at 10°, 20° and 30° and the lowest values in between these maxima, namely 14° and 26°. This suggests that the actual ratio of **bp** should not coincide with slot pitches **sp** when low torque ripple is wanted.

In section 3.2 the addition of an extra set of flux barriers improved the overall average torque and power factor compared to single flux barrier machines and should be considered as a design improvement if these quantities are wanted. The best double flux barrier machine, in terms of lowest torque ripple, compared well against those with only single flux barriers.

When cut-outs were introduced to the single- and double flux barrier rotors (section 3.1.1) the saliency ratio revealed a different story than in section 3.1 & 3.2. In these sections an increase in saliency indicated an increase in average torque or any other parameter except torque ripple. With the introduction of cut-outs the exact opposite is true where high saliencies are responsible for low average torques and vice versa.

The analysis in section 3.3.2 indicated that the cut-out height to rotor radius (**ch/rr**) should be as high as possible when low torque ripple and high average torque is wanted. This increased ratio, however, had a negative effect on the saliency and consequently the power factor due to reduced air-gap lengths.

The analysis of section 4.1 indicates that absolute minimum T_{ripple} for single flux barrier machines occurred at a current angle at 45° elec. This signified that these machines favour the current space phasor I_S to be exactly between the d- and q-axis. For the rest of the machines from section 3.2,3.3.1 and 3.3.2 this was not true as most parameters favoured the current space phasor to be closer to the q-axis. The optimum ranges are given below

- Minimum torque ripple: $45° \geq \delta \geq 74°$
- Maximum average torque: $54° \geq \delta \geq 57°$
- Maximum power factor: $66° \geq \delta \geq 70°$

The introduction of magnetic wedges un the stator slots (section 4.2) reduced the torque ripple significantly compared to machines with semi-closed slots. The negative effect on the average torque was minimal in most cases and can be assumed negligible in contrast to the significant reduction of the torque ripple.

Another advantage of these magnetic wedges is that they did not change the optimum barrier pitch for lowest torque ripple or maximum average torque and power factor. Therefore it should be considered as a design improvement to the stator when optimized machines are identified according to each desired parameter. With the introduction of different cut-out geometries of the rotor the same statement could not be made as these wedges reacted different to the change in the air-gap length.

In Chapter 5 the combination of rotor structures with different geometries were evaluated in order to counter for singular dominant torque harmonics. This method presented the best results towards torque ripple reduction, while maintaining sufficient values for high average torque, power factor and saliency. The study indicated that half of the rotor should consist of a single flux barrier rotor structure with **bp** = 18° while the other half consist of double set flux barriers with **bp** = 8°/34°. These optimum geometries hold true for machines with magnetic wedges or semi-closed.

In section 5.2.2, the FA analysis on these optimum machines (Fig 5.2.7 & 5.2.8) indicated that total torque harmonic compensation was achievable. This combination method of different rotor structures is therefore proposed to counter the fact of high torque ripple in stead of rotor skewing.

6.2 Future research

In section 3.1 & 3.2 the pitch of the flux barriers was increased in steps of 1° with respect to the d-axis. The change in torque ripple with each pitch changed significantly (Fig 3.1.2 & 3.2.2) while the change in average torque and power factor was minor. In order to identify more optimized flux barrier positions the increment between each **bp** should be decreased. The change of cut-out geometry indicated the same assessment.

In section 4.1 the optimization of the current angle was done only with the best performing machines with respect to low torque ripple from section 3.1, 3.2, 3.3.1 and 3.3.2 and comparisons made how different rotor geometries changed the optimized current angle. The same study should be done for non optimized machines. (i.e. is the optimum current angle the same for a machine with a flux barrier pitch of 16° to that of 24°).

Throughout this work a double layer winding distribution chorded by 2 slots were used. Bomela (2002) said: "With a single-layer winding the torque improvement may theoretically be as much as 10%, depending on what double layer winding is used." He did, however, mention that with a single layer winding distribution the space harmonics are less suppressed and therefore increased the deviation of the output torque. With the rotor combination method proposed in Chapter 5, using machines with geometries according to Chapter 3, the use of single layer windings could surely be considered for torque ripple reduction with the advantage of an increased average torque. Furthermore the general effects of triple layer windings should be investigated as well and even if the pitching (and direction of it) of the coils have any relevance.

In section 4.2, a comparison with respect to the performance characteristics (torque ripple, average torque, power factor, etc.) was done between machines with semi-closed slots and magnetic wedges. Although a reduction in torque ripple was achieved the power factor suffered significantly in most case. Therefore it is proposed that the permeability of the wedge itself should be investigated in order to achieve optimization for all parameters.

The success of reducing the torque ripple by means of the combination method from Chapter 5 presented the opportunity to investigate further improvements. The combination of only two sections was evaluated and presents the opportunity for multiple sections. The length per section could be varied in order to alter the magnitudes of certain dominant harmonics. The study was done for a chosen current angle and indicates that the same study can be done for any other current angle.

Since this machine was fed with sinusoidal currents it now needs to be investigated what influence harmonics in the current have on the torque- and on the flux harmonics. The question here is whether or not flux linkage harmonics always show a similar pattern as torque harmonics?

References

1) Bomela, X.B. & Kamper, M.J. 2002. Effect of Stator Chording and Rotor Skewing on Performance of Reluctance Synchronous Machine. *IEEE Transactions on Industry Applications*, 38(1): 91-100, January/February

2) Brinkman, J. 1965. Theoretische und experimentelle Untersuchung an einem Motor mit verbesserter Ausnutzung des Reaktionsprinzips. Unpublished PhD dissertation, Fakultät für Machinenwesen der Technischen Hochschule Carolo-Wilhelmina, Braunschweig, Jananuary

3) Brüderlin, R. 1924. Drehfeldmaschinen mit veränderlicher Reaktanz. *Archiv für Electrotechnik*. 13:12-29

4) Conti, G., Parasiliti, F. & Villani, M. 1996. Torque ripple analysis in synchronous reluctance motors. Mediamira Science Publisher, :188-193, October

5) Chang, L., Eastham, A.R. & Dawson, G.E. 1989. Permanent Magnet Synchronous Motor: Finite Element Torque Calculations, *IEEE Industry Applications Society Annual Meeting 24th*, San Diego, USA, :69-73, October

6) Chiricozzi, E., Conti, G., Parasiliti, F. & Villani, M. 1996. Design solutions to optimize torque ripple in synchronous reluctance motors. *Proceedings in International Conference on Electrical Machines*, Vigo, Spain, :148-153

7) Cruickshank, A.J.O., Anderson, A.F. & Menzies, R.W. 1971. Theory and performance of reluctance motors with axially laminated anisotropic rotors. *IEE Proceedings*, 118(7):887-894, July

8) Delaere, K., Sas, P., Belmans, R. & Hameyer, K. 1999. Weak Coupling of Magnetic and Vibrational Analysis using Local Forces. *IEEE International Electrical Machines and Drives Conference*, Seattle, Washington, USA, May

9) Deohar, R.P, Staton, A., Jahns, T.M. & Miller, T.J.E. 1996. Prediction of Cogging Torque Using Flux-MMF Diagram Technique, *IEEE Transactions on Industry Applications*, 32(3):569-576, May/June

10) Douglas, J.F.H. 1956. The theory of anisotropic field structures in synchronous machines. *AIEE Journal*, 75:84-86

11) El-Antably, A. & Hudson, T.L. 1985. The design and steady-state performance of a high efficiency reluctance rotor. *IEEE Industry Applications Society Annual Meeting*, New York, USA :770-776

12) Fick, P.D. & Kamper, M.J. 2004. Accurate Digital Current Control of the Reluctance Synchronous Machine with constant Current Angle, *The Transactions of the South African Institute of Electrical Engineers*, George, South Africa, :47-50, March

13) Fratta, A., Troglia, G.P., Vagati, A. & Villata, F. 1993. Evaluation of Torque Ripple in High Performance Synchronous Reluctance Machines. *IEEE Industry Application Society 28th Annual Meeting*, Toronto, Canada, 1:163-170, October

14) Haataja, J. 2003. A Comparative Performance Study of four-pole Induction Motors and Synchronous Reluctance Motors in Variable Speed Drives. Published PhD dissertation, Lappeenranta University of Technology, ISBN 951-764-772-7, June

15) Hanekom, A.N. 2004. A Study on Torque Harmonics in Reluctance Synchronous Machines. Unpublished Bachelors dissertation, Cape Technikon, December

16) Heaviside O., 1888, The Electro-magnetic Effects of a Moving charge, *The Electrician*, May

17) Hofmann, H. & Sanders, S.R. 2000. High-Speed Synchronous Reluctance Machine with Minimized Rotor Losses, *IEEE Transactions on Industry Applications*, 36(2):531-539, March/April

18) Honsinger, V.B. 1971. The Inductances L_d and L_q of Reluctance Machines. *IEEE Transactions of Power Applications and Systems*, 90(1):298-304, January

19) Howe, G.W.O., 1935. Some magnetic misconceptions, The Electrician, :601-602, November

20) Kamper, M.J. & Volschenk, A.F. 1994. Effect of rotor dimensions and cross magnetization on Ld and Lq inductances of reluctance synchronous machines with cageless flux barrier rotor. *IEE Proceedings on Electrical Power Applications.*, 141(4):213-220, July

21) Kamper, M.J.& Mackey, A.T. 1995. Optimum control of the reluctance synchronous machine with cageless flux barrier. *Transactions of the South African Institute of Electrical Engineers*, 86(2):49-56, June

22) Kamper, M.J. 1996. Design Optimization of Cageless Flux Barrier Rotor Reluctance Synchronous Machine. Unpublished PhD dissertation, University of Stellenbosch, December

23) Kostko, J.K. 1923. Polyphase reaction synchronous motors. *AIEE Journal*, 42:1162-1168

24) Kurscheidt, P. 1961. Theoretische und experimentelle Untersuchung einer neuartigen Reaktionsmaschine. Unpublished PhD dissertation, Fakultät für Machinenwesen und Elektrotechnik der Rheinisch-Westfälischen Technischen Hochschule, January

25) Lawrenson, P.J. 1964. Theory and performance of polyphase machines. *IEE Proceedings*, 111(8):1435-1445, August

26) Lawrenson, P.J. & Gupta, S.K. 1967. Developments in the performance and theory of segmental-rotor reluctance motor. *IEE Proceedings*, 114(5):645-653, May

27) Lee, J.W., Kim, H.S., Kwon, B.I. & Kim, B.T. 2004. New Rotor Shape Design For Minimum Torque Ripple of SRM Using FEM. *IEEE Transactions on Magnetics*, 40(2):754-757, March

28) Levi, E. & Panzer, M. 1966. Electromechanical Power Conversion, McGraw-Hill

29) Lin, C.Y. 1951. Characteristics of Reluctance Machines. *AIEE Journal*, 70(2):1971-1977

30) Malesani, L. 1994. Synchronous reluctance drives. *IEEE Industry Applications Society Annual Meeting*, Denver, CO, October

31) Parasiliti, F. & Villani, M. 1995. Optimization Analysis of Synchronous Reluctance Motor Design, *IEE Conference Publication on Electrical Machines and Drives*, 412: 276-280, September

32) Ren, Z., Ionescu, B., Besbes, M, & Razek, A. 1995. Calculation of Mechanical Deformation of Magnetic Materials in Electromagnetic Devices, *IEEE Transactions on Magnetics*, 31(3):1873-1876, May

33) Richardson, D.V. 1978. Rotating Electrical Machinery and Transformer Technology, Reston Publishing Company, Virginia, ISBN 0-87909-732-9

34) Talaat M.E. 1951. Steady-state and transient synthesis of 3-phase reluctance motors. *AIEE Journal*, 70(2):1963-1970

35) Thompson, S.P. 1911. Dynamo electric machinery, 8th ed. New York: M Strong: 389

36) Trickey, P. H. 1933. The non-excited synchronous motor. *Electric Journal*, 30:160-162

37) Trickey, P.H. 1946. Performance calculations on polyphase reluctance motor. *AIEE Journal*, 65:191-193

38) Trübenbach, R.A. 1993. Vector Control of a Reluctance Synchronous Machine. Unpublished Masters Dissertation, University of Stellenbosch, January

39) Vagati, A., Franceschini, G., Marongiu, I. & Troglia, G.P. 1992. Design criteria of high performance synchronous reluctance motor. *IEEE Industry Applications Society Annual Meeting Record*, 66-73, September

40) Vagati, A., Pastorelli, M., Franceschini, G. & Petrache, S.C. 1998. Design of Low-Torque-Ripple Synchronous Reluctance Motor. *IEEE Transactions on Industry Applications*, 34(4):758-764, July

41) Vagati, A., Canova, A., Chiampi, M., Pastorelli, M. & Repetto, M. 2000. Design Refinements of Synchronous Reluctance Motors through Finite-Element Analysis. *IEEE Transactions on Industry Applications*, 36(4): 1094-1102, July/August

42) Voss, E. & Kamper, M.J. 2004. On the use of magnetic wedges in synchronous reluctance machines". *Southern African Universities Power Engineering Conference*, University of Stellenbosch, Stellenbosh, January

43) Weh, H. & Schroder, U. 1985. Static inverter concept for multiphase machines with square-wave current-field distribution. *European Power Electronics Conference*, Brussels, :1147-1152

Appendix A

Derivation of Fundamental Quantities

A.1 Transformation of currents

To transform a set of variables from one system into another a specific transformation matrix, depending if it is from stator- to rotor frame or vice versa, has to be applied to the given equations above. To conversion process can be obtained by using

$$i_{dq0} = K \cdot i_{abc} \tag{A.1}$$

$$i_{abc} = K^{-1} \cdot i_{dq0} \tag{A.2}$$

where the Park transformation matrix K and it's inverse K^{1} are fined as

$$K = \frac{2}{3}\begin{bmatrix} \cos(\omega t) & \cos(\omega t - 120°) & \cos(\omega t + 120°) \\ -\sin(\omega t) & -\sin(\omega t - 120°) & -\sin(\omega t + 120°) \\ 1/2 & 1/2 & 1/2 \end{bmatrix}$$

(A.3)

and

$$K^{-1} = \begin{bmatrix} \cos(\omega t) & \sin(\omega t) & 1 \\ \cos(\omega t - 120°) & \sin(\omega t - 120°) & 1 \\ \cos(\omega t + 120°) & \sin(\omega t + 120°) & 1 \end{bmatrix} \tag{A.4}$$

The stator quantities i_a, i_b, i_c can now be transformed into three individual rotor quantities i_d, i_q, i_0 by using the following equations

$$i_d = \frac{2}{3}(i_a \cos(\omega t) + i_b \cos(\omega t - 120°) + i_c \cos(\omega t + 120°)) \tag{A.5}$$

$$i_q = -\frac{2}{3}(i_a \sin(\omega t) + i_b \sin(\omega t - 120°) + i_c \sin(\omega t + 120°)) \tag{A.6}$$

$$i_0 = \frac{1}{3}(i_a + i_b + i_c) \tag{A.7}$$

A.2 Calculation of flux linkages from vector potentials

From experience it can be said that the calculation of the flux linkages is done more accurately using average vector potentials than from a magnetic field surface integral. However, the ability to be precise and avoid errors can be markedly dependent on the model discretization, especially with respect to the number- and nature of the elements. The vector potential are assumed to vary linearly across each element leading to a constant permeability, flux density etc. within each element.

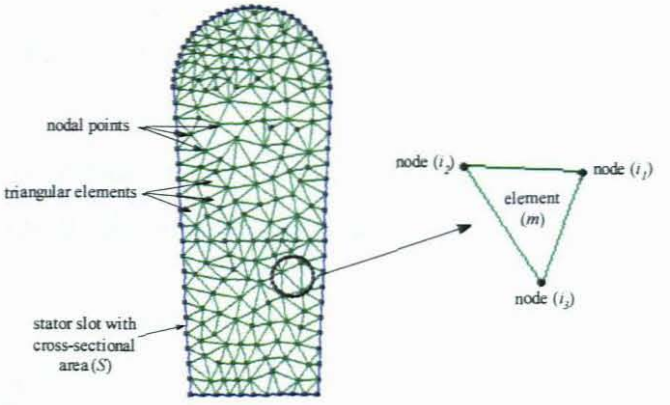

Fig A.2.1 Cross-sectional view of a meshed stator slot

Let us consider a stator slot (Fig A.2.1) consisting of a winding with N turns, modelled by a region of cross-sectional area S and let each node in the region represent a winding strand. The flux Φ_{mi} linked by such an individual winding strand corresponding to node i of element m is calculated from the product between the vector potential A_{mi} and the effective length ℓ_{mi} of the current strand at that specific node i (where i = 1, 2 or 3). Due to the cylindrical geometry of the machine the effective length of the current strand can be calculated accordingly

$$\ell_{mi} = 2\pi \cdot r_{mi} \tag{A.8}$$

where r_{mi} is the radius of the location of node i of element m. Since the calculation of the flux linked by an individual strand is established, the total flux linked experienced by the element itself can be determined by taking the average of the nodal points and can be presented accordingly

$$\Phi_m = \frac{1}{3}\sum_{i=1}^{3} 2\pi \cdot r_{mi} A_{mi} \tag{A.9}$$

To determine the actual flux linkage of each individual element one needs to consider the ratio between the cross-sectional area of the slot S_m (sum of all elements) and the element Δ_m itself. This is done to determine the amount of turns represented by each element assuming that conductors is uniformly distributed and is calculated by

$$\lambda_m = N\Phi_m \frac{\Delta_m}{S_m} = N\Phi_m \Delta_m \Big/ \sum_{m=1}^{M} \Delta_m \tag{A.10}$$

where N is the number of turns and M number of elements in the mesh region of the slot. From eq (A.9) & (A.10) the total flux linkage of the slot region can be calculated accordingly

$$\lambda = \sum_{m=1}^{M} \lambda_m = 2\pi N \left[\left(\sum_{m=1}^{M} \frac{\Delta_m}{S_m} \frac{1}{3} \sum_{i=1}^{3} r_{mi} A_{mi} \right) \Big/ \sum_{m=1}^{M} \Delta_m \right] \tag{A.11}$$

In cylindrical studies the solution potential includes the radius of each node which enables us to identify the part in square brackets as total weighted average solution potential A_{avg} over the whole slot region and present in short form as

$$\lambda = 2\pi N A_{avg} \tag{A.12}$$

In Cartesian coordinates the flux linkage needs to be expression as a function of the difference in weighted average vector potential on the "enter" side of the winding A_{avg+} and the weighted average vector potential on the "exit" side of the winding A_{avg-}. The concluding expression for winding to winding flux linkage becomes

$$\lambda = N\ell\left(A_{avg+} - A_{avg-}\right) \tag{A.13}$$

Appendix B

Construction of the Original RSM and Parameters of New Machines

B.1 Stator geometry specifications

The stator of the RSM in this analysis was taken from an "off the self" 3-phase, 4-pole, 5.5 kW induction motor with a D132S frame size. The laminations and windings was imbedding in a Class B insulation resin. The specifications of the stator are indicated below

Full load voltage	=	356 V
Full load current	=	10 A (rms)
Steady state frequency	=	50 Hz
Number of slots	=	36
Number of slots per phase per pole (q)	=	3
Core length	=	133.4 mm
Slot pitch (α_s)	=	10°
Winding layout	=	Double Layer
Pole pitch (τ_p)	=	9 slots
Coil span (τ_c)	=	7 slots
Pitching factor (k_p)	=	0.939
Distribution factor (k_d)	=	0.95
Winding factor (k_w)	=	0.902
Conductors in parallel per turn	=	3
Copper conductor diameter	=	(2 x 0.91mm) & (1 x 1.0mm)
Number of coils per phase	=	12
Number of turns per coil	=	11
Number of turns per phase	=	132
Actual winding resistance (20°C)	=	0.74Ω/phase
Operating winding resistance (75°C)	=	0.91Ω/phase

The full load voltage was calculated from equation 2.1.5 where the resistance of the phase winding r_s was taken at the operating temperature of 75°C. The calculation of the pitching-, distribution- and winding factors consequently indicated next

$$k_p = \sin\left(\frac{\tau_c}{\tau_p}\frac{\pi}{2}\right) \tag{B.1}$$

$$k_d = \frac{\sin(q\alpha_s/2)}{q\sin(\alpha_s/2)} \tag{B.2}$$

$$k_w = k_p \cdot k_d \tag{B.3}$$

B.2 Rotor and stator slot geometry of Original RSM

In Fig B.2.1 displays the geometrical dimensions of the original rotor, proposed by Honsinger (1971) and later by Kamper (1994), and used as the foundation design in this thesis. The same dimensions of the original semi-closed slot were used for machines in chapter 3.

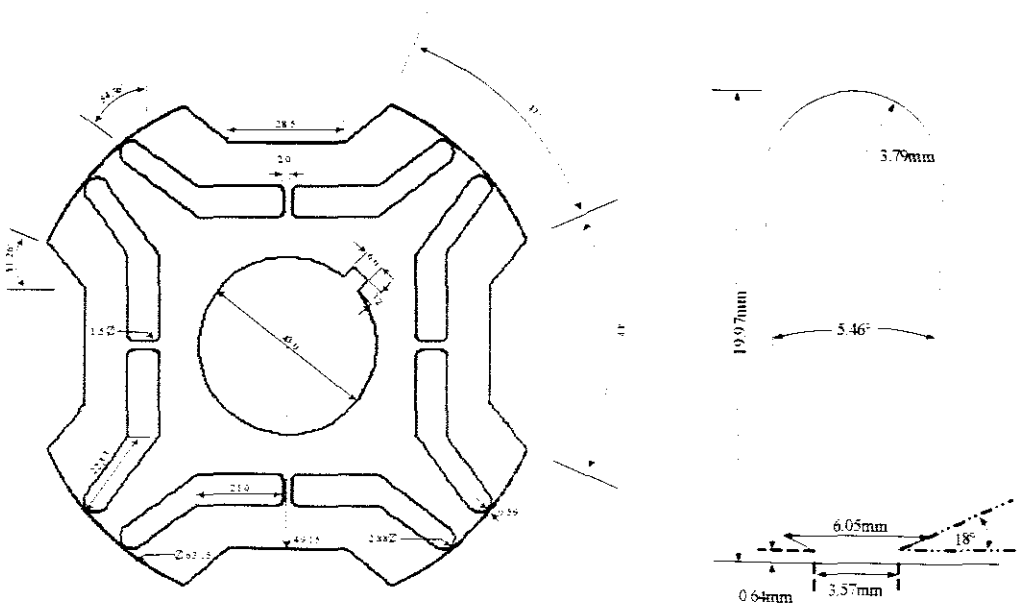

Fig B.2.1 Dimensional geometry of a rotor and stator slot of original RSM

B.3 Parameters of RSMs with different rotor geometries

The parameter results of the modelled machines from chapter 3 are indicated below according to the geometrical changes made to the rotor.

In this analysis the machine in Fig 3.1.1 is used for simulation where the pitch of the flux barriers **bp** with respect to the d-axis was changed each in 1° steps from 8° to 34° presenting 14 deferent machine prototypes. The performance of these machines are indicated in below

Table B.3.1 Single flux barrier machines without cut-outs in the rotor

	Parameters						
Machine	T_{avg} (Nm)	T_{ripple} (%)	$cos\varphi$	saliency σ	ΔL (mH)	L_d (mH)	L_q (mH)
BP8	18.694	104.41	0.565	3.63	81.20	112.11	30.91
BP10	19.695	107.73	0.586	3.86	85.59	115.56	29.97
BP12	20.276	78.16	0.6	4.01	88.02	117.26	29.24
BP14	20.611	49.47	0.61	4.13	89.74	118.40	28.66
BP16	20.948	57.7	0.617	4.22	90.97	119.19	28.22
BP18	21.141	80.54	0.621	4.29	91.77	119.69	27.92
BP20	21.211	105.73	0.623	4.32	92.21	119.99	27.78
BP22	21.264	86.12	0.624	4.32	92.34	120.13	27.79
BP24	21.27	68.22	0.624	4.30	92.10	120.05	27.95
BP26	21.054	44.3	0.62	4.23	91.43	119.71	28.28
BP28	20.815	73	0.612	4.14	90.34	119.09	28.75
BP30	20.455	107.03	0.601	4.02	88.84	118.24	29.40
BP32	20.055	101.18	0.589	3.88	87.04	117.22	30.18
BP34	19.546	99.49	0.574	3.73	84.86	115.99	31.13

In the second analysis the rotor will consist of double flux barriers where all possible combinations of different flux barrier pitches to be simulated. For the inner barrier the pitch will vary from 8° to 14° with respect to each other while the outer barrier will vary from 22° to 34° giving 22 possible combinations if no flux barriers where to overlap each other.

The stator dimensions will stay the same as the previous analysis keeping the rotor radius the same.

Table B.3.2 Double flux barrier machines without cut-outs in the rotor

	Parameters						
Machine	T_{avg} (Nm)	T_{ripple} (%)	$cos\varphi$	saliency σ	ΔL (mH)	L_d (mH)	L_q (mH)
BP8/22	19.521	43.49	0.661	4.90	84.79	106.501	21.715
BP8/24	20.759	59.56	0.679	5.25	90.10	111.28	21.18
BP8/26	21.771	87.4	0.694	5.56	94.53	115.24	20.71
BP8/28	22.555	100.6	0.705	5.83	98.11	118.42	20.31
BP8/30	23.103	109.41	0.712	6.01	100.45	120.48	20.03
BP8/32	23.276	95.55	0.715	6.09	101.18	121.04	19.86
BP8/34	23.506	77.34	0.72	6.19	102.76	122.55	19.79
BP10/24	20.78	62.35	0.68	5.27	90.20	111.34	21.14
BP10/26	21.915	88.5	0.695	5.60	95.17	115.84	20.67
BP10/28	22.802	108.96	0.707	5.90	99.19	119.45	20.26
BP10/30	23.521	117.7	0.716	6.13	102.30	122.24	19.94
BP10/32	23.943	103.14	0.721	6.33	105.15	124.87	19.72
BP10/34	24.067	80.05	0.723	6.33	104.61	124.23	19.62
BP12/26	21.043	99.64	0.687	5.41	91.41	112.13	20.72
BP12/28	22.0423	109.58	0.7	5.71	95.76	116.1	20.34
BP12/30	22.868	109.65	0.71	5.97	99.40	119.42	20.02
BP12/32	23.544	93.63	0.717	6.18	102.33	122.1	19.77
BP12/34	24.039	70.76	0.722	6.32	104.38	123.99	19.61
BP14/28	21.227	101.09	0.691	5.50	92.25	112.74	20.49
BP14/30	22.201	88.66	0.703	5.78	96.40	116.58	20.18
BP14/32	22.985	75.8	0.712	6.01	99.84	119.76	19.92
BP14/34	23.584	59.98	0.718	6.19	102.53	122.27	19.74

In the third study the two best performing machines from section 3.1 & 3.2 (BP26 and BP8/22) with respect to low torque ripple will be subjected to analysis. These machines will undergo geometrical changes by adding cut-outs to the rotor where the pitch and height of the latter will be the focus point. The geometry of the cut-outs is based on that of the original design presented in Fig 2.2.1. The first section of this analysis will introduce the machine to a cut-out pitch **cp** which will vary from 62° to 74° in steps of 2° giving a total of 14 possible prototypes for single and double flux barrier machines.

Table B.3.3 Best single- and double flux barrier machine with in creased cut-out pitch

Machine		Parameters						
		T_{avg} (Nm)	T_{ripple} (%)	$cos\varphi$	saliency σ	ΔL (mH)	L_d (mH)	L_q (mH)
SBP26	CP62	15.316	87.06	0.724	6.40	66.61	78.95	12.34
	CP64	17.04	92.98	0.727	6.48	74.08	87.61	13.53
	CP66	18.46	92.63	0.728	6.49	80.11	94.69	14.58
	CP68	19.5	68.73	0.725	6.40	84.74	100.44	15.7
	CP70	20.38	48.53	0.72	6.25	88.55	105.41	16.86
	CP72	21.13	52.8	0.714	6.08	91.76	109.84	18.08
	CP74	21.71	55.01	0.706	5.87	94.31	113.66	19.35
SBP8/22	CP62	14.02	66.79	0.765	7.95	60.92	69.69	8.77
	CP64	16.018	69.74	0.775	8.49	69.71	79.02	9.31
	CP66	17.59	48.79	0.778	8.68	76.46	86.41	9.95
	CP68	18.65	70.67	0.776	8.52	81.13	91.92	10.79
	CP70	19.411	61.13	0.77	8.19	84.4	96.14	11.74
	CP72	19.92	62.81	0.761	7.78	86.61	99.39	12.78
	CP74	20.28	50.78	0.752	7.36	88.17	102.04	13.87

With the most optimum span found the horizontal height of this cut-out **ch** will be increased from 2mm to 12mm in steps of 2mm giving 12 possible prototypes. From these simulations the best performing machines for single- and double flux barriers will be presented. The two machines subject to analysis will be the single flux barrier machine with a cut-out pitch of 70° and the double flux barrier machine with a pitch of 66°.

Table B.3.4 Best single- and double flux barrier machine with in creased cut-out height

Machine		Parameters						
		T_{avg} (Nm)	T_{ripple} (%)	$cos\varphi$	saliency σ	ΔL (mH)	L_d (mH)	L_q (mH)
BP26 with CP70	CH2	20.461	47.42	0.719	6.22	88.85	105.88	17.03
	CH4	20.52	45.88	0.717	6.16	89.13	106.39	17.26
	CH6	20.623	42.71	0.714	6.08	89.57	107.21	17.64
	CH8	20.753	38.53	0.709	5.95	90.13	108.34	18.21
	CH10	20.952	32.33	0.701	5.75	91	110.17	19.17
	CH12	21.28	27.33	0.684	5.36	92.44	113.62	21.18
BP8/22 with CP66	CH2	17.743	45.51	0.777	8.60	77.12	87.27	10.15
	CH4	17.847	41.79	0.774	8.44	77.57	88	10.43
	CH6	17.954	37.1	0.769	8.18	78.06	88.93	10.87
	CH8	18.096	30.47	0.761	7.78	78.65	90.25	11.6
	CH10	18.332	25.69	0.747	7.16	79.64	92.56	12.92
	CH12	19.255	23.31	0.718	6.19	83.65	99.78	16.13